MEDDELANDEN
FRÅN
STATENS SKEPPSPROVNINGSANSTALT
(PUBLICATIONS OF THE SWEDISH STATE SHIPBUILDING EXPERIMENTAL TANK)
Nr 68 GÖTEBORG 1971

THEORY AND OBSERVATIONS ON THE USE OF A MATHEMATICAL MODEL FOR SHIP MANOEUVRING IN DEEP AND CONFINED WATERS

BY

NILS H. NORRBIN

Extended version of a paper presented at
the Eighth Symposium on Naval Hydrodynamics
Pasadena, California, August 1970

AB ALLMÄNNA FÖRLAGET
STOCKHOLM

PRINTED IN SWEDEN BY
ELANDERS BOKTRYCKERI AKTIEBOLAG, GÖTEBORG 1971

Synopsis

This paper summarizes an experimental and analytical study of ship manoeuvring, with special emphasis on the use of a research-purpose simulator for evaluating the behaviour of large tankers in deep water as well as in harbour entrances and canals. In an introductory Section some new results from full-scale measurements and simulator studies are given to illustrate the demands put on a mathematical model in the two extreme applications: course-keeping in deep water and manoeuvring in a canal bend.

Well-known derivations of rigid body dynamics and homogeneous flow solutions for forces in the ideal case are included to form skeleton of the mathematical model. Separate equations handle helm and engine controls. Coefficients and parameters are made non-dimensional in a new system—here designated the "*bis*" system as different from the SNAME "*prime*" system generally used—in which the units for mass, length and time, respectively, are given by the mass of the ship, m, the length, L, and the time required for travelling one ship length at a speed corresponding to $V''=F_{nL}=1$, $\sqrt{\frac{L}{g}}$.

Semi-empirical methods are suggested for estimates of the force and moment derivatives. Special consideration is given to added masses and rudder forces in view of their predominant importance to course-keeping behaviour; the rudder forces measured on a scale model are corrected for differences in wake and screw loading before application to full-scale predictions. Non-linear contributions to hull forces are included in second order derivatives, relevant to the cross-flow concept.

The extension of the mathematical model to the confined-water case is based upon the theoretical results by NEWMAN, INOUE, and others, and upon relations found from special calculations and experiments. In the model the hydrodynamic interferences appearing in forces and moments due to the presence of port and starboard side wall restrictions and bottom depth limitations are represented by additional terms containing higher order derivatives with respect to three suitable confinement parameters, $\eta=\eta_s+\eta_p$, $\bar{\eta}=\eta_s-\eta_p$, and ζ.

In a canal the asymmetrical forces are considered as due to the added effects from port (p) and starboard (s) walls rather than as the effect of an off-centreline position; primarily η is a measure of this position, $\bar{\eta}$ a measure of the bank spacing.

The mathematical model is here applied for evaluation of model test data obtained for the Swedish 98,000 t.dw. tanker MALMÖHUS in the VBD laboratories. Oblique towing and rotating arm tests were performed in "deep" and shallow water. Oblique towing tests were also run at various distances from a vertical wall in the deep tank, and in two Suez-type canal sections. The effect of shallow water was especially large in force non-linearities. Missing data for bottom and wall effects on added mass and inertia are taken from theory and from test results due to FUJINO, respectively.

The deep-water predictions for zig zag test and spiral loop prove to be in good agreement with full-scale trial results. Analogue computer diagrams are given to show the effects of shallow water upon definite manoeuvres and upon course-change transients following auto-pilot trim knob settings. A few results are included to illustrate auto-pilot position control of the tanker in free water, in shallow water, between parallel walls and in a canal.

Essentially this report is a reproduction of a paper presented to the *Eighth Symposium on Naval Hydrodynamics*, held in Pasadena in August 1970. Part of Section 9 is new, however, as are some diagrams, and a final Section on conclusions and suggestions for future research has been added.

1. Introduction

On Course-Keeping in Deep Water

The average depth of the oceans is some 3800 m. Small native crafts still steer their ways between nearby islands in these oceans. New ships are built to transport ever larger quantities of containers or bulk cargoes at a minimum of financial expense between the continents.

It is not necessarily obvious that the helmsman shall be able to control a mammoth tanker on a straight course. A few years ago ship operators were stirred by the published results of an analytical study, interesting in itself, which in fact did indicate, that manual control of ships would be impossible beyond a certain size. Upon

request by the shipbuilders a series of real-time simulator studies were initiated at SSPA in autumn 1967 to investigate manual as well as automatic control of large tankers then building, [1].[1])

At an early stage of these tests the helmsman was found to constitute a remarkably adaptive control element, which could not be simulated by a simple transfer function. As could be expected a rate display proved to make course keeping more easy; the rate signal was even more essential to the auto-pilot.

The simulator findings were confirmed in subsequent prototype trials. The diagrams of Fig. 1 compare simulator and prototype rates of change of heading and yaw accelerations for a large tanker as steered by the author in a *Force 6* following sea. (In the simulator case the sea disturbance was represented by a cut-off pseudo-random white noise of predetermined root mean square strength, that was fed into the yaw loop.) This particular tanker is dynamically unstable on a straight course, and the steady-state $\dot{\psi}(\delta)$-diagram from a deep-water spiral test exhibits a hysteresis loop with a total height of 0.5°/s and a total width of a little more than 3° of helm. If yaw rate is maintained within some 40 per cent of the loop height value it has been found possible to control the straight heading by use of small helm only. This figure must not be generalized, however.

The use of the computer-type simulator for the prediction of ship behaviour implies the adoption of a suitable mathematical model and the knowledge of a number of coefficients in this model. An alternative technique that simulates full-scale steering by controlled free-sailing ship models is still in use. Mostly the steering has been exercised by manual operation of the controls, and it has been claimed that at least comparative results should then be valid. It is likely that the truth of this statement depends on the actual speed and size (and time constants) of the prototype ship as well as of the model scale ratio used.

Time is scaled as square root of length. Human response time may be "scaled" within certain limits only. The $\dot{\psi}(\delta)$-diagrams of Fig. 2 demonstrate results of simulated steering of the tanker prototype already referred to, as well as of her fictive models of four different sizes. (Note that curves run anti-clockwise with time.) The smallest "model" is in scale 1:100, i.e. it has a length of 3.1 m, which should permit free-sailing tests in several in-door facilities. The two helms-

[1]) The numbers within brackets refer to the list of references in Section 16.

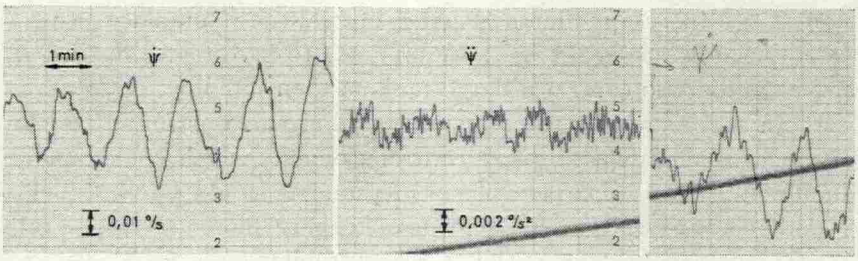

Full scale single-channel record (Helmsman: Author)

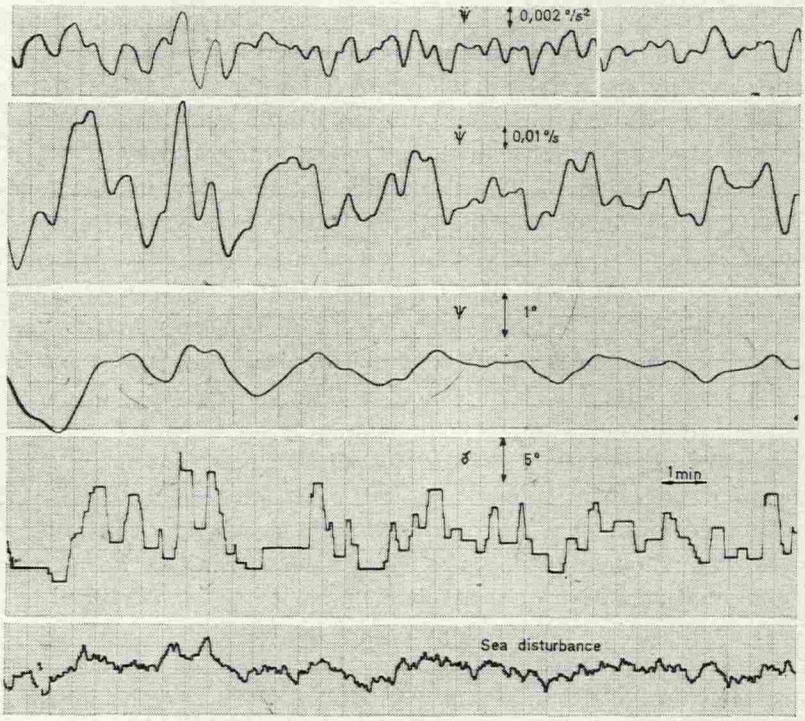

Simulator records (Helmsman: Author)

Fig. 1. Manual steering of an unstable 230,000 t.dw. tanker in quartering sea. Prototype and simulator records.

men, who both had their own kind of steering philosophy and who were allowed a short training period in each case, both failed to maintain the proper control of the two smaller "models".

The control of a ship on a straight course is governed mainly by the effective inertia, by the yaw damping moment, by the rudder

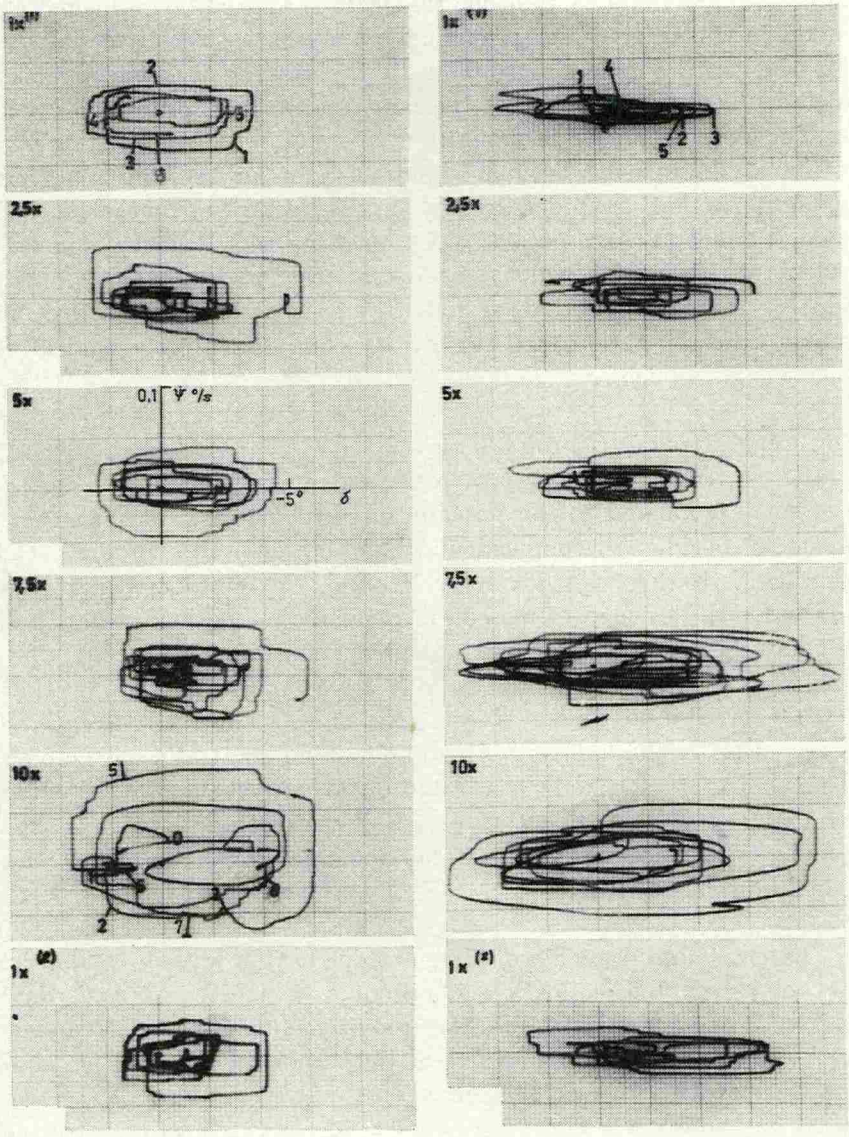

Fig. 2. Simulator tests of manual steering of an unstable 230,000 t.dw. tanker in real and speeded-up time. Yaw rate versus helm angle. (Numbers along curves indicate minutes in real time.)

force available, and by the time this force is applied. A mathematical model intended for studies of manual or automatic steering may therefore be quite simple; in contrast to the test basin model it may include proper corrections for the large scale effects often present in rudder force data. (Cf. Section 7.)

Fig. 3 repeats the original simulator $\dot{\psi}(\delta)$-curves from real-time straight running, recorded by use of the "complete" mathematical model, but it also presents results from tests with a linear model as well as with a model, which contains no other hydrodynamic contributions than those in lateral added inertias and rudder forces. No major differences were experienced in using these three models of increasing simplicity.

On Manoeuvring in Confined Waters

Manoeuvring, involving yaw rates and drift velocities which are not small compared to the forward speed, demands a mathematical model of considerable complexity. An useful presentation of non-linear characteristics has been given by MANDEL, [2]. One particular non-linear model designed to include manoeuvres in confined waters will be more fully discussed in subsequent Sections of this paper.

The average depth of the oceans is some 3800 m. But ocean voyages start and terminate at ports behind the shallow waters of the inner continental shelves. Additional confinements are presented by many of the important gateways of world trading, such as the Straits of Dover and Malacca, the Panama Canal, and the Suez Canal now closed.

The maximum draughts of "large" ships have always been limited by bottom depths of docks and harbours, and of canals and canal locks. With few exceptions the requirements placed on under-keel clearances—by ship owners or by authorities—have been chosen solely with a view to prevent actual ship grounding or excessive canal bed erosions. Thus the Suez Canal Authorities accepted a nominal blockage ratio of 1:4 for ships in northbound transit at a maximum speed of 13 kilometres per hour, corresponding to a mean back-flow velocity of some 1.5 m/s.

To-day new limits are imposed by the depths of ocean sills as well as by the depths and widths of open sea port approaches. The potential dangers of a large oil tanker navigating in such waters under, say,

"Complete" model:

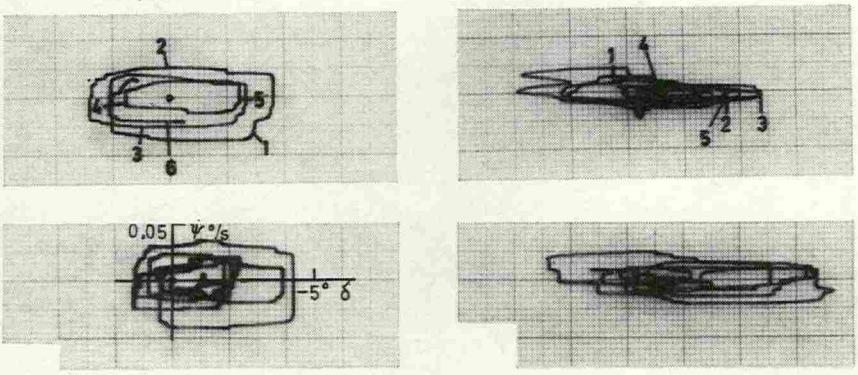

Linear model:

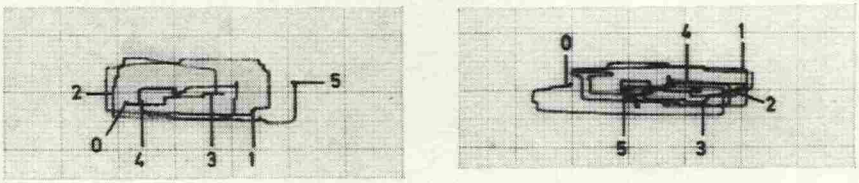

Model using inertia and rudder forces only:

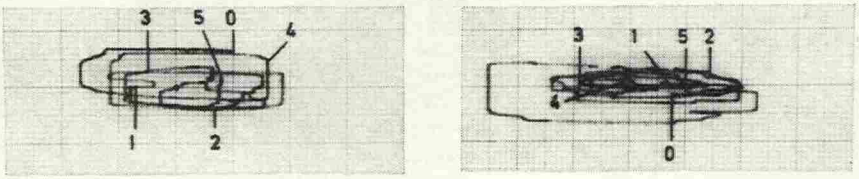

Helmsman N

Helmsman W

Fig. 3. Simulator tests of manual steering of an unstable 230,000 t.dw. tanker using alternative mathematical models. Yaw rate versus helm angle.

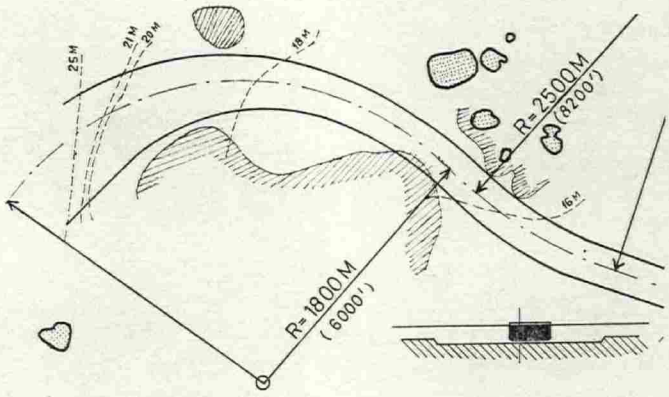

Plan and typical section of dredged channel

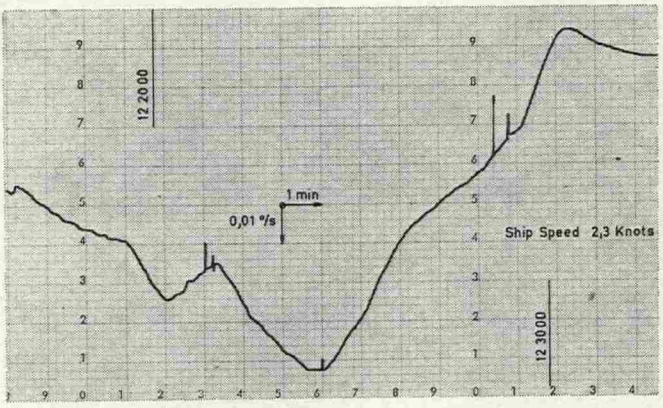

Part of yaw rate record in transit

Fig. 4. Example of yaw rates recorded on 210,000 t.dw. tanker in harbour approach.

the influence of an unexpected change of cross current must not be denied. Whatever nautical experience the master or pilot may possess, he is still in need of actual data and of means to convert this information to helm and engine orders. Automatic systems on a predictor basis are likely to appear in a near future, [3].

In the planning for dredged entrance channels and harbour turning basins the manoeuvring properties of the ships must no longer be overlooked. The upper drawing of Fig. 4, reproduced from ref. [4], shows part of the plan view and a typical section of the buoyed

channel for 200,000 t.dw. tankers unloading at a new oil terminal. Before entering the 90° starboard turn the speed is brought down to less than 2 knots, and the tanker then proceeds under slow acceleration by own power. Breaking tugs are used on quarters, and bow and stern tugs assist in the S-bend. The lower diagram of Fig. 4 is taken from SSPA records of yaw rates in the passage; the initial curvature corresponds to $r' = 0.175$, and the maximum rate of change of angular velocity is of the order of $0.0005°/s^2$ at a forward speed of 2.3 knots.

In general the lateral forces on the ship will all increase as water depth turns smaller, and the dynamical stability is also likely to increase. From extensive measurements by FUJINO it appears, however, that the picture is not so simple, and that for some ships there may be a "dangerous" range of depth-to-draught ratios, in which the dynamic stability gets lost, [5].

Recent model tests indicate that the large-value non-linearities, such as the lateral cross-flow drag at high values of drift, do increase even more than the linear contributions governing the inherent stability conditions. Whereas these non-linearities may be omitted in the mathematical model of the ship in a canal the bank effects here introduce destabilizing forces, that are again highly non-linear.

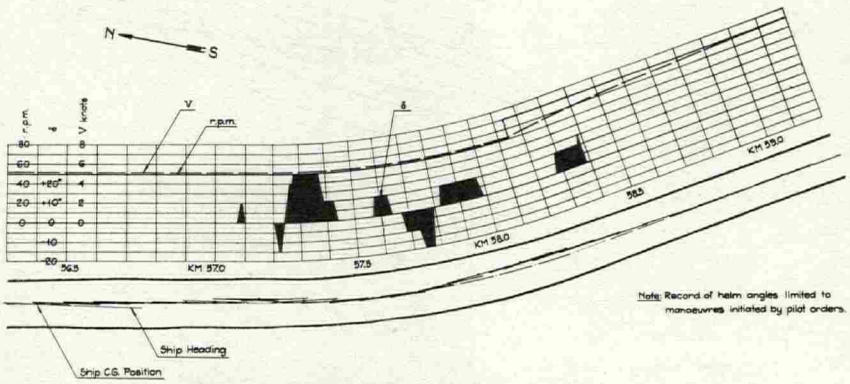

Fig. 5. 60,000 t.dw. tanker southbound through Suez Canal on 36′ draught. Abstract of records in *KM 57* bend.

The effects of well-known forces experienced by a ship sailing parallel to the bank of a canal are clearly apparent in the record from a Suez Canal transit here reproduced in Fig. 5, [6]. (The positions in the canal as well as the width between beach lines were derived from triangulation by use of two simple sighting instruments designed for the purpose.) Upon approach to the Km 57 bend the ship is slightly to port of the canal centre line. The pilot orders port helm for two minutes, by which the ship is pushed away from the near bank and the desired port turn is also initiated. Back on centre line the ship mainly turns with the canal. In spite of a starboard checking rudder she again moves closer to the port bank, and again port rudder has to be applied, etc.

So far analytical studies of ships moving in canals have been dealing with straight running. It is believed that the mathematical model which is presented here may also be extended to the case of slowly widening and bending canals.

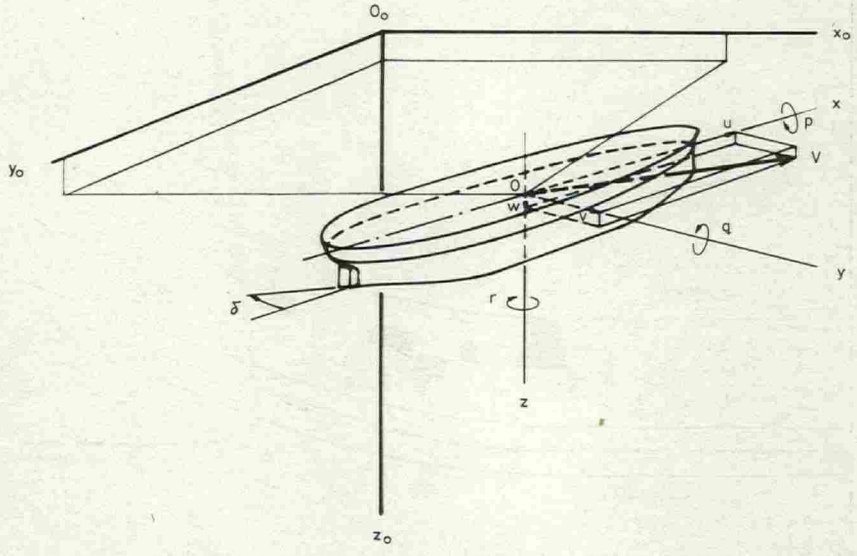

Fig. 6. Inertia frame and body axes, etc.

2. Symbols and Units, etc.

When applicable the symbols and abbreviations here used have been chosen in accordance with the ITTC recommendations, [7]. Some new symbols are introduced to define the position and orientation of a ship in confined waters. (See also Section 10.)

The system of axes fixed in space is $O_0x_0y_0z_0$, that fixed in the body or ship is $Oxyz$. The point of reference O lies at distance $L_{pp}/2$ forward of A.P. of the ship. (Cf. Fig. 6 and Section 4.)

Dimensional numbers are given in metric units unless otherwise stated. Generally coefficients and relations are expressed in non-dimensional forms. In addition to the non-dimensionalizing *"prime"* system usually adopted use is here made of a new *"bis"* system, further presented in Section 3.

A dot above a variable stands for a derivation with respect to time. Partial derivatives of forces and moments are designated by the proper subscript attached to the force or moment symbol.

Symbol	Definition	Physical Dimension	Remarks
A	Section area of hull	L^2	
A_c	Channel section area	L^2	
A_o	Midship section area	L^2	
A_{ij}	Added mass. $i=1,2,3$; $j=1,2,3$	M	
	Added mass. $i=4,5,6$; $j=4,5,6$	ML^2	
	Added mass. $i=1,2,3$; $j=4,5,6$	ML	
A_H	Added mass in horizontal oscill. in a free surface, neglecting gravity	M	
A'_H	Added mass in horizontal oscillation, unbounded fluid	M	
A_r	Total proj. area of rudder	L^2	
A_{rm}	Moveable proj. area of rudder	L^2	
B	Beam of hull	L	
C_D	Cross-flow drag coeff., 3-dim.	—	
D	Diameter of propeller	L	
$\mathbf{F}$	Force vector	MLT^{-2}	
F_{nh}	FROUDE number on depth	—	$F_{nh}=V/\sqrt{gh}$
F_{nL}	FROUDE number on length	—	$F_{nL}=V/\sqrt{gL}=V''$
I	Moment of inertia	ML^2	
I_{ij}	Mass product of inertia	ML^2	$I''_{zz}=k^2_{zz}$
J	Propeller advance coefficient	—	$J=u(1-w)/nD$
K	Rolling moment about x axis	ML^2T^{-2}	
K_Q	Propeller torque coeff.	—	$K_Q=-Q^P/\rho n^2D^5$
K_T	Propeller thrust coeff.	—	$K_T=T^P/\rho n^2D^4$
L	Length of hull	L	$L=L_{pp}$

Symbol	Definition	Physical Dimension	Remarks
M	Pitching moment about y axis	ML^2T^{-2}	
$\mathbf{M}$	Moment vector	ML^2T^{-2}	
N	Yawing moment about z axis	ML^2T^{-2}	$N''=N/mgL$
P	Step response quality number	—	
Q	Torque about propeller shaft	ML^2T^{-2}	Pos. driv. forw'd
R	Turning radius	L	$r'=L/R$
R	Resistance	MLT^{-2}	$X(R)=-R$
S	Surface area	L^2	
T	Hull draught	L	
T	Propeller thrust	MLT^{-2}	
T_L	Kinetic energy of liquid	ML^2T^{-2}	
$\mathbf{U}$	Total flow velocity	LT^{-1}	
$\mathbf{V}$	Velocity of origin of body axes	LT^{-1}	$V''=V/\sqrt{gL}$
$\mathbf{V}^c$	Speed of water current	LT^{-1}	
$\mathbf{V}_1$	Ship speed over ground	LT^{-1}	
W	Channel width in general	L	
$\overline{W}$	Bank spacing, half of	L	$2\overline{W}=W_s-W_p$
X,Y,Z	Hydrodynamic forces along body axes	MLT^{-2}	
Y^{RR}	Y-force due to rudder	MLT^{-2}	
Y^R	Y-force on rudder proper	MLT^{-2}	
a	Depth to top of rudder	L	
a	Half-distance between source and sink	L	
a	Water surface elevation	L	
a_A	Slope of lift coefficient curve	—	
b	Half-beam of body	L	
b	Height of rudder	L	
c	Flow velocity past rudder	LT^{-1}	
c_D	Cross-flow drag coeff., 2-dim.	—	
d	Distance of source and sink from wall	L	
g	Gap between rudder and hull	L	
$\mathbf{g}$	Gravity vector	LT^{-2}	
h	Depth of water	L	
$\mathbf{h}$	Vector in general	Undef.	
k_{ii}	Coefficients of accession to inertia	—	$i=1,2,3$
k'_{ii}	Do	—	$i=4,5,6$
k_r	Corr. factor for rudder inflow	—	Cf. eq. (7.4)
k_v	Do	—	
k_{zz}	Non-dim. radius of gyration	—	
l	Half-length of body	L	
m	Mass of body	M	$m''=1$
m	Strength of source	L^2T^{-1}	
n	Number of revs. of prop. in unit time	T^{-1}	
p	Pressure in general	$ML^{-1}T^{-2}$	
q	Stagnation pressure	$ML^{-1}T^{-2}$	
p,q,r	Angular velocity components of Ω	T^{-1}	
r_{ome}	Max. radius of equivalent body of revolution	L	
s	Lateral thrust factor	—	Cf. Section 7
s	Sinkage	L	

Symbol	Definition	Physical Dimension	Remarks
t	Time	T	$t''=t/\sqrt{\frac{L}{g}}$
t	Thrust deduction factor	—	
u,v,w	Components of **V** along body axes	LT^{-1}	
w	Wake fraction	—	
x,y,z	Orthogonal coordinates of a right-handed system of body axes	L	
x_0,y_0,z_0	Orthogonal coordinates of a right-handed system of space axes (inertia frame)	L	
Δ	Weight displacement	MLT^{-2}	$\Delta=\mu\rho g\nabla_0=mg$
∇	Volume displacement	L^3	Normal approx.: $\nabla=\nabla_0$
∇_0	Volume displacement at rest	L^3	
Λ	Aspect ratio	—	
$\underline{\Lambda}_r$	Aspect ratio of rudder	—	$\underline{\Lambda}_r=b^2/A_r$
Λ_r	Do for rudder + plane wall image	—	$\Lambda_r=2\Lambda_r$
Φ	Velocity potential	L^2T^{-1}	$\Phi''=\Phi/L\sqrt{gL}$
Ψ	Stream function	L^2T^{-1}	
Ω	Angular velocity of ship	T^{-1}	
α	Angle of attack	—	
β	Angle of drift	—	$\tan\beta=-v/u$
γ	Frequency parameter	—	$\gamma=V\omega/g=u''\omega''$
γ	Coeff. of heading error term in proportional rudder control	—	"Rudder ratio"
δ	Rudder angle (deflection)	—	
δ^*	Rudder angle ordered by auto pilot	—	
δ_e	"Effective" rudder angle	—	$\delta_e=\delta$ for $v=r=0$
ϵ	Phase lead angle	—	
ζ	Restricted water depth (under-keel clearance) parameter	—	$\zeta=T/(h-T)$
$\underline{\eta}$	Ship-to-bank distance parameter	—	$\underline{\eta}=\eta_s+\eta_p$
$\overline{\eta}$	Bank spacing parameter	—	$\overline{\eta}=\eta_s-\eta_p$
η_p	Port bank distance parameter	—	$\eta_p=L/(W_p-y_0)$
η_s	Starboard bank distance parameter	—	$\eta_s=L/(W_s-y_0)$
$\varkappa$	Engine output torque ratio	—	
θ	Angle of pitch	—	
μ	Body mass density ratio	—	$\mu=m/\rho\nabla_0$. For norm. surface ships $\mu=1$
ρ	Mass density of water	ML^{-3}	
σ	Coeff. of rate of change of heading term in proportional rudder control	T	"Rate (time) constant"
φ	Prismatic coefficient	—	
ϕ	Angle of roll or heel	—	
ψ	Angle of yaw, or heading error	—	
ω	Circular frequency	T^{-1}	$\omega''=\omega\sqrt{L/g}$
ω'	Reduced frequency	—	$\omega'=\omega L/V\approx\omega''/u''$

3. Non-Dimensionalizing by Use of the "Bis" System

The use of non-dimensional coefficients is accepted in all branches of ship theory, and when motion studies are considered even the variables of the equations are often normalized.

Within the field of manoeuvring a unit for time is usually the time taken by a body to cover the distance of its own length, and the unit for velocity then is most naturally given by the momentary speed $V=(u^2+v^2)^{1/2}$. If the body does not move forward this definition is less attractive. In the system just mentioned—which is recommended by ITTC and which in most cases is fully adequate—symbols for non-dimensional quantities usually are indicated by a prime.

The unit for length almost always is chosen equal to the length L of the body, and for the common surface ship more specified $L=L_{pp}$.

The unit for mass is mostly taken as the mass of a certain volume of the liquid, defined in terms of the body or ship geometry. In the "*prime*" system already referred to, reference volumes are, say, $\frac{1}{2}L^3$ [8] or $\frac{1}{2}L^2T$ [9], the latter one used with the reference area LT suggested by the wing analogy.

In case of bodies, which are supported mainly by buoyancy lift, the main hull contour displacement ∇_0 is perhaps the most natural reference volume: if body mass then is $m=\mu\cdot\rho\cdot\nabla_0$ the non-dimensional mass is equal to μ. (When treating heavy aircraft dynamics GLAUERT chose $\mu\rho\nabla$ in place of $\rho\nabla$ for the mass unit, [10].) In normal ship dynamics $\mu=1$, whereas for heavy torpedoes $\mu=1.3$–1.5, say; the symbol μ will be rejected in certain applications.

Here a consistent normalization of motion modes and forces will be made in a new system, the "*bis*" system, where the unit for mass is $m=\mu\rho\nabla_0$, the unit for length is L and the unit for linear acceleration is equal to g, the acceleration of gravity. From this the unit for time is $\sqrt{\frac{L}{g}}$, and it also follows Table I.

It will be noted that, in the system suggested, a non-dimensional velocity is given by the corresponding FROUDE number, and that all forces are related to the displacement gravity load $\Delta=\mu\rho g\nabla_0$ of the body. (Cf. quotients such as R/Δ, "resistance per tons of displacement", used in other fields of applied naval architecture.)

Table I.

Unit for	"Bis" system	"Prime" system	
Mass (M)	$\mu\rho\nabla_0$	$\frac{\rho}{2}L^3$	$\frac{\rho}{2}L^2T$
Length (L)	L	L	L
Time (T)	$\sqrt{\frac{L}{g}}$	$\frac{L}{V}$	$\frac{L}{V}$
Linear velocity	$\sqrt{gL}$	V	V
Linear acceleration	g	$\frac{V^2}{L}$	$\frac{V^2}{L}$
Angular velocity	$\sqrt{\frac{g}{L}}$	$\frac{V}{L}$	$\frac{V}{L}$
Angular acceleration	$\frac{g}{L}$	$\frac{V^2}{L^2}$	$\frac{V^2}{L^2}$
Force	$\mu\rho g\nabla_0$	$\frac{\rho}{2}V^2L^2$	$\frac{\rho}{2}V^2LT$
Moment	$\mu\rho g\nabla_0 L$	$\frac{\rho}{2}V^2L^3$	$\frac{\rho}{2}V^2L^2T$
Reference area	$\mu\frac{2\nabla_0}{L}$	L^2	LT

It is custommary to form a non-dimensional force coefficient by dividing by the product of a stagnation pressure ($q=\frac{\rho}{2}V^2$) and a reference area, and of course the new system will not demand any different rules. In place of the velocity V, however, here is choosen that particular velocity which corresponds to $F_{nL}=1$, i.e. the normalized stagnation pressure is $q=\frac{\rho}{2}gL$. The reference area then is seen to equal $\mu\frac{2\nabla_0}{L}$, or, for the normal surface ship, $\frac{2\nabla}{L}$.

4. Kinematics in Fixed and Moving Systems

The two orthogonal systems of axes here used, $O_0x_0y_0z_0$ fixed in space—the inertia frame—and $Oxyz$ fixed in the body, are shown in Figs. 6 and 7. The orientation of the body axes may be derived, from an original identification with the inertia frame, by the successive rotations through the angle of yaw, ψ, the angle of pitch, θ, and the angle of roll, ϕ, respectively, defined around the body axes z, y, and x in their progressively changed positions.

In a certain moment of time the relation between the space vector $\overline{\mathbf{O_0P}}=\mathbf{x}_{0P}$ and radius vector $\overline{\mathbf{OP}}=\mathbf{x}_p$, invariant in the body system, is given by

$$\mathbf{x}_{0P}-\mathbf{x}_{0O}=\Lambda\mathbf{x}_p \tag{4.1}$$

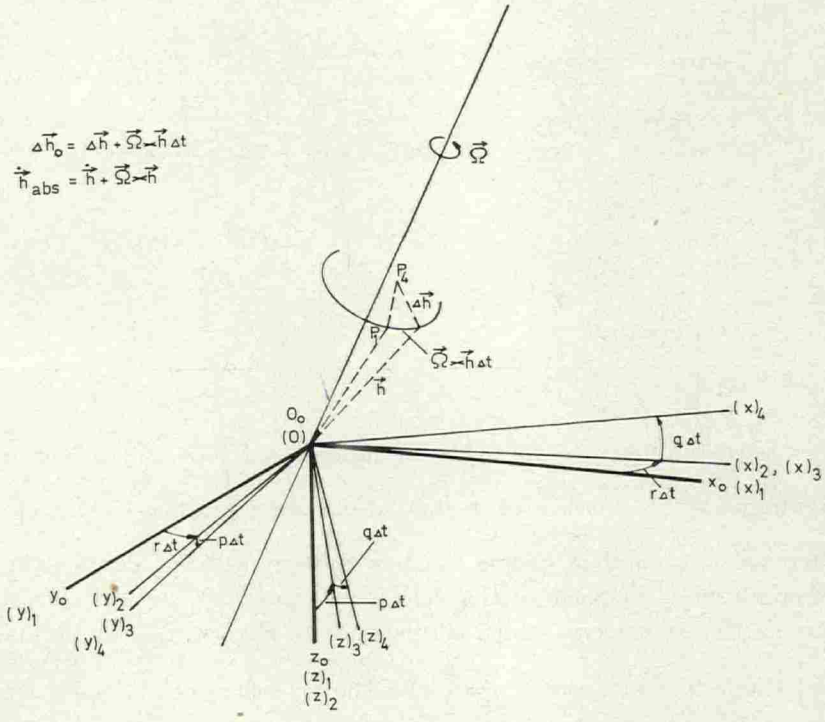

Fig. 7. Graphical deduction of the absolute time derivative of a vector $\overline{\mathbf{OP}}_1=\mathbf{h}$ defined in the moving body system.

where the orthogonal transformation matrix reads

$$\Lambda=\begin{bmatrix}\cos\psi\cos\theta & -\sin\psi\cos\phi+\cos\psi\sin\theta\sin\phi & \sin\psi\sin\phi+\cos\psi\sin\theta\cos\phi\\ \sin\psi\cos\theta & \cos\psi\cos\phi+\sin\psi\sin\theta\sin\phi & -\cos\psi\sin\phi+\sin\psi\sin\theta\cos\phi\\ -\sin\theta & \cos\theta\sin\phi & \cos\theta\cos\phi\end{bmatrix} \tag{4.2}$$

When applied in opposite direction the transformation is

$$\mathbf{x}_P=\Lambda^{-1}(\mathbf{x}_{0P}-\mathbf{x}_{00})=\tilde{\Lambda}(\mathbf{x}_{0P}-\mathbf{x}_{00}) \tag{4.3}$$

where $\tilde{\Lambda}$ is the transposed matrix, in which rows and columns appear in interchanged positions.

In particular, note that the gravity vector $\mathbf{g}_0=g\hat{z}_0$ will be given by the column vector

$$\mathbf{g}=\tilde{\Lambda}\begin{vmatrix}0\\0\\g\end{vmatrix}=\begin{vmatrix}-g\cdot\sin\theta\\ g\cos\theta\sin\phi\\ g\cos\theta\cos\phi\end{vmatrix} \tag{4.4}$$

in the moving system.

From Fig. 7 will be seen how the absolute (total) value of the time derivative of any vector $\mathbf{h}$ in the body system may be calculated from the relation

$$\dot{\mathbf{h}}_{abs}=\dot{\mathbf{h}}+\boldsymbol{\Omega}\times\mathbf{h} \tag{4.5}$$

The angular velocity vector $\boldsymbol{\Omega}$ may now be expressed in terms of the Eulerian angles and their time derivatives: For the vector $\mathbf{h}$ there is $\mathbf{h}_0=\Lambda\mathbf{h}$ and

$$\dot{\mathbf{h}}_{abs}=\tilde{\Lambda}(\Lambda\dot{\mathbf{h}}+\dot{\Lambda}\mathbf{h})=\dot{\mathbf{h}}+\tilde{\Lambda}\dot{\Lambda}\mathbf{h} \tag{4.6}$$

and so the column vector $\boldsymbol{\Omega}$ is obtained from the corresponding anti-symmetric angular velocity matrix for the product $\tilde{\Lambda}\dot{\Lambda}$,

$$\boldsymbol{\Omega}=\begin{vmatrix}p\\q\\r\end{vmatrix}=\begin{vmatrix}\dot{\phi}-\dot{\psi}\sin\theta\\ \dot{\psi}\cos\theta\sin\phi+\dot{\theta}\cos\phi\\ \dot{\psi}\cos\theta\cos\phi-\dot{\theta}\sin\phi\end{vmatrix} \tag{4.7}$$

The angular velocity components resolved in the inertia frame are

$$\left.\begin{aligned}\dot{\phi}&=p+q\sin\phi\tan\theta+r\cos\phi\tan\theta\\ \dot{\theta}&=q\cos\phi-r\sin\phi\\ \dot{\psi}&=r\cos\phi\sec\theta+q\sin\phi\sec\theta\end{aligned}\right\} \tag{4.8}$$

In the special case of motion in a horizontal plane in absence of rolling and pitching it is $\dot{\psi}=r$.

In Section 8 an expression will be required for the absolute acceleration of a mass element dm at station $P(x, y, z)$ in a body moving through the water with velocity $\mathbf{V}$. From (4.5) then

$$\mathbf{V}_P=\begin{vmatrix} u \\ v \\ w \end{vmatrix}+\begin{vmatrix} 0 & -r & q \\ r & 0 & -p \\ -q & p & 0 \end{vmatrix}\begin{vmatrix} x \\ y \\ z \end{vmatrix}=\begin{vmatrix} u-ry+qz \\ v+rx-pz \\ w-qx+py \end{vmatrix} \tag{4.9}$$

and by a repeated application of the transformation formula

$$(\mathbf{a}_P)_{abs}=\begin{vmatrix} \dot{u}-rv+qw-(q^2+r^2)x+(pq-\dot{r})y+(rp+\dot{q})z \\ \dot{v}-pw+ru-(r^2+p^2)y+(qr-\dot{p})z+(pq+\dot{r})x \\ \dot{w}-qu+pv-(p^2+q^2)z+(rp-\dot{q})x+(qr+\dot{p})y \end{vmatrix} \tag{4.10}$$

In presence of a homogeneous steady current $\mathbf{V}_0^c$ a term $\tilde{\Lambda}\mathbf{V}_0^c$ is to be added to the right hand member of eq. (4.9). In practical applications this current may be assumed to take place in planes parallell to the horizontal, so that $\mathbf{V}_0^c$ is fully identified by u_0^c and v_0^c; ~~the body "speed over ground" is then given by $u_1=u+u_0^c\cdot\cos\psi+v_0^c\cdot\sin\psi$ and $v_1=v+v_0^c\cdot\cos\psi-u_0^c\cdot\sin\psi$.~~ It is easy to show that ~~whereas the two upper rows of~~ the column matrix for the acceleration in (4.10) will remain unchanged, ~~the lower row defining the acceleration of the point P along the axis of z will now contain the terms $-qu_1+pv_1$ in place of $-qu+pv$. According to this result, which is often overlooked in the literature, the motion of a submarine will in fact be influenced by a steady horizontal current~~. To the surface ship in horizontal manoeuvres, ~~however~~, this homogeneous current will only mean a steady shift of the path; alternatively, if a certain straight course is required heading shall compensate for the steady drift. The local finite current, on the other hand, generates varying outer disturbances and shall be handled by other means.

5. Flow Phenomena and Forces on a Ship in Free Water

Ideal-fluid Concepts

As a source of reference for further discussions this Section recapitulates some of the characteristics of the flow past a ship in free or open water.

When a double-body ship form—i.e., a body which is symmetrical about the xy-plane—moves forward in a large volume of ideal-fluid water the streamlines adjust themselves according to the laws of continuity. The shape of those stream-lines remain the same at all speeds. The increase of relative velocity past the wider part of the body corresponds to a back-flow or return flow of the water previously in rest. This disturbance in the potential flow pattern extends far into the fluid volume—a beam-width out from the side of the body the super-velocity still has a value, which is some 80 per cent of that just outside the body.

From a resistance point of view the steady forward motion within this ideal homogeneous fluid may lack some realism. According to the D'ALEMBERT's Paradox the body will experience no resultant force. However, if the body is to be accelerated the kinetic energy of the fluid must be increased. This energy increase is manifested by a resistance, which for a given geometrical form is proportional to the mass of displaced fluid and the amount of acceleration, i.e. to the product of an "added mass" and the acceleration component in the direction considered. The resultant force is not necessarily orientated in the same direction.

In the simple steady motion the total energy certainly will remain constant, but as the body moves forward through virgin fluid there takes place in each transverse section a repeated particle acceleration and transformation of energy. The impuls pressure distribution thus generated will normally be unsymmetric, and so a free moment results on the body. This moment may be expressed by a combination of total-body added mass coefficients.

In the general case of a complex motion in the ideal homogeneous fluid all the forces and moments will then be available in terms of added masses and inertias, according to the theories originated by KIRCHOFF [11] and LAMB [12]. In spite of the fact that these forces will be modified by the presence of viscosity in the real fluid, and that new forces will also be generated by the viscous effects, these ideal results should be considered when formulating the mathematical model.

If **U** is the velocity vector of the local fluid element the total kinetic energy is given by $T_L = \frac{\rho}{2} \int U^2 \, d\tau$, or in a potential flow generated by the impulse pressure $\rho\Phi$

$$T_L = -\frac{\rho}{2}\int \Phi \frac{\partial \Phi}{\partial n}\, dS \tag{5.1}$$

The integration is to be extended over the total boundary, i.e. over the wetted surface of the body. Let the potential be written in linearized form as

$$\Phi = \Phi_1 u + \Phi_2 v + \Phi_3 w + \Phi_4 p + \Phi_5 q + \Phi_6 r \tag{5.2}$$

with respect to the six component body velocities u_i. The six coefficients Φ_i then are functions of the body geometry and of the position in relation to the body.

The condition for fluid velocity $-\dfrac{\partial \Phi}{\partial n}$ at the body boundary to equal the body normal velocity may be formulated by use of the directional cosines for the normal in the *Oxyz*-system, whereby

$$2T_L = \sum_{i=1}^{6}\sum_{j=1}^{6} A_{ij}\, u_i u_j \text{—with } A_{ij} = \rho \int \Phi_i \frac{\partial \Phi_j}{\partial n} dS \text{— or}$$

$$\left.\begin{aligned} 2T_L = &-X_{\dot{u}}u^2 - Y_{\dot{v}}v^2 - Z_{\dot{w}}w^2 - 2Y_{\dot{w}}vw - 2X_{\dot{w}}wu - 2X_{\dot{v}}uv \\ &-K_{\dot{p}}p^2 + M_{\dot{q}}q^2 - N_{\dot{r}}r^2 - 2M_{\dot{r}}qr - 2K_{\dot{r}}rp - 2K_{\dot{q}}pq \\ &-2(X_{\dot{p}}u + Y_{\dot{p}}v + Z_{\dot{p}}w)p - 2(X_{\dot{q}}u + Y_{\dot{q}}v + Z_{\dot{q}}w)q \\ &-2(X_{\dot{r}}u + Y_{\dot{r}}v + Z_{\dot{r}}w)r \end{aligned}\right\} \tag{5.3}$$

Here there are 21 different added masses (A_{ij}) or "acceleration derivatives". Force derivatives with respect to a linear acceleration are of dimension M, and moment derivatives with respect to an angular acceleration are of dimension ML^2, as are the mass moments of inertia. Cross coupling derivatives such as $X_{\dot{p}} = -A_{14}$ are of dimension ML.

If the body has a plane of symmetry there remain 12 different acceleration derivatives, and for a body of revolution generated around the x axis there are only the three derivatives A_{11}, A_{22} and A_{66}.

The motion of the ideal liquid takes place in response to the force and moment expended by the moving solid. At any time this motion may be considered to have been generated instantaneously from rest by the application of a certain impuls wrench. The rate of change —cf. eq. (4.5)—of the impulse wrench is equal to the force wrench searched for. Again, the work done by the impulse is equal to the increase of kinetic energy, and as shown by MILNE-THOMSON [13] the force and moment on the body may therefore be expressed in terms of the kinetic energy of the liquid,

$$\left.\begin{aligned}\mathbf{F} &= -\frac{d}{dt}\left(\frac{\partial T_L}{\partial \mathbf{V}}\right) - \boldsymbol{\Omega} \times \frac{\partial T_L}{\partial \mathbf{V}} \\ \mathbf{M} &= -\frac{d}{dt}\left(\frac{\partial T_L}{\partial \boldsymbol{\Omega}}\right) - \boldsymbol{\Omega} \times \frac{\partial T_L}{\partial \boldsymbol{\Omega}} - \mathbf{V} \times \frac{\partial T_L}{\partial \mathbf{V}}\end{aligned}\right\} \tag{5.4}$$

(The partial derivations shall be considered as gradient operators.) The complete formal expressions for the inertia forces in the ideal fluid have been derived from eqs. (5.3) and (5.4) by IMLAY [14], and they are given in eq. (5.5).

$$\left.\begin{aligned}
\bar{X}_{id} &= X_{\dot{u}}\dot{u} + X_{\dot{w}}(\dot{w}+uq) + X_{\dot{q}}\dot{q} + Z_{\dot{w}}wq + Z_{\dot{q}}q^2 + X_{\dot{v}}\dot{v} + X_{\dot{p}}\dot{p} + X_{\dot{r}}\dot{r} \\
&\quad - Y_{\dot{v}}vr - Y_{\dot{p}}rp - Y_{\dot{r}}r^2 - X_{\dot{v}}ur - Y_{\dot{w}}wr + Y_{\dot{w}}vq \\
&\quad + Z_{\dot{p}}pq - (Y_{\dot{q}} - Z_{\dot{r}})qr \\
\bar{Y}_{id} &= X_{\dot{v}}\dot{u} + Y_{\dot{w}}\dot{w} + Y_{\dot{q}}\dot{q} + Y_{\dot{v}}\dot{v} + Y_{\dot{p}}\dot{p} + Y_{\dot{r}}\dot{r} + X_{\dot{v}}vr - Y_{\dot{w}}vp \\
&\quad + X_{\dot{r}}r^2 + (X_{\dot{p}} - Z_{\dot{r}})rp - Z_{\dot{p}}p^2 - X_{\dot{w}}(up - wr) + X_{\dot{u}}ur \\
&\quad - Z_{\dot{w}}wp - Z_{\dot{q}}pq + X_{\dot{q}}qr \\
\bar{Z}_{id} &= X_{\dot{w}}(\dot{u} - wq) + Z_{\dot{w}}\dot{w} + Z_{\dot{q}}\dot{q} - X_{\dot{u}}uq - X_{\dot{q}}q^2 + Y_{\dot{w}}\dot{v} + Z_{\dot{p}}\dot{p} + Z_{\dot{r}}\dot{r} \\
&\quad + Y_{\dot{v}}vp + Y_{\dot{r}}rp + Y_{\dot{p}}p^2 + X_{\dot{v}}up + Y_{\dot{w}}wp - X_{\dot{v}}vq \\
&\quad - (X_{\dot{p}} - Y_{\dot{q}})pq - X_{\dot{r}}qr \\
\bar{K}_{id} &= X_{\dot{p}}\dot{u} + Z_{\dot{p}}\dot{w} + K_{\dot{q}}\dot{q} - X_{\dot{v}}wu + X_{\dot{r}}uq - Y_{\dot{w}}w^2 - (Y_{\dot{q}} - Z_{\dot{r}})wq \\
&\quad + M_{\dot{r}}q^2 + Y_{\dot{p}}\dot{v} + K_{\dot{p}}\dot{p} + K_{\dot{r}}\dot{r} - (Y_{\dot{q}} - Z_{\dot{r}})vr + Z_{\dot{p}}vp \\
&\quad - M_{\dot{r}}r^2 - K_{\dot{q}}rp + X_{\dot{w}}uv - (Y_{\dot{v}} - Z_{\dot{w}})vw - (Y_{\dot{r}} + Z_{\dot{q}})wr \\
&\quad - Y_{\dot{p}}wp - X_{\dot{q}}ur + (Y_{\dot{r}} + Z_{\dot{q}})vq + K_{\dot{r}}pq \\
&\quad - (M_{\dot{q}} - N_{\dot{r}})qr + Y_{\dot{w}}v^2 \\
\bar{M}_{id} &= X_{\dot{q}}(\dot{u} + wq) + Z_{\dot{q}}(\dot{w} - uq) + M_{\dot{q}}\dot{q} - X_{\dot{w}}(u^2 - w^2) - (Z_{\dot{w}} - X_{\dot{u}})wu \\
&\quad + Y_{\dot{q}}\dot{v} + K_{\dot{q}}\dot{p} + M_{\dot{r}}\dot{r} + Y_{\dot{p}}vr - Y_{\dot{r}}vp - K_{\dot{r}}(p^2 - r^2) \\
&\quad + (K_{\dot{p}} - N_{\dot{r}})rp - Y_{\dot{w}}uv + X_{\dot{v}}vw - (X_{\dot{r}} + Z_{\dot{p}})(up - wr) \\
&\quad + (X_{\dot{p}} - Z_{\dot{r}})(wp + ur) - M_{\dot{r}}pq + K_{\dot{q}}qr \\
\bar{N}_{id} &= X_{\dot{r}}\dot{u} + Z_{\dot{r}}\dot{w} + M_{\dot{q}}\dot{q} + X_{\dot{v}}u^2 + Y_{\dot{w}}wu - (X_{\dot{p}} - Y_{\dot{q}})uq - Z_{\dot{p}}wq \\
&\quad - K_{\dot{q}}q^2 + Y_{\dot{r}}\dot{v} + K_{\dot{r}}\dot{p} + N_{\dot{r}}\dot{r} - X_{\dot{v}}v^2 - X_{\dot{r}}vr - (X_{\dot{p}} - Y_{\dot{q}})vp \\
&\quad + M_{\dot{r}}rp + K_{\dot{q}}p^2 - (X_{\dot{u}} - Y_{\dot{v}})uv - X_{\dot{w}}vw + (X_{\dot{q}} + Y_{\dot{p}})up \\
&\quad + Y_{\dot{r}}ur + Z_{\dot{q}}wp - (X_{\dot{q}} + Y_{\dot{p}})vq - (K_{\dot{p}} - M_{\dot{q}})pq - K_{\dot{r}}qr
\end{aligned}\right\} \tag{5.5}$$

Forces in Horizontal Motions—General

Especially, for a body which is symmetrical with respect to its xz-plane and which is moving in the extension of its xy-plane, there are

$$\left.\begin{aligned}
\bar{X}_{id} &= X_{\dot{u}}\dot{u} - Y_{\dot{v}}vr - Y_{\dot{r}}r^2 \\
\bar{Y}_{id} &= Y_{\dot{v}}\dot{v} + X_{\dot{u}}ur + Y_{\dot{r}}\dot{r} \\
\bar{N}_{id} &= N_{\dot{r}}\dot{r} + (Y_{\dot{v}} - X_{\dot{u}})uv + Y_{\dot{r}}(\dot{v} + ur)
\end{aligned}\right\} \quad \left\{\begin{aligned}
&+ X_{\dot{v}}(\dot{v} - ur) + X_{\dot{r}}\dot{r} \\
&+ X_{\dot{v}}(\dot{u} + vr) + X_{\dot{r}}r^2 \\
&+ X_{\dot{v}}(u^2 - v^2) + X_{\dot{r}}(\dot{u} - vr)
\end{aligned}\right\} \tag{5.6}$$

By careful application of sound reasoning it is suggested that terms to the right of the bar may be dropped. Terms containing the coefficient $Y_{\dot{r}}$ have been retained in view of the fore-and-aft unsymmetry present particularly in propelled bodies.

The coefficients for $\dot{u}$ in X, for $\dot{v}$ in Y, and for $\dot{r}$ in N —with signs reversed—are the most commonly well-known added masses and added moment of inertia respectively. These inertia coefficients also appear in some of the cross-coupling terms.

LAMB's "coefficients of accession to inertia" relate added masses to the mass of the displaced volume ∇ (k_{ii}, $i=1, 2, 3$) and added moments of inertia to the proper moments of inertia of the same displaced volume (k'_{ii}, $i=4, 5, 6$). LAMB calculated k_{11}, $k_{22}=k_{33}$ and $k'_{55}=k'_{66}$ for the sphereoid of any length-to-diameter ratio, [15]. For ellipsoids with three unequal axes the six different coefficients were derived by GUREWITSCH and RIEMANN; convenient graphs are included in ref. [16]. For elongated bodies in general the total added inertias may be calculated from knowledge of two-dimensional section values by strip methods, applying the concept of an equivalent ellipsoid in correcting for three-dimensional end effects. (See further below.)

Of special interest in eq. (5.6) is the coefficient $Y_{\dot{v}}-X_{\dot{u}}$ in the "MUNK moment", [17]. (See also discussion in [18].) This free broaching moment in the stationary oblique translation within an ideal fluid defines the derivatives

$$N''_{uv}=-\frac{k_{22}-k_{11}}{\mu};\quad N'_{\beta}=\frac{2\nabla}{L^3}\,(k_{22}-k_{11}) \tag{5.7}$$

(Cf. Table I.) The factor $k_{22}-k_{11}$ may be looked upon as a three-dimensional correction factor.

Due to energy losses in the viscous flow of a real fluid past a submerged body the potential flow picture breaks down in the afterbody. In oblique motion there appears a stabilizing viscous side force. So far no theory is available for the calculation of this force, but semi-empirical formulas give reasonable results for conventional bodies of revolution. Force measurements on a divided double-body model of a cargo ship form have demonstrated that some de-stabilizing force is still carried on the afterbody but that most of the moment is due to the side force on the forebody, predictable from low-aspect-ratio wing or slender body theories, [18].

Similar measurements on a divided body in a rotating arm shall be encouraged. Contrary to the case of stationary pure translation the pure rotation in an ideal fluid involves non-zero axial and lateral forces. From eq. (5.6) the side force is given by $X_{\dot{u}}ur$, whereas the moment here is $Y_{\dot{r}}ur$. For bodies of revolution the distribution of the lateral force may be calculated as shown by MUNK [17] whereas strip theory and two-dimensional added mass values may be used for other forms. The magnitude of ideal side force as well as moment are small, however, and in a real fluid the viscous effects are dominating.

There are reasons to believe that the main results of the theories for the deeply submerged body will also apply to the case of a surface ship moving in response to control actions at low or moderate forward speeds. Potential flow contribution to damping as well as inertia forces depend on the added mass characteristics of the transverse sections of the hull, and as long as these characteristics are not seriously affected by the presence of the free surface the previous statement comes true. However, an elongated body performing lateral oscillations of finite frequencies will generate a standing wave system close to the body as well as progressive waves, by which energy is dissipated. The hydrodynamic characteristics then are no longer functions of the geometry only. At a higher speed or in a seaway displacement and wave interference effects will further violate the simple image conditions.

6. Calculations and Estimates of Hull Forces

On Added Mass in Sway and Added Inertia in Yaw

A brief review will here be given of the efforts made to calculate the added mass and inertia of surface ships in lateral motions. Four facts will be in support of this approach: The added masses are mainly free from viscous effects; the added masses appear together with rigid body masses in the equations of motions, and relative errors are reduced—this is especially true in the analytical expression for the dynamic stability lever, which involves only the small $X_{\dot{u}}$; the added masses are experimentally available only by use of non-stationary testing techniques, and in many places experimental data must therefore be supplemented with calculated values; the added masses are no unique functions of geometry only, and experiments must be designed to supply the values pertinent to the problems faced.

The velocity potential for the two-dimensional flow past a section of a slender body must satisfy the normal velocity condition at the contour boundary as well as the kinematical condition for the relative depression velocity at the free constant-pressure surface. In case of horizontal as well as vertical oscillations this latter linearized condition is $\omega^2+g\frac{\partial\Phi}{\partial z}=0$—cf. LAMB [12]—or, introducing the non-dimensional potential $\Phi''=\Phi/L\sqrt{gL}$ and $\omega''=\omega\sqrt{\frac{L}{g}}$,

$$\frac{\partial\Phi''}{\partial z''}=-\omega''^2\cdot\Phi'' \tag{6.1}$$

For a steady horizontal drift at moderate forward speeds one finds a similar condition

$$\frac{\partial\Phi''}{\partial z''}=\beta^2\cdot F_{nL}{}^2\cdot\frac{\partial^2\Phi''}{\partial y''^2} \tag{6.2}$$

which shall govern the local accelerations of the flow in the transverse plane penetrated by the moving body [18].

As is seen from the two equations above the vertical velocities at the water surface are zero in the limit of zero frequency or zero drift, and negligible for $\omega\ll\sqrt{\frac{g}{L}}$ or $\beta^2F_{nL}{}^2\ll 1$. The water surface may therefore be treated as a rigid wall, in which the underwater hull and streamlines are mirrored, i.e. the image moves in phase with the hull.

For high frequencies, where $\omega\gg\sqrt{\frac{g}{L}}$, the condition at the free surface is $\Phi=0$. The water particles move up and down normal to the surface, but no progressive waves are radiated. At the juncture of the horizontally oscillating submerged section contour and the free surface this condition may be realized by the added effect of an image contour, which moves in opposite phase. (Cf. WEINBLUM, [19].) The value of added mass in this case, "neglecting gravity", is smaller than the deeply submerged value by an amount equal to twice the image effect.

Added masses A_H' for two-dimensional forms oscillating laterally with very low frequencies in a free surface have been calculated by

GRIM [20] and by LANDWEBER and MACAGNO [21], using a LAURENT series with odd terms to transform the exterior of a symmetric contour into the exterior of a circle (THEODORSEN mapping). By retaining the first three terms this transformation yields the well-known two-parameter LEWIS forms, [22]; other combinations of three terms have been studied by PROHASKA in connection with the vertical vibrations of ships, [23]. Two terms (and one single selectable parameter for the excentricity) define the semi-elliptic contour as that special case with given draught, for which the added mass is a minimum. LANDWEBER and MACAGNO also made calculations of the added masses A_H in the high-frequency case. For the semi-elliptic contour $A_H/A_H' = \frac{4}{\pi^2}$, which result was first found by LOCKWOOD-TAYLOR, [24].

A basic theory for the dependence of the hydrodynamic forces on finite frequencies was developed for the semi-submerged circular cylinder by URSELL, [25]. By use of a special set of non-orthogonal harmonic polynomials he found the velocity potential and stream function that satisfied the boundary conditions and represented a diverging wave train at infinity. Based upon similar principles TASAI extended the calculations of added masses (and damping forces) for two-dimensional LEWIS forms to include the total practical range of swaying frequencies, [26]. His results are condensed in a number of convenient tables and diagrams; the added mass values are seen to vary even outside the limit values corresponding to zero and infinite frequencies.

An application of a generalized mapping function technique to ship section forms of arbitrary shape was performed by PORTER, who studied the pressure distribution and forces on heaving cylinders, [27]. A way of solving the two-dimensional problem without resort to conformal mapping was developed by FRANK, who represented the velocity potential by a distribution of wave sources over the submerged part of the contour, now defined by a finite number of off-sets. The varying source strength was determined from an integral equation based on the kinematical boundary condition, [28].

VUGTS [29] contributed an extensive experimental and theoretical study of the hydrodynamic coefficients for pure and coupled swaying, heaving and rolling cylinders, based on the previous works by URSELL, PORTER and DE JONG, [30]. The coefficients of the THEODORSEN mapping function were defined by a least square fit of the geometry of the cylinder contours to off-sets in 31 points. Of special interest is

the good agreement obtained between experiments and theoretical predictions for the added mass of a typical midship section; the oscillation experiments do not cover the very low frequencies, however. Although small the difference in the calculations for the actual section fit and for an approximate LEWIS form was mainly confirmed by the experiments.

When used with the strip method the integrated section contributions to total added mass and inertia shall be reduced by the appropriate "longitudinal inertia factors" for three-dimensional effects. Following LEWIS these factors are usually taken equal to those derived for the prolate sphereoid in a similar mode of motion. This is only an engineering artifice, and it is certainly not correct, say, in case of accelerations in yaw for normal hull forms; thus these correction factors are mostly omitted in hydrodynamic studies of sufficiently slender bodies.

In a discussion of the strip theory TUCK [31] included the results of all the added mass and damping coefficients of a surface ship at zero forward speed, calculated by use of FRANK's close-fit method with 15 off-sets for each of 23 stations. The total added mass (A^0_{22}) and moment of inertia (A^0_{66}) of a *Series* 60 *Block* .70 form are here represented by full lines in Fig. 8. TUCK also examined the forward speed corrections to be applied to the integrated values; thus, especially, he put $A_{66}=A^0_{66}+\frac{U^2}{\omega^2}\cdot A^0_{22}$, or in present notation

$$N''_{\dot{r}}(u'', \omega'')=N''_{\dot{r}}(\omega'')_{u''=0}+\frac{u''^2}{\omega''^2}\cdot Y''_{\dot{v}}(\omega'')_{u''=0} \tag{6.3}$$

(Note that the strip theory is not valid for small "reduced frequencies" $\omega'=\omega''/u''$, where it shall be replaced by a slender body theory, [31].) The dotted curves in the diagrams indicate predictions for $F_{nL}=u''=0.20$.

The *Series* 60 *Block* .70 form was subject to oscillator experiments in lateral modes at several frequencies and forward speeds by VAN LEEUWEN [32]. The results for the naked hull with rudder at $F_{nL}=0.20$ are compared with the predictions from strip theory in Fig. 8. The experimental values fall well below these predictions in the entire range of frequencies, especially in case of the moments in yaw. Although it is inherent in the testing technique that very low frequencies could not be included VAN LEEUWENS results do cover the critical range around $\omega''\cdot u''=\frac{1}{4}$.

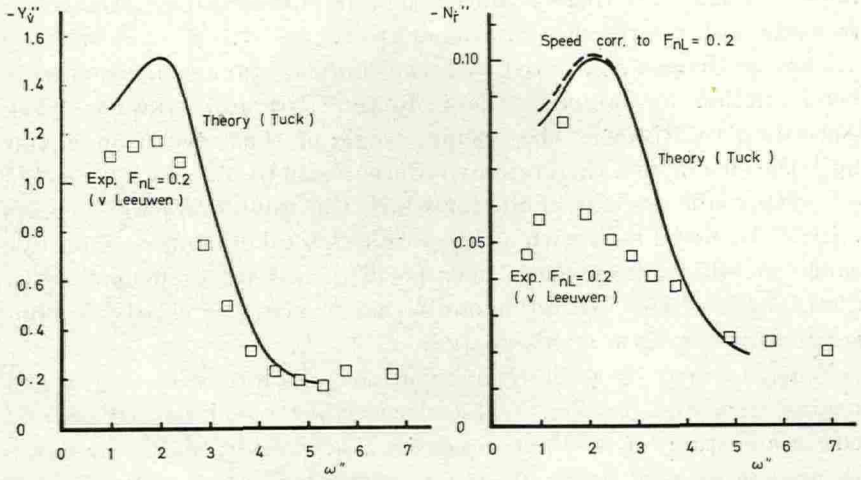

Fig. 8. Total added mass and added moment of inertia for a Series 60 Block .70 form according to theory and experiments.

Consider a surface body in steady motion along the centreline between two parallel walls width W apart; the diverging bow wave displays an angle to the centreline. If the motion is steady the reflected wave will pass aft of the body only if $\frac{W}{L} > \tan \beta$, regardless of the speed. For the simple travelling pressure point the cusp line angle is equal to 19°47 according to the KELVIN theory, whereas slightly different values may be observed for real ship forms. In case the body is oscillating at rest (as in the simple example may be illustrated by a pulsating source) radiating waves propagate in concentric circles at the speed $\frac{g}{\omega}$. In the general case a rather complicated wave system is generated around the moving body, characterized by the velocity ratio $\gamma = u : \frac{g}{\omega} = u''\omega''$. A typical value for γ, using the exiting frequency on a ship in a head sea, may be $\gamma = 0.8$, say, in which case the ship wave pattern at a distance from the ship is not yet very different from that of a non-oscillating ship. If the oscillating frequency of a body (model) moving in calm water is progressively reduced the radiated waves move faster, the diverging wave front

folds forward, and there is now a new requirement on basin width to avoid wall interference in a model test.

The phenomena associated with the complex wave generation have been studied by, among others, BRARD [33] and NEWMAN [34]. According to NEWMAN the opening angle of the wave front equals 90° at $\gamma=0.272$, and then rapidly reduces again to 55° as γ approaches $\gamma=\frac{1}{4}$; this is a singular point, for which the wave damping becomes critical. In model tests with a ship form in lateral oscillations a narrow range of critical frequencies may be identified by a change of the distribution of the hydrodynamic forces, which was clearly demonstrated by VAN LEEUWEN's analysis.

Whereas there is a discrepancy in the absolute values of added masses compared in Fig. 8 this discrepancy could be reduced by the application of a three-dimensional corrector; more elaborate theories of forward speed effects for slender bodies at low frequencies may further improve the comparison. In the main, therefore, it may be stated that the variation of added mass with frequency is well documented.

Added Masses in Manoeuvring Applications

The performance problems set up in manoeuvring studies usually involve a short-time prediction of a transient response to a control action, and it is therefore convenient to be in the position to use ordinary non-linear differential equations with constant coefficients. This, of course, is in contrast to the linearized spectrum approach to the statistical sea-keeping problem, which will more readily accept frequency-dependent coefficients. (Frequency- or time-dependence as a result of viscous phenomena will be touched upon below.) Which values of added mass are now to be used in the equations for the manoeuvring ship? It shall be noted that it is hard to judge from the behaviour of a free-sailing ship or ship model which is the correct answer unless special motions are carefully examined.

It was early suggested by WEINBLUM that the low added mass values of the high-frequency approximation should be adequate for use in dealing with problems of directional stability, where starting conditions should simulate impulsive motion, [19]. WEINBLUM also drew attention to ref. [35], in which HAVELOCK proved that the high-frequency values appeared in horizontal translations with uniform acceleration, regardless of the initial velocity.

The impulsive pressures experienced on the tapered bow and stern portions of a slender body in oblique translation may be calculated from the sectional area curve slope and the added mass characteristics of the transverse sections, as shown by MUNK [17] and experimentally veryfied for the submerged double-body ship form in ref. [18]. The good agreement obtained between total yawing moments measured on this form and its surface ship geosim suggests that the deeply submerged added mass values should apply in this case. It is observed, however, that the water particles in way of a certain section station here are not repeatedly accelerated from rest as is the case when considering the cylindrical part of the hull. Again, if the principle of superposition of damping and inertia components to the total hydrodynamic force shall be retained for general motions it shall be necessary to adopt the zero-frequency added mass values.

An illustrative discussion of added masses with special application to the design and analysis of experiments is due to MOTORA in ref. [36]. For the determination of the added mass in sway to be used in the aperiodic equations of a manoeuvring ship he recorded the direction of the acceleration imparted to a model by a force suddenly applied in a certain direction. The added mass then could be found from a reasonable estimate of virtual mass in surge. To obtain the added moment of inertia in yaw he recorded the angular acceleration following the impact by a pendulum, the momentum loss of which was also known. He suggested that the inertia values so derived should correspond to the impact or high-frequency type, but the results included from tests with a series of ship models indicate sway mass values of the same order as those valid for the deeply submerged case, and moments of inertia in yaw of magnitudes corresponding to finite frequency surface values.

In a recent paper MOTORA and co-authors [37] compare the results of new experiments and calculations of an "equivalent" added mass for a ship model in a sway motion, which is initiated by a ramp- or step-form impact input of finite duration. The calculations are based on TASAI's section values in the frequency domain, [26], and in agreement with the experiments they confirm that the value of the equivalent added mass defined is a function of impact duration. (Cf. Fig. 9.) If the duration is infinitely small only the equivalent added mass is equal to its high-frequency value, and it becomes larger the longer the duration. Thus these results help to explain the earlier findings for added masses as well as for added moments of inertia,

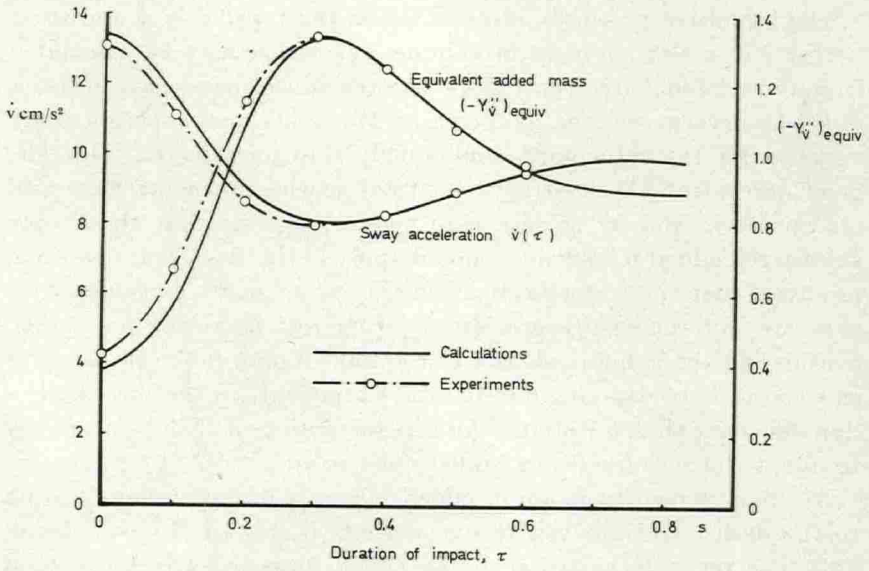

Fig. 9. MOTORA's equivalent added mass coefficient as defined by acceleration due to step input impact of duration τ.

for which latter the impact technique then used did generate rather short input impulses.

For application to normal ship manoeuvres it may now seem justified to use the low-frequency or deeply submerged values.

In recent years it has been widely accepted that the acceleration derivatives for a surface ship model may be evaluated from a set of "planar-motion-mechanism" tests in pure sway or yaw. The acceleration amplitudes are varied by an adjustment of oscillator amplitudes, whereas the frequency is kept as low as running length permits, [32]. A typical reduced frequency $\omega' = \omega \cdot \frac{L}{V}$ will be of order 0.5, corresponding to $\omega'' = \frac{\gamma}{u''} = \omega' \cdot u'' = 0.1$ in Fig. 8. The derivatives so obtained may be expected to be somewhat higher than the zero-frequency values.

The theoretical zero-frequency added mass values for two-dimensional LEWIS forms as well as for semi-submerged ellipsoids of finite lengths indicate the main dependence on principal geometrical characteristics. Especially, for very large length-to-draught ratios the

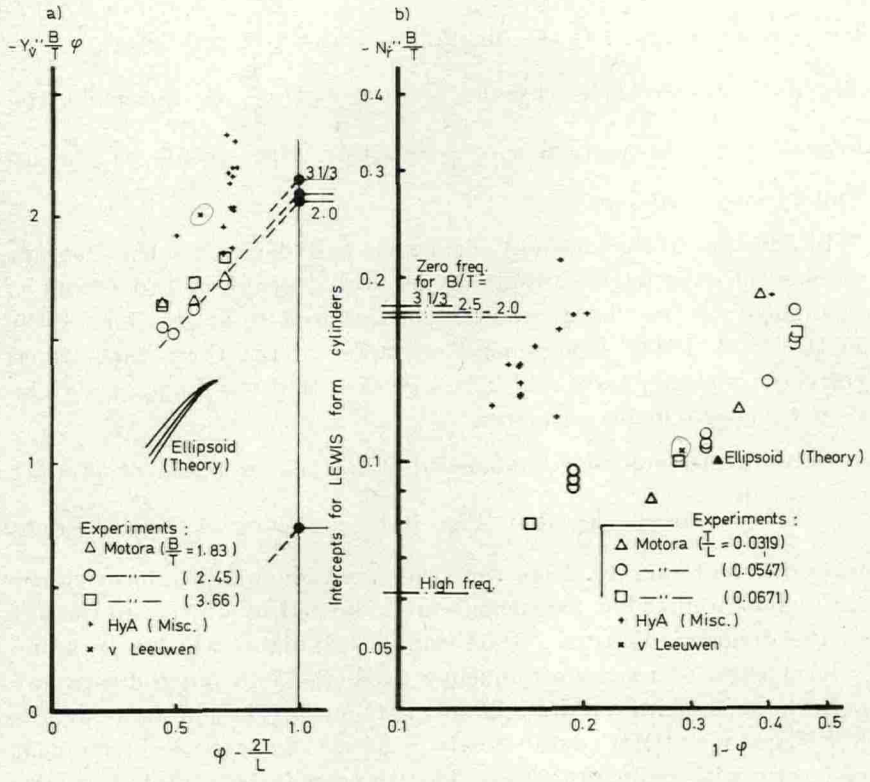

Fig. 10. Non-dimensional added mass (a) and added moment of inertia (b) from theory and experiments.

ellipsoid values tend to those of a semi-elliptic cylinder, $\frac{\pi}{2} \rho T^2$, so that $-Y_v'' = \frac{T}{B}$. Moreover, it will be seen from [21] that for LEWIS forms in general $-Y_v''$ likewise is rather close to $\frac{T}{B}$ for fullness coefficients corresponding to midship sections.

The ellipsoid family has a constant prismatic coefficient $\varphi = \frac{2}{3}$. The correction for finite length involves a slight dependence on $\frac{B}{T}$, as may be seen from Fig. 10. In a more general case this correction will

also depend on φ and on lateral profile, etc. For the inclusion of ship form values in Fig. 10a the diagram is drawn to a base of $\varphi - \frac{2T}{L}$. The ordinates are given by the product $-Y''_{\dot{v}} \frac{B}{T} \varphi$, by which the intercepts on the vertical $\varphi - \frac{2T}{L} = 1$ then corresponds to the infinitely long cylinders.

In addition to the ellipsoid and LEWIS cylinder values the diagram include the experimental results by MOTORA just referred to as well as a number of oscillator results, chiefly from tests run for SSPA in the HyA PMM. The general character of the three-dimensional corrector is clearly seen, and it is suggested that the diagram may be used for approximate estimates.

Non-dimensional added moments of inertia, in terms of product $-N''_{\dot{r}} \frac{B}{T}$, are displayed in Fig. 10 b, compiling experiment data from different sources. Here the two-dimensional LEWIS-form values for high as well as low frequencies are indicated by off-sets to the left in the diagram. MOTORA's 1960 impact test data, which appear on a level close to the high-frequency prediction, do not indicate any definite dependence on draught-to-length ratio. These data as well as low-frequency PMM data clearly indicate an increase of moment of inertia with reduced fullness. This trend may be expected in view of the deep and narrow bow and stern sections in fine forms—certainly the deeply-submerged ellipsoid is not representative for a ship form in yaw acceleration.

Semi-Empirical Relations for the Four Basic Stability Derivatives

Among the large number of first-order force and moment derivatives, that are used to describe the linearized hydrodynamics of the moving hull, only four appear in the analytical criterion for inherent dynamic stability with fixed controls. These are the stability derivatives proper, Y_{uv}, N_{uv}, Y_{ur} and N_{ur}. From simple analogy with the zero-aspect-ratio wing theory of JONES [38] they turn out as in Table II.

Table II.

Non-dim. system:		"*Prime*"			"*Bis*"	
Ref. area:		LT	L^2		$2\nabla/L$	
Symbol and analogy value:	$Y'_v = -Y'_\beta$	$-\frac{\pi}{2}\cdot\frac{2T}{L}$	$-\pi\cdot\left(\frac{T}{L}\right)^2$	Y''_{uv}	$-\frac{\pi}{2}\cdot\frac{LT^2}{\nabla}$
	$N'_v = -N'_\beta$	$-\frac{\pi}{4}\cdot\frac{2T}{L}$	$-\frac{\pi}{2}\cdot\left(\frac{T}{L}\right)^2$	N''_{uv}	$-\frac{\pi}{4}\cdot\frac{LT^2}{\nabla}$
	Y'_r	$\frac{\pi}{4}\cdot\frac{2T}{L}$	$\frac{\pi}{2}\cdot\left(\frac{T}{L}\right)^2$	Y''_{ur}	$\frac{\pi}{4}\cdot\frac{LT^2}{\nabla}$
	N'_r	$-\frac{\pi}{8}\cdot\frac{2T}{L}$	$-\frac{\pi}{4}\cdot\left(\frac{T}{L}\right)^2$	N''_{ur}	$-\frac{\pi}{8}\cdot\frac{LT^2}{\nabla}$

Remembering that Y'_v is made non-dimensional by use of the instantaneous velocity V it shall be observed that, strictly,

$$Y''_{uv} = \frac{L^3}{2\nabla}\,(Y'_v + Y'_{uv}) \tag{6.4}$$

where the conversion factor relates to the *prime-L^2*-alternative. Similar expressions are valid for the other derivatives. In most cases Y'_{uv} has been taken equal to zero, which makes the conversion to the new system especially simple. (The forward-speed-dependence of Y''_{uv} will be considered below.)

Although this wing analogy has been verified in principle for a submerged double-body model as well as for the surface model at small FROUDE numbers, [18], it shall not be expected to furnish an adequate numerical prediction. It suffices to point to the alternative relation for a closed body in a perfect fluid, given by eq. (5.7), and to the fact that at least some negative lift is still carried on the run of a normal ship-form hull. The bow lift or transverse force is not concentrated to the leading edge as in case of a rectangular wing but distributed over the fore-body as an effect of fullness and section shape. Certain modifications to the hull form are known to affect the force derivatives, but do not appear in the simple form parameters of Table II. The fin effect of screw and rudder contributes to the derivatives even in the case of vanishing aspect ratio of the hull.

From the analysis of a large number of derivatives it has been found that the scatter of data in a plot of, say, Y''_{uv} versus the parameter $\frac{LT^2}{\nabla}$ is somewhat smaller than the scatter of Y'_v on base of aspect ratio $\frac{2T}{L}$.

The diagrams Figs. 11–12 include stability derivative data for normal ship form models with normal-sized rudders propelled at medium FROUDE numbers on even keels. The dotted lines shown correspond to the simple wing analogy. The full lines are derived by linear regression and upon the tentative assumption of a $-1:2$ relation of moment and force intercepts at zero aspect ratio. Their equations are given as

$$\left.\begin{aligned} Y''_{uv} &= -2.66\,\frac{LT^2}{\nabla} - 0.04 = -1.69 \cdot \frac{\pi}{2} \cdot \frac{LT^2}{\nabla} - 0.04 \\ N''_{uv} &= -1.01\,\frac{LT^2}{\nabla} + 0.02 = -1.28 \cdot \frac{\pi}{4} \cdot \frac{LT^2}{\nabla} + 0.02 \\ Y''_{ur} &= \;\;1.02\,\frac{LT^2}{\nabla} - 0.18 = \;\;1.29 \cdot \frac{\pi}{4} \cdot \frac{LT^2}{\nabla} - 0.18 \\ N''_{ur} &= -0.74\,\frac{LT^2}{\nabla} + 0.09 = -1.88 \cdot \frac{\pi}{8} \cdot \frac{LT^2}{\nabla} + 0.09 \end{aligned}\right\} \qquad (6.5)$$

and of the data 100, 86, 67 and 79 per cent, respectively, appear within ± 20 per cent of these mean values.

Simultaneously to the original presentation of these diagrams SMITT independently published similar diagrams of the *prime*-form stability derivatives, using zero intercepts, [39].

It must be borne in mind that the data in Figs. 11–12 as well as those of ref. [39] are obtained from cubic fits to the experimental force measurements, whereas the mathematical model here put forth makes use of square fits to the same non-linear relations. (Cf. below.) As a matter of fact this latter procedure furnishes linear derivatives, which are closer to the prediction from the simple wing analogy.

It is obvious that these expressions should be regarded as guide values only, but they may also be used for comparative studies, especially when steering on a straight course is of main concern. In this latter case it is more important to have a proper knowledge of

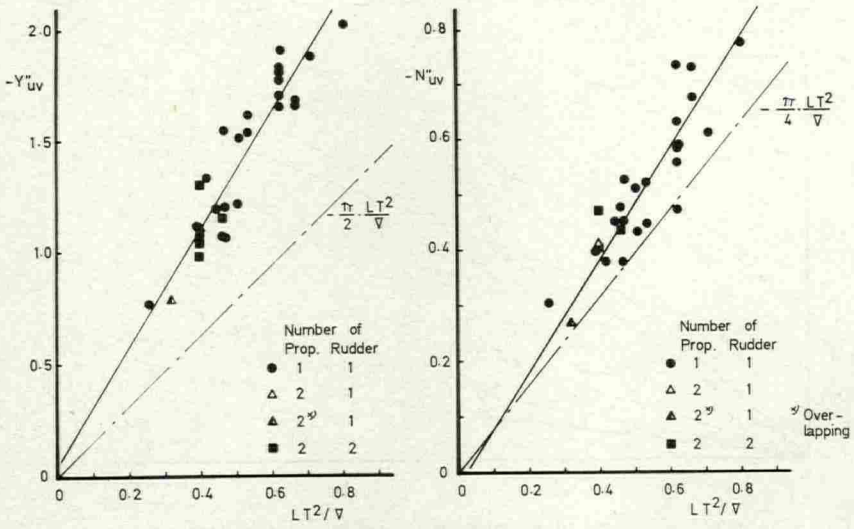

Fig. 11. Stiffness force and moment derivative data with mean regression line.

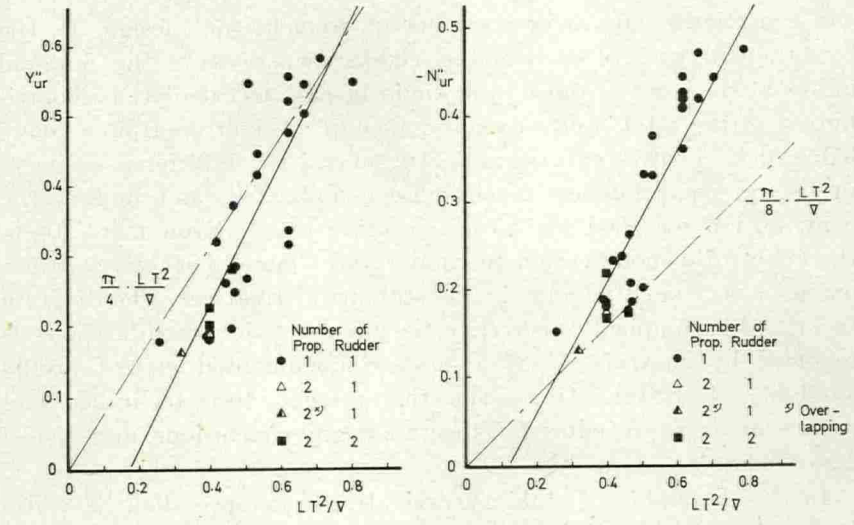

Fig. 12. Rotary force and moment derivative data with mean regression line.

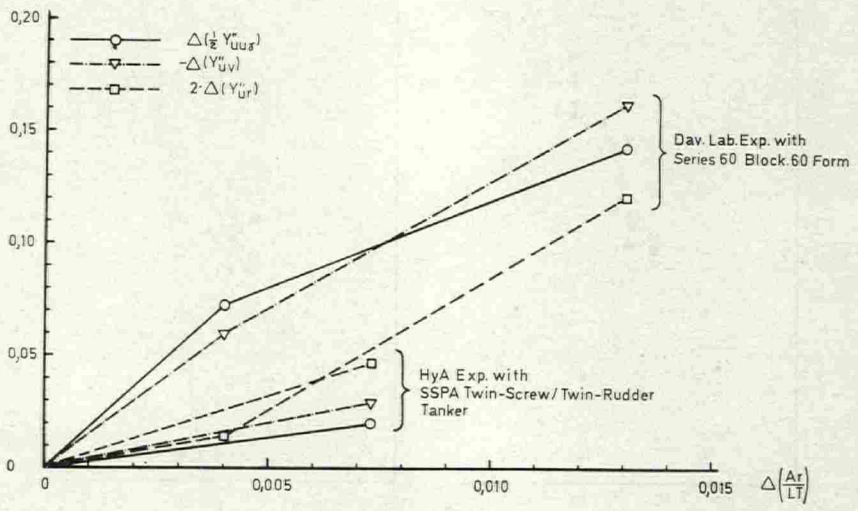

Fig. 13. Change of control force derivatives and total force derivatives in sway and yaw with change of relative size of rudder.

the control derivatives, whereas eq. (6.5) may furnish adequate estimates for the hull forces; they again shall be corrected for alternative control arrangement alternatives, however.

In the next Section an approximate method will be given for finding the control derivatives of a rudder of conventional design. In the hypothetical case of an isolated rudder experiencing the nominal inflow at the stern of the ship it would be easy to calculate its contribution to the total "hull+rudder amidship" derivatives from a knowledge of its control effectiveness. In general the interference effects in behind condition are much more complicated, and in fact the contribution searched for mostly is quite small. Even more, then, the effect of a modification to rudder and control derivatives comes out as a very small change in the stability derivatives. The diagram in Fig. 13 is compiled to correlate the effects of such modifications as reported by EDA and CRANE [40] and documented in test results available at SSPA. Obviously the present test technique and routine analysis procedure fail to support any conclusions, and special experiments are required.

In the discussion of stability derivatives reference shall here also be given to the methods of estimating these derivatives for surface ships suggested and successfully tested by JACOBS, [41].

The aerodynamic wing analogy should only be valid for small FROUDE numbers as the limit solution of a general lifting surface integral equation. The effects of finite FROUDE numbers on the lateral stability derivatives of a thin ship of small draught-to-length ratio were studied by HU, [42]. According to HU the force and moment derivatives at $F_{nL}=0.1$ are increased by some 20 per cent above their zero-speed values, an increase which is not fully realized in model tests. A comparison of the results of this theory with various experiments—including those of ref. [18]—is presented by NEWMAN [43]. NEWMAN also points out that the free surface may give rise to a steady side force as a thickness effect, and indicates a solution to that problem.

From an inspection of the experimental results for the drift moment, which are the more consistent, a first approximation to the speed dependence is given by

$$(N''_{uv})_{u''}=(N''_{uv})_0+\tfrac{1}{2}\,N''_{uuv}u'' \tag{6.6}$$

where $\frac{1}{2}\,N''_{uuv}\approx 1.3(N''_{uv})_0$. This suggests that the zero-speed values will be some 20 per cent lower than those indicated by the mean line of Fig. 11.

Viscous Frequency Effects and Small-Value Non-Linearities in Lateral Forces

In dealing with the free-surface effects on added masses it was concluded that so far the frequencies involved in manoeuvring motions were to be regarded as low, but that frequency (or memory) effects should be expected to appear in time histories were viscous phenomena were of more concern.

The extreme exemplification is furnished by the pitching submarine, the stern planes of which are operating in the down-wash behind the bow planes, but in case of submarines as well as normal surface ships also the very stern portion of the hull is exposed to velocities induced by vortices trailing from upstream hull and appendages. Moreover, local separation within the three-dimensional boundary layer flow over the stern directly affects the cross-flow momentum and the impulsive pressures. The forces and moments experienced by the hull in transient motions can then only be calculated by use of convolution integrals over the entire time history, such as derived by BRARD in case of a special descriptive model, [44].

For application to the mathematical model defined by ordinary differential equations it is again still possible to use frequency dependent coefficients, but unfortunately this frequency dependence is likely to be subjected to scale effects. It is therefore advisable to design experiments for STROUHAL numbers or reduced frequencies, which are low enough to produce steady-state values. From a summary of published data in ref. [43] the limiting frequency will be expected to be somewhere in the region $1<\omega'<4$. From a more recent analysis of sinusoidal free-sailing tanker model data NOMOTO suggests that this limiting frequency is approached already at $\omega' \approx 0.5$, [45]. This indicates that the high-frequency part of a normal ship steering transfer function is obscured by the viscous frequency dependence. (Cf. Section 8.)

The steady motion of a full form may also be accompanied by a non-steady separation and shedding of vortices, which will violate captive measurements, or it will modify the force field and be a cause of unpredictable scale effects. In ref. [46] NOMOTO drew the attention to an "unusual" kind of separation, which had been observed not on the leeward but on the outer side of the afterbodies of turning models. (Later on he reported the same phenomenon taking place on full scale ships with high block coefficients and low length-to-beam ratios.) This separation may be responsible for an almost constant increase in yaw damping moment—see diagram in Fig. 14 a—and so indirectly for the small-rate non-linearity displayed in the yaw-rate-versus-helm diagram from spiral tests with these hulls.

Unsymmetrical separation may also take place on a hull moving along a straight line with a small angle of drift. If transverse force and moment both are mainly linear functions of angle of drift the centre of pressure will remain in a forward position, only gradually moving aft with onset of viscous cross-flow. A three-dimensional separation, which suddenly develops on one side of the hull, may explain the strange behaviour of the centre-of-pressure curve of a tanker model tested by BOTTOMLEY [47], here reproduced in Fig. 14 b. New tests with modern hulls sometimes indicate similar trends.

It is fully possible to approximate these effects by a small-value non-linearity term in the mathematical model, which may then be used, say, for the prediction of a ship behaviour which is extremely sensitive to winds of varying directions, [48]; if the separation is peculiar to the model only, this prediction is meaningless, however.

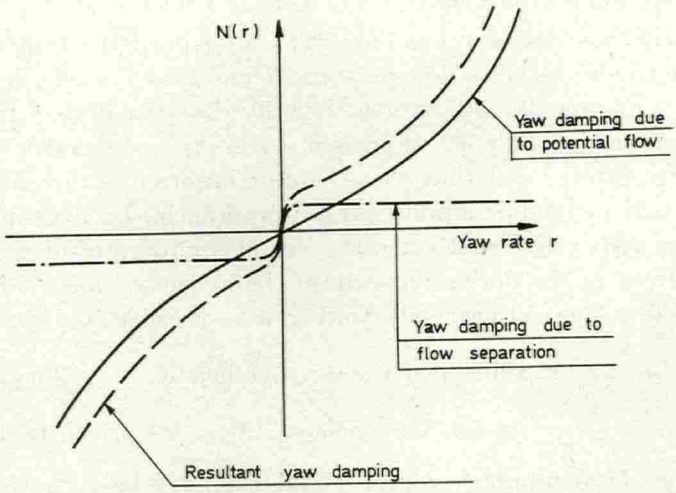

a) Nomoto's explanation of effect of 3-dim. stern flow separation (Above)

b) Lateral force centre of pressure acc. to measurements by Baker and Bottomley (Below)

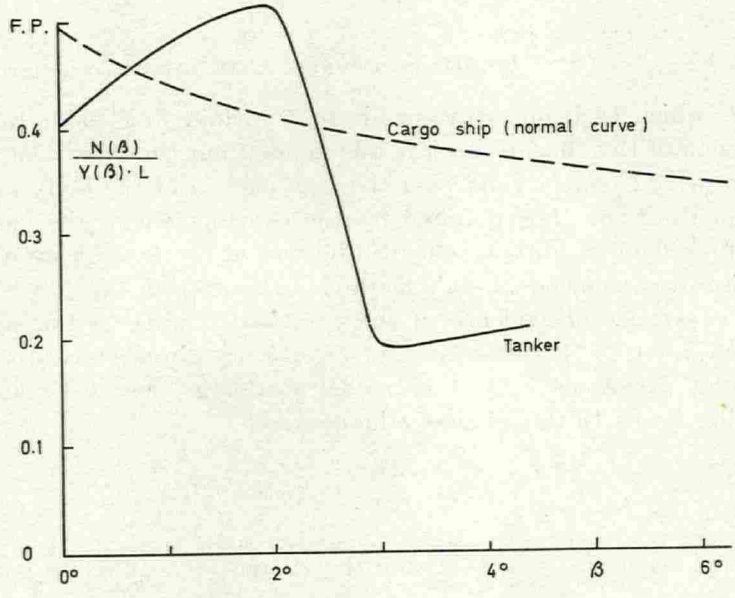

Fig. 14. Small-value non-linearities in full form model testing.

Large-Value Non-Linearities in Lateral Forces

The predominant non-linearities present in the lateral forces are due to viscous cross-flow resistances, and they can only be established by experimental procedures. It will be assumed that the empirical relationships may be expressed by finite polynomials, derived by curve-fitting, and that these same relationships therefore also may be fully defined by a finite number of terms in the TAYLOR expansions. This convention motivates the use of appropriate numerical factors in front of the derivatives within the hydrodynamic coefficients.

From pure athwartship towing it is possible to define an Y-force $-C_D \cdot LT \cdot v^2$, the sign of which is governed by $\frac{|v|}{v}$. Thus $Y(v^2, \frac{|v|}{v}) = \frac{1}{2} Y_{vv} \frac{|v|}{v} \cdot v^2 \frac{|v|}{v}$, or, for convenience, $\frac{1}{2} Y_{|v|v} |v|v$. Note that the factor $\frac{1}{2}$ has been retained, which should not have been the case if v and $|v|$ had been treated as independent variables; this, however, would only have been a formal artifice with no physical significance.

In straight-line oblique motion the non-dimensional lateral force is $Y''(u'', v'', v''^2, \frac{|v''|}{v''})$, or, in accepted writing,

$$Y''(u'', v'') = Y''_{uv} u'' v'' + \tfrac{1}{2} Y''_{|v|v} |v''| v'' \tag{6.7}$$

where $\frac{1}{2} Y''_{|v|v} = -C_D \cdot \frac{L^2 T}{2\nabla}$. It is obvious that here two terms are added, which each one corresponds to a certain flow field. In the discussion of the "linear" term it was pointed out that the ideal flow picture would remain valid over the bow portion of the hull, and in view of the finite time required for the development of the viscous cross-flow these conditions may still be true at larger angles of drift. See also discussion on INOUE's methods in Section 9.

An experimental evidence of the practical validity of the superposition in eq. (6.7) is illustrated in Fig. 15, based on force measurements at SSPA on a 3.55 m model of a cargo liner with rudder and bilge keels. In this diagram the quotient

$$Y / \frac{\rho}{2} V^2 LT = \frac{2\nabla}{L^2 T} \; Y'' / (u''^2 + v''^2)$$

is plotted versus $\beta = -\tan^{-1} \frac{v}{u}$, and the viscous cross-flow component is seen to dominate the entire range of $10° < \beta < 90°$.

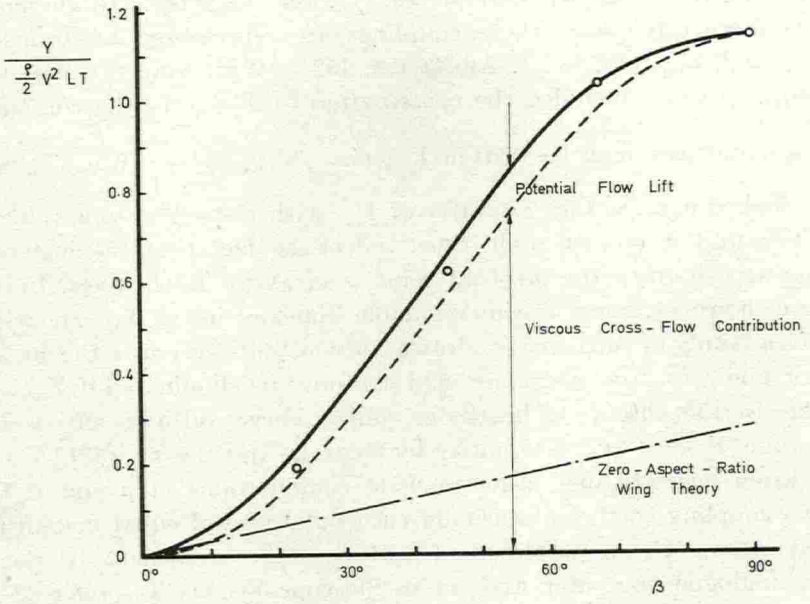

Fig. 15. Calculated and measured lateral forces on a cargo liner model in oblique towing.

The variation of cross-flow drag coefficients with drifting speed and hull geometry has also been discussed in several papers by THIEME and by other authors, [49, 50, 51]. In lack of experimental results for a special case in the non-linear range it shall be possible to use these results; a typical value of cross-flow drag of a tanker form is $C_D=0.7$. The contribution of cross-flow drag to moment-due-to-sway may then be ignored.

In a similar way it is possible to approximate the non-linear rotary derivatives. If $c_D(>C_D)$ is the mean section drag coefficient the moment-due-to-yaw derivative is $\frac{1}{2}N''_{|r|r} = -\frac{c_D}{32} \cdot \frac{L^2T}{2\nabla}$, except for a three-dimensional correction factor. (For rough estimates $\frac{1}{2}N''_{|r|r} = 0.03 \cdot \frac{1}{2}Y''_{|v|v}$, which is verified from experiments.) The force-yaw velocity derivative now is zero to this approximation. Additional effects of skegs and screws contribute to non-zero values of $\frac{1}{2}N''_{|v|v}$ as well as $\frac{1}{2}Y''_{|r|r}$.

In the general case the local cross-flow resistance is proportional to $|v+xr|(v+xr)$, and from symmetry relations the coupling terms

are seen to include the derivatives $Y_{|v|r}$ and $Y_{|v|r}$, etc. (In the cubic fits more often used these couplings are represented by terms in Y_{vvr} and Y_{vrr}, etc. — cf. ABKOWITZ, [52].) With only the first two coupling terms included the contribution to Y due to the combined sway and yaw may be written $Y_{|v|r}|v|v\,\frac{r}{v} + Y_{v|r|}|r|r\,\frac{v}{r}$, i. e. $Y_{|v|r}$ may be looked upon as the derivative of $Y_{|v|r}$ with respect to yaw velocity r per unit v, etc. It shall, thus, reflect the fact that the instantaneous position of the pivoting point is of major importance. In this case, however, there are unavoidable knuckles in the $Y(v, r)$-curves. For a family of such curves, drawn for constant r versus v the breaks (for non-zero r) as v changes sign can only be elliminated if $Y_{|v|r}=0$; likewise the absence of breaks in similar curves on basis of r would require $Y_{v|r|}=0$. (Cf. alternative by GERTLER and HAGEN, [53].)

From curve-fitting, using realistic combinations of v and r, the two coupling coefficients usually turn out to be of equal magnitude but of opposite sign. (The identification of the coefficients by use of an analogue computer and an oscilloscope display is preferred in place of digital regression analysis.)

Forward Speed and Resistance

The principal effects of viscous and free-surface phenomena on the resistance to steady forward motion are well-known to naval architects. The correlations of wavemaking and separation with ship geometry are still less satisfactory. However, alternative methods are available for full scale powering predictions from standard series or project model data. As will be further discussed in next Section the adequate synthesis should supply information not only on shaft horse power and r.p.m. but also on hull resistance and wake fraction. Speed trial data therefore require an analysis such as proposed and used by LINDGREN; in case of very large and slow-running ships it may be necessary to include scale effects also in the open-water characteristics of the screw propeller, [54].

A simple guide to ship resistance values may be obtained from the mean line of Fig. 16, which summarizes the results of a limited number of SSPA trial trip data in terms of the total specific resistance $\frac{R}{\Delta} = -[X']_{v=r=0}$ on basis of FROUDE number F_{nL} or u''. (A similar plot of "total resistance in lbs to displacement in long tons" versus TAYLOR speed-length quotient, based on model data,

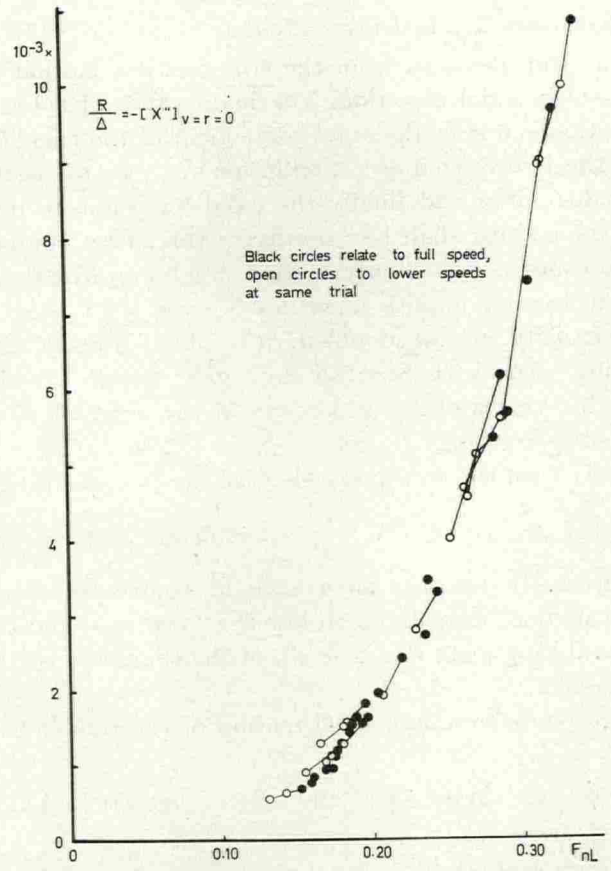

Fig. 16. Specific resistance figures as evaluated from ship trial data at SSPA.

was published by SAUNDERS [55].) The mean line also reflects the general trend of the resistance-speed-dependence for the individual ships in the proximities of their design speeds.

A close approximation to a resistance curve with typical humps and hollows requires a multi-term polynomial in u. Established practice in naval architecture makes use of a single exponential term $R_1 \cdot \left(\frac{u}{u_1}\right)^p$ to characterize the curve in the vicinity of u_1. For large slow-running tankers $p \approx 2$ over the entire speed range of interest, which is associated with an almost constant advance ratio for the screw. In confined waters it may be necessary to include a higher-order term; see Section 9.

Forward Resistance due to Lateral Motions

When the ship deviates from the true forward motion, additional forces appear in axial direction. The main cause of speed loss in a turning motion is due to the axial component of the centrifugal mass force and the hydrodynamic contribution $X_{rv} \cdot rv$, of second importance is rudder drag and finally the axial force due to oblique-hull lift and wave-making shall be considered; this latter component will be of more concern in a steady motion involving drift due to wind.

Ideal-flow hydrodynamics identifies X_{rv} with $-Y_{\dot{v}}$, i.e. the mass effect is virtually almost doubled. (Cf. (5.6).) Recent evaluations from turning trials with Swedish ships give, within a wide scatter, most probable values of X_{rv} which are of the order of 20 to 50 per cent of ideal $(-Y_{\dot{v}})$ only.

In a steady turn the ship proceeds with her bow pointing inwards, so that $(m+X_{rv})rv = -(m+X_{rv})\frac{V^2}{R} \cdot \beta$ indicates a force opposed to forward thrust. In running on a straight course the frequency of the yawing motion normally is so low that yaw rate and drift angle are in phase during most (but not all) of the time, and so an average resistance results.

Let the response to a sinusoidal motion of the rudder be

$$\dot{\psi} = \dot{\psi}_a \cdot \sin(\omega t + \epsilon_r) \quad \text{and} \quad \beta = \beta_a \cdot \sin(\omega t + \epsilon_\beta).$$

Averaging over a number of complete periods gives

$$\overline{r\beta} = \frac{r_a \beta_a}{2} \cos(\epsilon_r - \epsilon_\beta) \tag{6.8}$$

The normal merchant ship will pivot round a point closely aft of the bow at low frequencies and a rough estimate of the average product

is given by $\overline{(rv)}_{\omega \to 0} \approx -\frac{L}{2} \cdot \frac{\overline{OP}}{L} \dot{\psi}_a^2$

A plane wing in a uniform flow will experience an induced drag as given by $C_{Di} = \frac{1}{\pi \Lambda} C_L^2$. According to certain experiments this

simple relation may still be used with a correction factor for the twisted flow over a rudder behind a screw. The calculation of rudder lift will be shortly discussed in the next Section; using a nominal aspect ratio equal to twice the geometrical one, the correction factor just mentioned will be of the order of 1.2–1.4.

Typical estimates for fullscale tankers give as a guide value a relative increase in forward resistance due to a rudder deflection of δ radians equal to 3,5 or 4 δ^2. For small sinusoidal helm angles on a straight course the quasi-stationary application gives $\frac{\Delta X(\delta)}{X(u)} \approx 1.75$ or $2\,\delta_a{}^2$, which may be compared with the relation given from propulsion tests with a MARINER ship model in Japan, $\frac{\Delta T(\delta)}{T} = 2 \cdot \delta_a{}^2$, [56].

At propeller advance conditions removed from the steady forward motion state the induced rudder drag will be given by $\frac{1}{4}X_{cc\delta\delta} \cdot c^2\delta^2$, where $c=c(u, n)$ is the effective flow velocity past the rudder and where the coefficient $\frac{1}{4}X''_{cc\delta\delta}$ is proportional to the product of the ratio $a_{\bar{\Lambda}}/\bar{\Lambda}$ and the control derivative $\frac{1}{2}Y''_{cc\delta}$. (See Section 7.) In computer applications a soft-type limiter will be used to simulate the conditions for a stalled flow.

The viscous lift experienced by a slender ship hull in oblique translation is also accompanied by an induced drag, but the axial component of the resultant force still is expected to be positive. (According to the zero-aspect-ratio wing analogy the resultant force will bisect the angle between the normal to the hull and the normal to the flow. With increasing aspect ratio the resultant moves towards the normal to the flow.) The break-down of the ideal flow over the stern causes a change of viscous pressure resistance, however, and wave-making effects will cause a further increase of forward resistance.

These effects are here illustrated in Fig. 17 by results of axial force measurements on the surface ship model and the submerged double-body form otherwise described in ref. [18]. From an inspection of these and other surface ship model experiments it is suggested to use a term

$$X(u, v) = \tfrac{1}{6}X_{u|v|vv}u|v|v^2 \tag{6.8}$$

to represent the axial force due to lateral drift. An approximate value of the derivative is given by $\frac{1}{6}X''_{u|v|vv} = -200$.

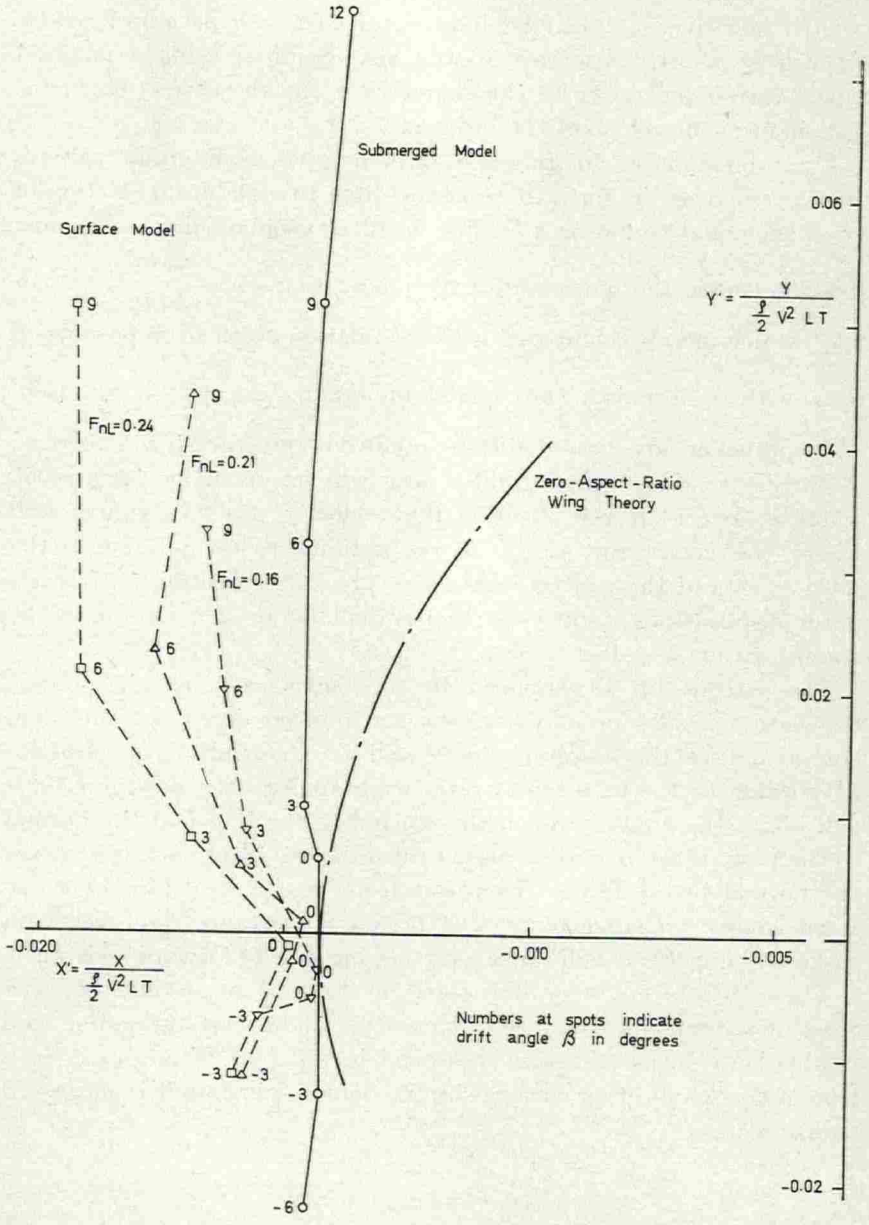

Fig. 17. Change of longitudinal force with hull lift in oblique towing of ship model and submerged double-body geosim.

7. Speed and Steering Control

Some General Observations

In general the subject of steering and manoeuvring may not be separated from that of propulsive control, and this is specially true in case of ship behaviour at slow speeds. Moreover, in model testing the interactions between hull, propeller, and rudder are likely to cause the main problems of model-to-ship-conversion, including scale effects of a hydrodynamic nature as well as other model effects due to the dynamics of the testing equipment.

Large seagoing ships are usually propelled by a single centre line screw, or by wingward twin screws. In case of a tandem contra-rotating propeller arrangement most of the characteristics discussed below may be calculated for an equivalent single propeller. In case of close-shafted twin screws of overlapping or interlocking types the interaction with the rudder should be specially considered.

It has been repeatedly proven by handling experience that twin screw ships should be fitted with twin rudders. Recent model tests indicate that with a suitable design of the rudders, including a certain neutral position toe-out, this arrangement may favourable compete with the centre line rudder alternative also from a propulsive performance point of view.

In the application of the first-order steering theory, [57], first introduced by NOMOTO in 1956 and strictly valid only for inherently stable ships, there appear only two constants: a (desired high) "gain" K, which represents the ratio of rudder turning moment to yaw damping, and a (desired low) "time constant" T, which measures the sluggishness of the ship response, and which represents the ratio of ship inertia to yaw damping. As was subsequently also shown by NOMOTO [58] the non-dimensional quotient K'/T' turns out to be proportional to the parameter LA_r/∇ for ships with similar stern arrangements. This quotient may therefore be looked upon as a rudder-on-ship effectiveness factor, proportional to the initial yaw acceleration imparted to the ship by a given helm. It is also closely related to the P-value introduced by the author as a non-dimensional measure of the initial change of course in response to a rudder step manoeuvre, [59].

Some ten years ago manoeuvring trials were run with three tankers of the Götaverken 40,000 t.dw. series, all similar except for the stern arrangements, [60]. The SSPA analysis of zig-zag tests with respect

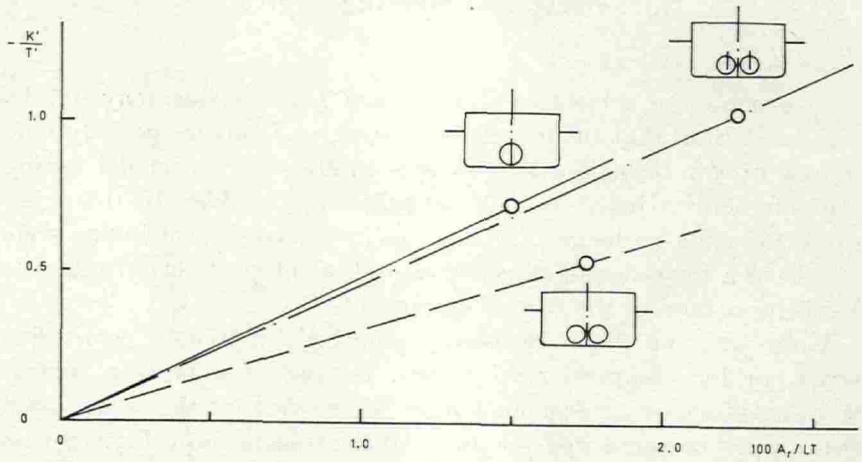

Fig. 18. Results from first-order analysis of full-scale zig zag tests with three 40,000 t.dw. tankers, similar except for stern arrangements.

to the rudder-on-ship effectiveness factor just mentioned offers an unique illustration of the merits of these arrangements, Fig. 18. In particular, note that the two alternatives with rudder behind screw (screws) prove to be equivalent in case of same total area of rudder, and that the use of the larger area of a twin alternative therefore is especially favourable.

A propeller or a rudder, or the combination of a propeller and a rudder, acts as a stabilizing fin as well as a manoeuvring device; the contributions to the fin effect from the propeller and from the rudder-behind-propeller are of equal order. It should be realized that a minor modification to a rudder does not appreciably affect this fin effect or the size of a hysteresis loop in the yaw-velocity-versus-steady-helm diagram of an unstable ship. However, the higher control force per degree of helm then possibly achieved, will help in actual directional control, where the history of yaw velocities and helm angles takes place well within the height of the steady-state loop. (See also Section 1.)

The general propulsion case will be represented by an arrangement including one centre line screw and two wing screws, developing thrusts T_c, T_s and T_p, respectively. Hull interference generates axial forces $t_c T_c$, $t_s T_s$ and $t_p T_p$, in the opposite directions, as well as lateral or sideward forces $s_s \cdot T_s$ and $s_p \cdot T_p$. In order to adhere to the thrust

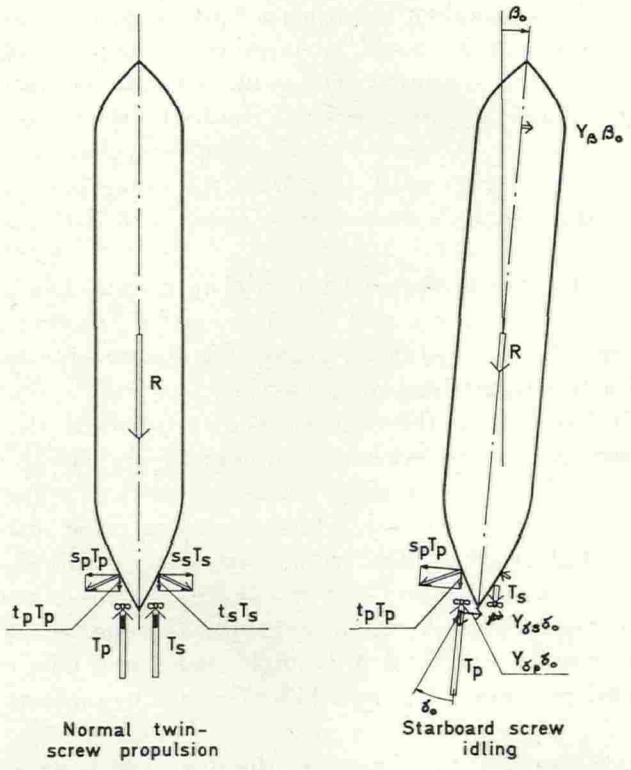

Fig. 19. Force fields on twin-screw tanker on straight steady course.

deduction concept the factors t—which are not necessarily constants—will be taken as positive, so that the force in positive x direction is $-t \cdot T$. The factor s_s will be positive, and $s_p = -s_s$. Roughly $s_s = t_s \cdot \cot \alpha$, where α is the effective waterline angle in front of the propeller.

Normally the lateral forces due to T_s and T_p are in balance, but if $T_p \neq T_s$ there is a resultant force applied some $0.4L$ behind the $C.G.$ of the ship. The turning moment thus obtained is much larger than that produced by the axial forces along the shaft lines, [61].

The diagrams in Fig. 19 illustrate the symmetric force field around a twin-screw tanker in normal straight course conditions, and the steady state situation when running with starboard propeller idling. The non-symmetric suction force on the port quarter is balanced by the forces due to drift and checking rudders. The drift angle is a fraction of a degree only, and some 90 per cent of the compensation

force is due to the rudders, set at some 5 to 7 degrees. With the twin rudder arrangement it should be possible to maintain 75 per cent of the speed in this condition. The induced resistance due to rudder lift would be larger in case of a single rudder between the propellers, but the main cause of speed loss of a ship propelled by one of its screws only is the additional drag from the idling propeller; again, that drag may well be increased by a factor of 3 if the propeller is locked.

The characteristics of a propeller in axial open-water flow are usually given by tables or curves of well-known K_T and K_Q coefficients versus advance ratio J. In yawed flow the propeller also experiences a lateral force and a (small) pitching moment, [62].

In behind conditions the effective angle of drift at the propeller still is roughly $\frac{2}{3}$ of the nominal local angle, high enough to let the propeller contribute the fin effect already mentioned. (The sidewash behind the propeller then has a further straightening effect on the flow to the rudder.) The effective advance ratio is modified by the effective wake in the factor $1-w$; here w will be chosen as for thrust identity. The effective wake, again, is modified by the drift of the ship, being higher for a starboard drift angle than for a port one and a right-handed propeller, [63]; here that effect will be taken as of second order.

Finally, the vertical asymmetry of the flow field is responsible for the appearance of a lateral force on the propeller of a ship even if drift or yaw are zero. In case of a single screw ship this latter force may be put equal to 3 to 5 per cent of the thrust, [64]. A right-handed screw tends to throw the stern of a loaded ship towards starboard, thus requiring a small starboard helm to be carried on straight course. Other free-running model tests prove that draught conditions may change this picture, and that the ship on light draught may have a tendency to turn to starboard, [65].

The hydrodynamic thrust $T(T_c, T_p, T_s)$ and torque $Q(Q_c, Q_s, Q_p)$ —which is negative in case of a righthanded screw on a driving shaft—will be given as quasi-stationary functions of instantaneous values of forward ship speed, u, and screw r.p.s., $n(n_c, n_s, n_p)$. The thrust is a major factor governing the flow velocity past the rudder, and this velocity likewise will be given in terms of u and n. Rudder control derivatives usually are determined from model tests in one or two conditions of screw loading only. In order to find an adequate prediction of full scale control derivatives for the more

general propulsion case it is necessary to combine model results with a simple procedure for calculating the total control force due to rudder deflection.

From the hydrodynamical point of view the typical allmovable rudder in behind condition is equivalent to a twisted wing on a pointed afterbody. There are a number of additional complications, however: The spanwise velocity distribution is highly non-uniform, the flow along the chord is accelerating or decelerating, the gap between wing and body is within a retarded boundary layer flow and it also varies with the angle of deflection, the boundary conditions at the free surface violate the vertical symmetry aspect even if there is no suction-down of air, the shape of the body stern is far from say a simple axisymmetric cone. The modern half-spade rudder on a fixed horn (the MARINER-type) is a hybrid of the allmovable and the flapped types, and other common forms all have their special characteristics. The procedure here adopted is not a substitute for the detailed calculations necessary for a certain project design, but it will furnish a good estimate of control forces and make possible the extended use of model results referred to above.

The Rudder or "Control" Derivatives

It will be assumed that for each rudder configuration may be defined "equivalent" values of rudder area, rudder aspect ratio, rudder angle and rudder advance velocity.

A detailed study of the velocity field in the slip-stream of a propelled tanker model and of the pressure distribution over the rectangular rudder fitted to this model was reported by LÖTVEIT, [66]. The distorsion of the spanwise loading due to slip-stream rotation was clearly demonstrated, but the diagrams did not indicate any definite influence of the rudder image in the hull and free surface; the gap distance from top of rudder to stern profile was some 12 per cent of rudder height. Straight-forward calculations of rudder lift from known relations of lift curve slope versus geometric aspect ratio and an average advance velocity based on the simple momentum theory proved to give good agreement with the rudder forces measured by a force balance or integrated from the pressure field.

Unfortunately in this case no simultaneous measurements were made of the total hull-and-rudder forces, and there is still a lack of such data for normal surface ship forms. However, already from the old experiments by BAKER and BOTTOMLEY [67] it was seen that

the total force due to rudder deflection was increased by some 40 per cent in presence of a deep cruiser stern close above the rudder, and that a third of the total force then was carried by the hull.

Let b be the height of the rudder at the stock, or the higher value forward of it, and let a be the depth to top of rudder at the same station. With a projected area A_r of the rudder the aspect ratio of rudder+plane image is equal to $\bar{\Lambda}=2\,\frac{b^2}{A_r}$. The lift curve slope $a_{\bar{\Lambda}}$ is taken from the theoretical curve derived from the WEISSINGER theory, [68], or from empirical curves available.

The geometrical aspect ratio usually is of the order of 1.5, i.e. the rudder is not a low-aspect-ratio fin, but it seems still to be possible to make use of the results for wing-body interferences applicable to such fins. In particular, the ratio of the lift on a rigid combination of a wing and a cylindrical central body, $L_{\alpha\alpha}^{WB}$, to the lift of the abridged wing alone, $L_{\alpha}^{\overline{W}}$, is simply given by $\left(1+\frac{a}{a+b}\right)^2$, [69]. Next, for calculation of the lift carried on the axially orientated body and on the wing deflected to the flow, it is observed that the exact theory by MIRELS [70] may be approximated by

$$L_{\alpha 0}^{WB} \approx \sqrt{L_{\alpha}^{\overline{W}} \cdot L_{\alpha\alpha}^{WB}} = L_{\alpha}^{\overline{W}}\left(1+\frac{a}{a+b}\right).$$

Except for a correction factor the control derivative for the ship will be calculated as

$$\frac{1}{2}\,Y_{cc\delta}'' = \frac{L^3}{2\nabla}\cdot\frac{u^2}{c^2}\cdot Y_{\delta}' = a_{\bar{\Lambda}}\left(1+\frac{a}{a+b}\right)\frac{A_r}{LT}\,\frac{L^2T}{2\nabla} \qquad (7.1)$$

where $Y_{cc\delta}''$ unlike Y_{δ}' is defined also for zero forward speed. The modern half spade or MARINER type rudder has a fixed horn, which divides the upper part of the rudder in ratio $A_h/(A_u-A_h)$. The right hand member of (7.1) may then be multiplied by a factor $1-\frac{1}{4}\cdot\frac{A_h}{A_r}$.

The effective rudder advance velocity c (squared) is calculated from the mean square velocity of the screw race and an estimated mean square velocity past the rudder outside the race. If w is the wake factor as integrated by the propeller (thrust identity) the effective square velocity above the race in a normal single screw

arrangement may be taken as $u^2(1-\frac{4}{3}w)^2$. Inside the race, which in average conditions has a diameter some 10 per cent smaller than the propeller, the ultimate mean square velocity is given by

$$u^2(1-w)^2\left(1+\frac{8}{\pi}\cdot\frac{K_T}{J^2}\right), \text{ where, for } u>0,$$

$$K_T=K_{T00}+\frac{J}{|J|}\cdot K_{T0}+K_{TJ}J+\frac{1}{2}K_{TJJ}J^2 \tag{7.2}$$

is to be approximated from the open water propeller diagram. Whereas the thrust may be analytically defined for all combinations of u and n—see below—the working conditions of the rudder are known only for a positive thrust, in which case

$$c^2=\tfrac{1}{2}c^2_{uu}u^2+c^2_{un}un+\tfrac{1}{2}c^2_{|n|n|}n|n+\tfrac{1}{2}c^2_{nn}n^2 \tag{7.3}$$

From an analysis of a large number of control derivative measurements on models it appears that a correction factor of 0.7–0.8 shall be applied to (7.1) when combined with (7.3) to give the force

$$Y(u,n,\delta)=\rho\frac{\nabla}{L}\cdot\tfrac{1}{2}Y''_{cc\delta}\cdot c^2\delta.$$

This correction factor is understood to take care of gap effects and non-ideal geometry of the hull+rudder arrangement, etc.

The three constants in eq. (7.3) depend on screw characteristics and wake factors, and they are therefore unique for the model scale. To facilitate a correction for this scale effect in the control derivatives the diagram in Fig. 20 has been compiled, chiefly from ref. [71] and data available at SSPA. The slope of curves of wake factors against ship or model lengths increases with hull fullness; especially SSPA experience of full scale tanker trials only rarely include effective wake factors above 0.38.

In Fig. 21 the control moment derivative N''_δ for a 98,000 t.dw. tanker is presented as a function of forward speed u and shaft speed n, for a 1:70 scale model as well as for the prototype. (Extrapolation to slowly reversed propeller is shown dotted.) In particular it is seen from the diagram that the turning moment from the rudder at self propulsion point of ship is only some 60 per cent of the model test value.

During a manoeuvre the effective change of angle of attack of the rudder is a function of nominal helm deflection δ, drift v, and

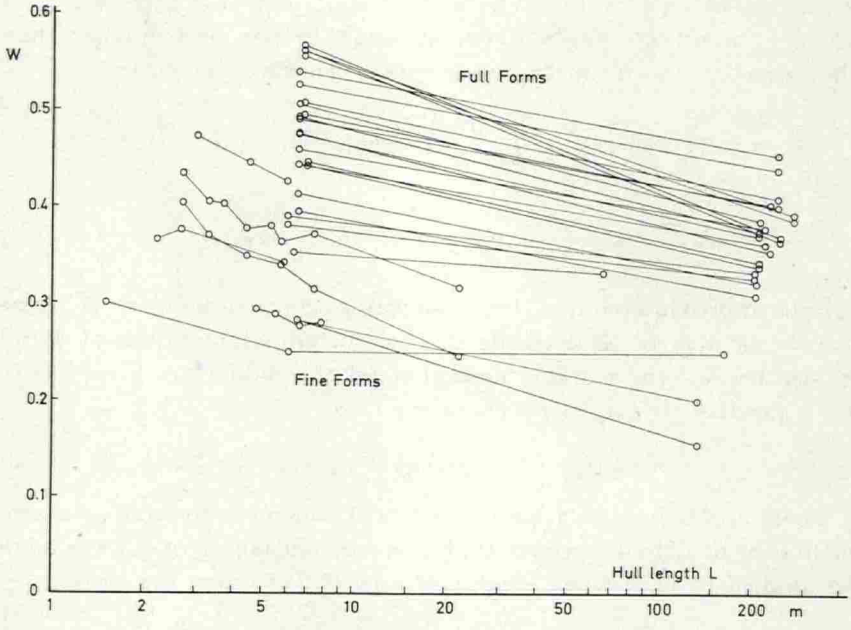

Fig. 20. Scale effects on wake factor w as integrated by propeller in model and full scale.

yaw rate r, and change of screw loading. Again accepting this quasi-stationary model it is

$$\delta_e = \delta + \left(k_v \cdot \frac{v}{c} + k_r \frac{L\dot{\psi}}{2c} \right) |\delta| \tag{7.4}$$

where typical values are $k_v = -0.5$ and $k_r = 0.5$. This relation reflects a kind of ECK-effect; note that the force contribution from the rudder in midship position is included in the total force derivatives. (An alternative but less explicit method to include the same phenomena is given by STROM-TEJSEN and CHISLETT, [72], who make use of a number of coupling derivatives such as $Y'_{\delta rr}$, etc.)

Helm Control

The manual or automatic pilot excerts the control through the steering gear, which is supposed to have a time constant T_E, causing a small delay in the rudder angle δ obtained. The value of T_E may vary say between 0.4 and 4 s, the first figure being a good catalogue

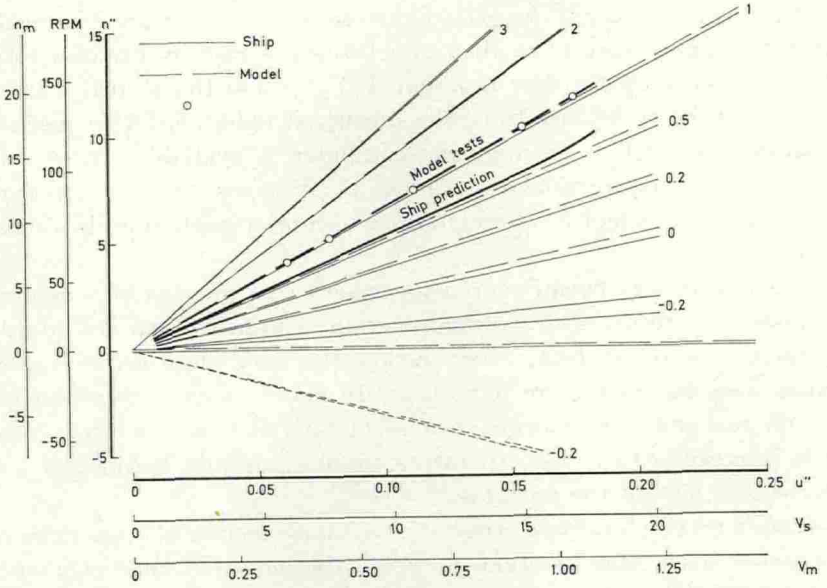

Fig. 21. Relative change of rudder control force with change of propeller advance conditions for 3.6 m model and 98,000 t.dw. tanker prototype. Diagram based on model tests at VBD and SSPA, and on speed trials.

value and the second one not seldom realized in shipboard testing. The steering gear or telemotor system often has a back-lash of about half a degree.

The function of an auto-pilot may be said to be essentially of the "*proportional+rate control*" type, although an integrator control shall be added to take care of stationary deviations. Commercial type auto-pilots include special features, which shall be included in simulator applications.

With the simple ideal auto-pilot "calling for" the rudder angle $\delta^* = \gamma\psi + \sigma\dot{\psi}$ the transfer function of the feed-back loop is

$$Y_2 = Y_{\delta\delta^*} \cdot Y_{\delta^*\Psi} = \frac{\gamma[1+(\sigma/\gamma)s]}{1+T_E s} \tag{7.5}$$

Typical values for the gain or "rudder ratio" γ and rate constant σ of a tanker auto-pilot in deep water setting are $\gamma = 3$ (degrees helm per degree heading error) and $\sigma = 135$ seconds (or 135 degrees helm per degree per second of change of heading). (See Section 13.)

Although the course keeping characteristics of say an inherently unstable tanker may be studied in a BODE diagram by use of a total system open loop transfer function $Y_1 Y_2$, where the ship dynamics open loop Y_1 is defined from the linearized equations, this method is mostly avoided if an analogue computer is available. In case of small value non-linearities—such as dead zones or lags—in gyro compass and telemotors the equations-of-motion technique is almost unavoidable.

Much effort has been devoted to present the function of a manual helmsman in terms of a transfer function. The helmsman is a highly adaptive control system, which makes the task more difficult, but which also makes it more important. In many cases it is impossible to run real-time simulations because of lack of time, in other cases it is impossible to run comparative simulations just because of the learning ability of the operator.

HOOFT tried to evaluate criteria for manual steering of large tankers by use of a transfer function, in which the gain and time constants were derived by extrapolation from high frequency pilot dynamics, [73]. Undoubtedly new basic information is required.

Propeller Thrust and Shaft Torque

A majority of ocean-going ships are propelled by fixed-blade screws driven by diesel engines or steam turbines, the normal steady state outputs of which in principle are characterized by constant torque Q^E—proportional to fuel pump stroke—and constant power—proportional to steam inlet pressure—respectively. In running conditions the mechanical torque losses Q^F depend on sign of r.p.m. but are more or less independent of its magnitude. Shaft r.p.m. is governed by the simultaneous equations for longitudinal resistance and for thrust and torque, for $u > 0$ here given as

$$\left.\begin{aligned} gT'' &= L^{-1} \cdot \tfrac{1}{2} T''_{uu} u^2 + T''_{un} un + L \cdot \tfrac{1}{2} T''_{|n|n} |n| n + L \cdot \tfrac{1}{2} T''_{nn} n^2 \\ (Q^{E''}_{\dot{n}} - Q''_{\dot{n}}) \dot{n} &= L^{-1} g \cdot Q^{E''}_{\varkappa} \varkappa + L^{-1/2} g^{1/2} \cdot Q^{E''}_{n} \cdot n + L^{-1} g \cdot Q^{F''} n / |n| \\ &\quad + L^{-2} \cdot \tfrac{1}{2} Q''_{uu} u^2 + L^{-1} Q''_{un} un + \tfrac{1}{2} Q''_{|n|n} |n| n + \tfrac{1}{2} Q''_{nn} n^2 \end{aligned}\right\} \quad (7.6)$$

$$\text{with } \frac{1}{2} T''_{uu} = \frac{L^3/\nabla}{(L/D)^2} \cdot (1-w)^2 \cdot \frac{1}{2} K_{TJJ}, \text{ etc.}$$

The steady-state hydrodynamic thrust and torque are given as

functions of forward speed, u, and rate of revolutions, n, based on open water K_T and K_Q characteristics; K_T and K_Q are first approximated by square functions of $J = \frac{u}{nD}(1-w)$ or $1/J$. (Note that a linearization of these characteristics does not result in a linearization of the (u, n)-dependence.) The NORDSTRÖM data [74] may be used when reversing or transient manoeuvres are considered. In general it is then necessary to confine the analytical functions to limited ranges of propeller advance coefficients, i.e. to use alternative coefficients as in eq. (7.2). The use of modified advance coefficients of several forms has been discussed by BAKER and PATTERSON, [75]. HARVALD has presented useful information on the propulsive factors at arbitrary steady-state advance conditions, [76]. Transient state flows and especially the effects of a separating boundary layer along the stern of a retarding ship are still less predictable.

The added mass and moment of inertia involved in unsteady manoeuvring of the propeller are functions of the momentaneous advance coefficients as well as of the rate of change of r.p.m. In small changes from normal propulsive conditions the added inertia is small as blade angles of attack are small. Naval architects often use a value of 30 per cent of rigid screw inertia for the added inertia; although this figure originates from model tests with screws oscillating at zero advance coefficient it may still be used as an effective average value during the short reversing stage of an engine manoeuvre. In fact this stage is dominated by the large control torques and by the way they are used.

When simulating manoeuvres with diesel-powered ships it shall be observed that normal r.p.m. control is not possible for n less than some 35–40 per cent of design shaft speed n_0. The torque delivered is here rapidly reduced, mainly due to loss of charge air pressure. (For high r.p.m. Q_n^E is almost zero.) Slow speed manoeuvring must be performed by intermittent use of the propeller, which requires repeated starting of the engine. Reversing manoeuvres must often await drop of speed to some 60 per cent of the full speed, at which lower speed braking air may be applied. There is also a certain astern r.p.m. which must be attained before fuel may be injected to start engine back. For a discussion of detailed features of diesel manoeuvring the reader is referred to a paper by RITTERHOFF, [77].

The energy-converting efficiency of a turbine wheel has a maximum of some 80 per cent at a certain ratio of blade velocity to nozzle

steam velocity, attainable at the design point. Assuming this ratio equal to 0.5, and a parabolic curve of efficiency symmetric to the design point, the following simple formula is obtained for the torque output:

$$Q^E = 2\varkappa Q_0^E \left(1 - \frac{1}{2} \cdot \frac{n/n_0}{\varkappa}\right) \tag{7.7}$$

Here Q_0^E and n_0 refer to torque and shaft speed at design conditions for full steam inlet $\varkappa = 1$. The formula furnishes a good approximation also for present multi-staged ship turbines. In practical applications to studies of slow-speed port approach manoeuvring it must be realized that steam production may then be limited to say $\varkappa = 0.7$.

8. Modelling the Deep-Water Horizontal Manoeuvre

The General Case

The ship will be regarded as a rigid body moving under the influence of the gravity force $m\mathbf{g}$ and the buoyancy force $-\rho \cdot \nabla_0 \cdot \mathbf{g}$ — where ∇_0 is the volume displacement at rest—as well as under that of the external forces, including the control forces applied by use of rudders and thrusters. Before reducing the problem to the normal merchant ship case the more general form of the rigid body dynamics will be included.

The centres of mass (G) and buoyancy (B) may be off-set from the origin of the moving system (O), and it is then practical to apply NEWTON's laws in a summation of the acceleration forces on the mass elements (cf. (4.10) and (4.4)):

$$\left.\begin{aligned}
&\sum \begin{bmatrix} dm & 0 & 0 \\ 0 & dm & 0 \\ 0 & 0 & dm \end{bmatrix} \begin{bmatrix} a_x \\ a_y \\ a_z \end{bmatrix}_{\text{abs}} = \begin{bmatrix} X \\ Y \\ Z \end{bmatrix} + \begin{bmatrix} m-\rho\nabla_0 & 0 & 0 \\ 0 & m-\rho\nabla_0 & 0 \\ 0 & 0 & m-\rho\nabla_0 \end{bmatrix} \tilde{\Lambda} \begin{bmatrix} 0 \\ 0 \\ g \end{bmatrix} \\
&\sum \begin{bmatrix} dm & 0 & 0 \\ 0 & dm & 0 \\ 0 & 0 & dm \end{bmatrix} \begin{bmatrix} 0 & -z & y \\ z & 0 & -x \\ -y & x & 0 \end{bmatrix} \begin{bmatrix} a_x \\ a_y \\ a_z \end{bmatrix}_{\text{abs}} = \begin{bmatrix} K \\ M \\ N \end{bmatrix} + \\
&+ \begin{bmatrix} 0 & -(mz_G - \rho\nabla_0 z_B) & my_G - \rho\nabla_0 y_B \\ mz_G - \rho\nabla_0 z_B & 0 & -(mx_G - \rho\nabla_0 x_B) \\ -(my_G - \rho\nabla_0 y_B) & mx_G - \rho\nabla_0 x_B & 0 \end{bmatrix} \tilde{\Lambda} \begin{bmatrix} 0 \\ 0 \\ g \end{bmatrix}
\end{aligned}\right\} \tag{8.1}$$

Upon summation the coefficient matrices of the acceleration terms, the mass and inertia tensors, expose as

$$\left.\begin{aligned} m&=\begin{bmatrix} m_{xx} & 0 & 0 \\ 0 & m_{yy} & 0 \\ 0 & 0 & m_{zz} \end{bmatrix}=\sum dm \\ I&=\begin{bmatrix} I_{xx} & -I_{xy} & -I_{zx} \\ -I_{xy} & I_{yy} & -I_{yz} \\ -I_{zx} & -I_{yz} & I_{zz} \end{bmatrix}=-\sum \mathbf{xx}\, dm \end{aligned}\right\} \tag{8.2}$$

where the elements are defined by

$$\left.\begin{array}{lll} \sum x\, dm=m\cdot x_G & \sum(y^2+z^2)\, dm=I_{xx} & \sum xy\, dm=I_{xy} \\ \sum y\, dm=m\cdot y_G & \sum(z^2+x^2)\, dm=I_{yy} & \sum yz\, dm=I_{yz} \\ \sum z\, dm=m\cdot z_G & \sum(x^2+y^2)\, dm=I_{zz} & \sum zx\, dm=I_{zx} \end{array}\right\} \tag{8.3}$$

Many authors prefer to introduce the virtual masses and moments of inertia into the equations given above. Here the "added" masses will consistently be assigned to the hydrodynamic reaction forces in the right-hand members; in Section 5 it was seen that these forces may include other inertia terms otherwise easily overlooked.

In most practical applications the xz-plane is a plane of symmetry, so that $y_G=y_B=0$ and $I_{xy}=0$. Except in a few special cases, such as when dealing with hydrofoil crafts, etc.—the discussion of which is outside the scope of this paper—other terms may be safely ignored in view of the smallness of the products of inertia and the perturbation velocities involved.

The Merchant Type Displacement Ship

In what follows the discussion is restricted to displacement ships, for which $m=\rho\nabla_0$ and $\nabla\approx\nabla_0$. Forward speed is always associated with a sinkage and change of trim, most obvious as "squatting" in waters of finite depth, but the manoeuvring dynamics will be sufficiently well described by the equations in four degrees of freedom, i.e. the surge, sway, roll and yaw.

Then

$$\left.\begin{aligned} &m\{\dot u-rv-x_Gr^2+z_Grp\}=X \\ &m\{\dot v+ru+x_G\dot r-z_Gpr\}=Y \\ &I_{xx}\dot p-I_{zx}\dot r-mz_G(\dot v+ru)=K-mg(z_G-z_B)\sin\phi \\ &I_{zz}\dot r-I_{zx}\dot p+mx_G(\dot v+ru)=N \end{aligned}\right\} \tag{8.4}$$

Whereas the initial roll as well as the steady outward heel may be appreciable in case of, say, a high-speed destroyer these angles are also known to be quite insignificant in the tanker case. In steady turning a heel, proportional to $-\frac{L}{R_c} \cdot F_{nL}^2$, may produce an effective camber of the waterline flow around a fine hull, but this hardly applies to tankers, [65].

Leaving out the roll equation the present deep-water model is given as in eq. (8.5).

$$
\begin{aligned}
(1-X_{\dot{u}}'')\dot{u} &= L^{-1}\cdot\tfrac{1}{2}X_{uu}''u^2+L^{-2}g^{-1}\cdot\tfrac{1}{24}X_{uuuu}''u^4+g\cdot T''(1-t)\\
&\quad+(1+X_{vr}'')v\dot{\psi}+L(x_G''+\tfrac{1}{2}X_{rr}'')\dot{\psi}^2\\
&\quad+L^{-2}g^{-1}\tfrac{1}{6}X_{u|v|vv}''u|v|v^2+L^{-1}\tfrac{1}{4}X_{cc\delta\delta}''c^2\delta_e^2\\
(1-Y_{\dot{v}}'')\dot{v} &= L(Y_{\dot{r}}''-x_G'')\ddot{\psi}+(Y_{ur}''-1)u\dot{\psi}+L^{-1/2}g^{-1/2}\cdot\tfrac{1}{2}Y_{uur}''u^2\dot{\psi}\\
&\quad+L^{-1}Y_{uv}''uv+L^{-3/2}g^{-1/2}\cdot\tfrac{1}{2}Y_{uuv}''u^2v\\
&\quad+L^{-1}\tfrac{1}{2}Y_{|v|v}''|v|v+L\cdot\tfrac{1}{2}Y_{|r|r}''|\dot{\psi}|\dot{\psi}+Y_{|v|r}''|v|\dot{\psi}\\
&\quad+Y_{v|r|}''v|\dot{\psi}|+L^{-1}\cdot\tfrac{1}{2}Y_{cc\delta}c^2\delta_e+k_Ygr''\\
(k_{zz}^2+N_{\dot{r}}'')\ddot{\psi} &= L^{-1}(N_{\dot{v}}''-x_G'')\dot{v}+L^{-1}(N_{ur}''-x_G'')u\dot{\psi}\\
&\quad+L^{-3/2}g^{-1/2}\tfrac{1}{2}N_{uur}''u^2\dot{\psi}+L^{-2}N_{uv}''uv\\
&\quad+L^{-5/2}g^{-1/2}\tfrac{1}{2}N_{uuv}''u^2v+L^{-2}\cdot\tfrac{1}{2}N_{|v|v}''|v|v+\tfrac{1}{2}N_{|r|r}''|\dot{\psi}|\dot{\psi}\\
&\quad+L^{-1}\cdot N_{|v|r}''|v|\dot{\psi}+L^{-1}\cdot N_{v|r|}''v|\dot{\psi}|\\
&\quad+L^{-2}\tfrac{1}{2}N_{cc\delta}''c^2\delta_e+L^{-1}k_Ngr''
\end{aligned}
\qquad (8.5)
$$

It shall be pointed out that the derivative Y_{ur}'' includes the potential-flow contribution $X_{\dot{u}}''$ and the derivative N_{ur}'' the potential-flow contribution $Y_{\dot{r}}''$. In the forward speed equation X_{vr}'' is given a value much smaller than its ideal value equal to $-Y_{\dot{v}}''$. (Cf. page 46.)

Eq. (8.5) is to be combined with Eqs. (7.3), (7.4) and (7.6). In case of twin-screw ships (7.6) is to be properly modified and terms corresponding to $s_p \cdot T_p$ and $s_s \cdot T_s$ are to be introduced in (8.5).

Some Elementary Concepts

So far as small motions are considered forward speed and r.p.m. remain almost constant and the rudder force and moment may be regarded as functions of nominal helm δ. The yaw-rate/helm relation is given by the transfer function

$$Y_{\dot{\psi}\delta} = K \cdot \frac{1+T_3 s}{1+(T_1+T_2)s+T_1 T_2 s^2} \tag{8.6}$$

and the ship heading response by $Y_1 = \frac{1}{s} \cdot Y_{\dot{\psi}\delta}$, which may be used with Y_2 from eq. (7.5) to study the closed-loop system with transfer function $F = Y_1/(1+Y_1 Y_2)$, [9].

The static gain and the three time constants in (8.6) are built up from the coefficient of eq. (8.5). T_3 is always positive. The two constants T_1 and T_2 are given by the roots of the characteristic equation. If $s_1 = -\frac{1}{T_1}$, the root to the right on the real axis, turns positive the ship is inherently unstable. The analytical criterion for dynamic stability suggests the dynamic stability lever

$$l_r'' - l_v'' = \frac{x_G'' - N_{ur}''}{1 - Y_{ur}''} - \frac{N_{uv}''}{Y_{uv}''} \tag{8.7}$$

to be a suitable measure for the degree of stability. In particular it provides a good illustration when studying the effects onto the stability characteristics of changes in the stability derivatives. A typical value for an unstable tanker may be, say $l_r'' - l_v'' = 0.30 - 0.45 = -0.15$. The relation between the magnitude of this negative stability lever and the height of the hysteresis loop is very sensitive to the form of the mathematical model chosen.

A first-order approximation to the transfer function (8.6) yields a step response, which is correct for large values of t provided the effective time constant T is defined by $T = T_1 + T_2 - T_3$. With $T_3 \ll T_1 + T_2$ the quotient K'/T', discussed in the beginning of Section 7, is

$$K'/T' = -\frac{\frac{1}{2} N_{cc\delta}'' \frac{c^2}{u^2}\left(1 + \frac{l_v''}{2}\right)}{k_{zz}^2 - N_{\dot{r}}'' + \frac{N_{ur}''}{Y_{uv}''}\left(1 - Y_{\dot{v}}''\right)} \tag{8.8}$$

i.e., it is proportional to the ratio of rudder-induced turning moment over ship inertia; the magnitude of K'/T' given by (8.8) is roughly just about a quarter of the value predicted for an uncoupled yawing

motion. It will be seen that denominator as well as numerator increases in shallow water, but that the over-all change will mean a reduction of this rudder-on-ship effectiveness factor.

Most modern large tankers are slightly unstable, or marginal stable, i.e. $l_r = l_v$. For such ships the pivoting point is given by the simple relation

$$\frac{\overline{OP}}{L} = -\frac{1 - Y''_{ur}}{Y''_{uv}} \tag{8.9}$$

which may be approximated by $\frac{\overline{OP}}{L} = 0.45 + \frac{1}{3}(\delta_{pp}\frac{B}{T} - 2)$. For a typical tanker this corresponds to $OP/L = 0.5$. (The formula in fact indicates an acceptable value also for the destroyer, about 0.3.) Again, the pivoting point position—or the drift angle β—is a critical parameter to study when entering shallow waters.

9. Confined Water Flow Phenomena and Some Results from Theory

Mainly on Resistance

In his notes for a third volume of "Hydrodynamics in Ship Design" SAUNDERS collected a number of citations, ranging from SCOTT-RUSSEL to MOODY, which all illustrate the classical picture of ship behaviour in confined waters as it has been derived from observations in full scale and in model tests, [78]. He also concluded that, by 1960, the ventures and progresses made in analytical studies of ship manoeuvring in shallow waters remained scarce. One exception was offered by the papers by BRARD, [79]. The problems of interaction between meeting or passing ships, or between ships travelling abreast —closely related to the bank effect problem of the single ship—had been dealt with by WEINBLUM [80], HAVELOCK [81], and SILVERSTEIN [82].

Undoubtedly much more effort had by then been devoted to the changes of frictional and wave resistance of ships in axial motion in confined waters, and an important survey and contribution had been given by SCHUSTER [83].

Ocean-going ships generally move at low speeds in shallow or narrow waterways, and hence the deformation of the wave system

is small. According to SCHUSTER the wave resistance is not notably affected by a limited depth for speeds below $F_{nh}=0.7$, at which speed the excentricity of the orbital ellipse corresponds to a diameter difference of about 5 per cent. In case of a bottom depth of 15 m this again corresponds to a ship speed of 16 knots.

In ref. [84] WEINBLUM demonstrated that the wave-making in a canal is a complicated function of speed, depth and width. In general it is therefore not possible to define a single effective length to characterize the canal dimensions in a speed number. However, effective canal speed includes the back-flow, and just as a critical speed in shallow water is defined by the speed of the solitary wave, $\sqrt{gh}$, experimental evidence advocates a critical speed in a certain canal corresponding to a certain BOUSSINESQUE number $B=F_{nh}\sqrt{\frac{h}{\overline{W}}+1}$. (Here $\overline{W}$ is equal to half the mean width of the section.) For a rectangular section MÜLLER proved that the maximum wave resistance occured at $F_{nh}=(2\frac{h}{\overline{W}}+1)^{-1/2}$, [85]. In a canal 15 m deep and 120 m wide this correspond to $F_{nh}=0.81$. Again, let it be assumed that a significant change of the wave resistance due to the confinements will be found only at a speed equal to or higher than 70 per cent of this critical speed: this now gives a speed of about 13 knots, much to high to be experienced in canal transits involving normal blockage ratios. It may be concluded that the additional resistance terms to appear in the speed equation normally need not to account for the oscillatory wave-making components.

Reference shall here be given to recent studies of the unsteady flow conditions existing within a critical speed range for a ship in a canal; this range tends to zero when the width of the canal tends to infinity, [86], [87].

At sub-critical speeds the wave-making itself may influence the lateral force and moment on a ship moving along a bank, as shown by SILVERSTEIN, [82]. In case of the low FROUDE numbers met with in practice also these effects may probably be ignored, and the water surface thus be treated as a solid wall. At $F_{nL}=0.078$ or $F_{nh}=0.32$, realized for a 98,000 t.dw. tanker proceeding at a speed of 14 km/h through the Suez canal, the longitudinal waves will have a length of some 10 m, i.e. only 4 per cent of the length of the ship.

The back-flow producing an increase of frictional resistance will

also produce an increase of sinkage, and in case of small bed clearances this will of course indirectly affect the lateral forces sensitive to the clearance. These secondary effects must be born in mind when comparing predictions from theory with results from force measurements on models, which are free to heave and trim. In the normal evaluation and presentation of such measurements, however, it will be considered more practical always to use the nominal under-keel clearance.

The viscous resistance, including frictional as well as viscous pressure resistance, may be calculated accepting a plate friction line and a form factor, characteristic for the supervelocities along the hull. This resistance now may be written $[X^v]_{\overline{W}=h=\infty}=\frac{1}{2}X^v{}_{uu}u^2$, where u is the forward speed of the ship. In confined waters there are additional supervelocities, the effect of which is equivalent to a back-flow along the hull and waterway bottom, where another boundary layer is generated. The two boundary layers will reduce the effective under-keel clearance, which tend to increase the trim by stern. Separation and unsymmetrical eddy-making within the boundary layers may initiate yawing tendencies in straight running, or change the behaviour of the ship in manoeuvres.

GRAFF has suggested to consider part of the mean back flow, ΔU_b, to be due to the lateral restriction, and the other part, ΔU_h, to be due to the finite depth, [88]. In normal applications ΔU is small compared to u, so that

$$X^v=\frac{1}{2}X^v_{uu}u^2\left(1+\frac{2\Delta U_b}{u}\right)\left(1+\frac{2\Delta U_h}{u}\right)=\frac{1}{2}X^v_{uu}u^2(1+K_b)(1+K_h) \tag{9.1}$$

The effects of a plane bottom at distance h below the ship waterline and a pair of parallell vertical walls, each one at distance $\overline{W}$ from the ship centreline, are those produced by an infinite array of image bodies with spacings equal to $2h$ and $2\overline{W}$ respectively. At the double-body ship centreline the lateral perturbation velocities cancel whereas the axial components add together. (This simple concept is not valid for $\overline{W}$ or h small compared to B or T, in which case additional doublet distributions are required to prevent a deformation of the body contour.) GRAFF choose to calculate an approximate value of K_b for an elliptic cylinder, extending from the surface down to the bottom and having a beam given by the three-dimensional form displacement. (Thus K_b is dependent on canal depth,

although the final calculation is purely two-dimensional.) For the calculation of K_h he used an equivalent spheroid and results for supervelocities earlier published by KIRCH, [89]. His final results are given in graphs and compared with model measurements, which confirm that this method offers acceptable values of resistance allowances for moderate confinements. It is thereby also possible to define a suitable form of resistance derivatives to be evaluated from model experiments from case to case.

In particular, a limited re-analysis of some of the data given by GRAFF indicates that the resistance increase in shallow water will be proportional to the increase of an under-keel clearance parameter $\zeta = \frac{T}{h-T}$. Further analysis of the results for sinkage in shallow water according to TUCK's theory are likewise in favour of the use of this parameter. (See below.)

In waterways severely restricted in width as well as in depth the increase of resistance is a complex function of blockage conditions. From model tests with a Rhine vessel [90] it appears that the added resistance at a given forward speed may be approximated by an expression of the form $\Delta R = a \cdot \frac{BT}{Wh} + b \cdot \frac{BT}{Wh} \cdot \zeta$, or, roughly,

$$\Delta X(u, \zeta, \bar{\eta}) = \tfrac{1}{2} X_{uu\zeta\bar{\eta}} u^2 \zeta \bar{\eta} + \tfrac{1}{4} X_{uu\zeta\zeta\bar{\eta}} u^2 \zeta^2 \bar{\eta} \tag{9.2}$$

where $\frac{\bar{\eta}}{2} = \frac{L}{\overline{W}}$ is a bank spacing parameter defined from the mean width $2\overline{W}$ of the canal cross section. (See Section 10.)

The higher resistance in confined waterways is associated with a lower propeller efficiency, and the total propulsive efficiency is further reduced by an increase of the thrust deduction. The influence of flow restrictions on thrust deduction and wake factors has also been considered in a paper by GRAFF, [91]. In most simulator applications this latter influence may be ignored. However, the computed values of r.p.m. and speed attained at a given engine setting should be compared with, say, diagrams compiled by SJOSTROM, [92].

Sinkage and Lateral Forces in Shallow Water

Within the last decade the application of slender-body theory has furnished new understanding and quantitative estimates to the old

experience on sinkage and lateral motions in confined waters. Further developments of the theories and more accurate measurements are required to bridge a gap still remaining in force predictions.

In an essentially forward motion of the ship in shallow water the back-flow is increased all round the frame sections, and according to the first-order theory of TUCK the dynamic pressure is largely constant in the water around a cross-section of the hull and over the bottom bed close below it, [93]. Upon assumption of a water depth of same order as the draught, the draught and beam being small compared to the length of ship and waves, and by use of the new technique of "matched asymptotic expansions" TUCK derived formulas for the vertical forces and so also for the sinkage and trim at sub- and super-critical speeds.

In case of ships with fore-and-aft symmetry the theory predicts zero trim for subcritical speeds, and zero sinkage for supercritical speeds. For small to moderate FROUDE numbers based on depth the sinkage varies as speed squared, and, using the under-keel clearance parameter defined here, according to the upper curve of Fig. 22.

In ref. [94] TUCK has extended the theory to canals of finite width, in which the ratio of sinkage into the water (or trim) in the canal to the sinkage (or trim) in shallow water is given by a unique curve on basis of a simple width-and-speed parameter. Replotting this curve as in the lower diagram of Fig. 22 TUCK's results are shown to yield a square dependence on the bank-spacing parameter $\bar{\eta}$ when $F_{nh}{}^2 \ll 1$.

In canals presenting higher blockage the total sinkage or "squat" is dominated by the contribution from water level lowering as a consequence of flow continuity. From the BERNOULLIE and continuity equations an approximate relation for the hydrostatic ship sinkage in terms of ship lengths is given by

$$\sqrt{\frac{\varphi_L}{\alpha_{WL}}} \cdot \frac{\dfrac{A_o}{A_c} \cdot F_{nL}{}^2}{1 - \dfrac{A_o}{A_c} - \dfrac{LW_{beach}}{A_c} \cdot F_{nL}{}^2} \tag{9.3}$$

Here φ_L and α_{WL} are the prismatic and waterline-area coefficients of the ship. Other methods of the practical calculation of squat are discussed in ref. [95].

At low speeds wave making is concentrated to bow and stern of the ship, were changes of the local velocities do not influence the

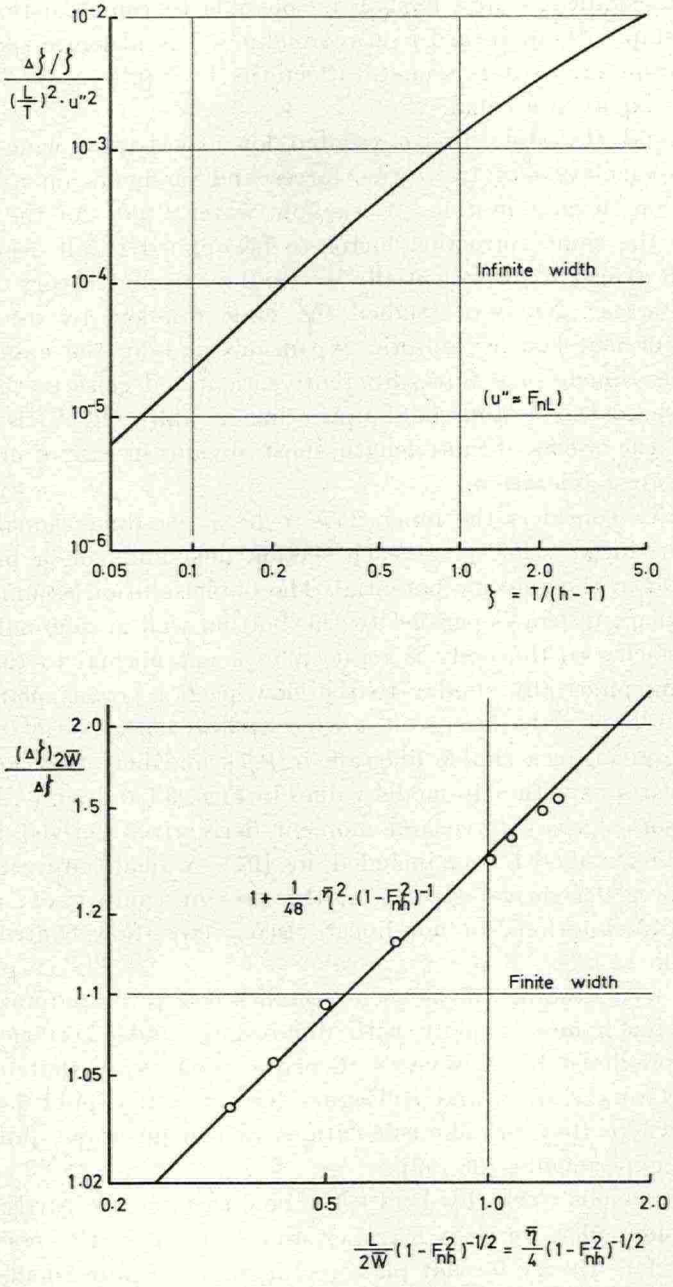

Fig. 22. Sinkage in shallow water of infinite and finite width, recalculated from TUCK's results.

blockage conditions, and it shall be possible to calculate the forces on the ship without regard to wave making. The absolute speed still is a parameter, as it is seen to affect the hydraulic as well as the dynamic squat in a canal.

KAN and HANAOKA first presented low-aspect-ratio wing results for the calculation of transverse forces and moments on a ship in oblique or turning motions in shallow water, [96]. As the theory predicts the same correction factor to be applied to all deep-water values it seems to be essentially a two-dimensional theory as it is in deep water. NEWMAN studied the same problem by use of the method of matched asymptotic expansions and by the assumption of a three-dimensional flow, differently orientated close to the body and close to the bottom (and upper image wall), [97]. His results bear out the effects of finite length, most obvious in case of moments due to yaw acceleration.

NEWMAN considers the inner flow to be a two-dimensional cross-flow of reduced velocity, at each section depending on a blockage parameter in the velocity potential. The outer solution assumes flow to take place in planes parallel to the bottom wall at nominal transverse velocity as the body is reduced to a cut normal to the flow, this being physically similar to the flow past a porous plate. The results as applied to forces on a wing of low aspect ratio (or to a ship) are given in a simple diagram in [97], and here they are used for comparisons with ship model values in Figs. 38 and 39. (A limited comparison of sway force and moment derivatives derived for the SSPA tanker model was included in [97]. A small adjustment of model force derivative appears in the present comparison, due to modified assumptions for non-linear viscous cross-flow contribution; cf. Section 11.)

Model tests results will be seen to indicate that the lateral forces increase much more rapidly with diminishing under-keel clearance than is predicted by NEWMAN's theory as well as by that of KAN and HANAOKA. INOUE and colleagues have recently published two papers, where they present calculations, which do agree quite well with the experiments, [98, 99].

As in previous works by INOUE the new theories are partly based on the main ideas of VON KÁRMÁN and BOLLAY in the non-linear lifting surface theory for flat plate rectangular wings of small aspect ratio, [100]. BOLLAY assumed a constant strength of bound vortices and downwash along the span, and calculated the variation of vortex

intensity along the chord as well as the effective angle at which the horse-shoe trailing vortices leave the tip chord from the boundary conditions. The general results for the normal force coefficient include a linear term, which agrees with the PRANDTL solution for infinite aspect ratio in the one extreme, but also a non-linear term, which in the other extreme of zero aspect ratio equals NEWTON's value for inelastic impact, $2 \sin^2 \alpha$. In Section 6 above the linear contribution was taken to be predicted by JONES' zero-aspect-ratio wing theory, which postulates an elliptical distribution of vortex strength along the span [38], whereas the non-linear effects then were estimated from a separate consideration of cross-flow drag. It appears that both approaches may be accepted on the assumption that the constancy of vortex strength along the span in BOLLAY's theory is mainly attributed to the non-linearities; INOUE also introduced correction factors to account for viscous effects.

In ref. [98] the shallow water effects in the four stability derivatives were derived in analogy with the unbounded flow case but by inclusion of infinite arrays of vortex images. In Fig. 23 the results are presented as recalculated on basis of the under-keel clearance parameter ζ; comparisons with experiments are given in Fig. 38. The final results for Y_{uv} and N_{uv} in channels of finite width were obtained by use of additional infinite images [99], and they are here compared with experimental values in Figs. 40 and 41.

Side Wall Effects in Deep and Shallow Waters

The lateral forces acting on a body in an unsymmetrical field of flow are well known to their effects: bank suction and interaction between ships on parallel courses have already been mentioned in the beginning of this Section.

A full-bodied deep-draughted ship that proceeds parallel to the vertical bank on one side of a wide canal presents an almost two-dimensional problem of great importance; the simple flow around a RANKINE oval in presence of a vertical wall will be derived to illustrate the geometry of the interference, but also the failure of this approach for small wall clearances. (The oval in a symmetrical flow between two parallel walls has been studied by BORDEN, [101].)

Consider a two-dimensional homogeneous flow U_0 parallel to the negative axis x, into which are introduced a line source at $(a, -id)$ and a line sink at $(-a, -id)$, both of strength m per unit length

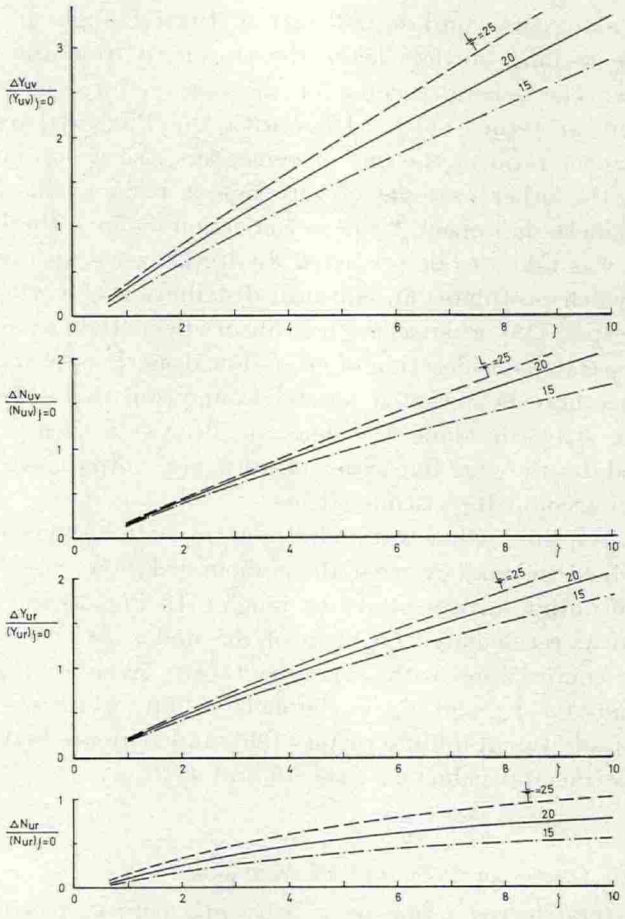

Fig. 23. Relative change of the stability derivatives with variation of water depth parameter ζ, as predicted by INOUE theory for hulls with different L/T ratios.

perpendicular to the complex plane $\xi = x + iy$. The dividing streamline (with $\Psi = -U_0 d$) defines a RANKINE oval of length $2l$ and beam $2b$.

The length-to-beam ratio is governed by the parameter $\frac{m}{aU_0}$ through the relations

$$\left.\begin{aligned} \frac{b}{a} &= \frac{2m}{aU_0}\tan^{-1}\frac{a}{b} \\ \left(\frac{l}{a}\right)^2 &= 1+2\cdot\frac{m}{aU_0} \end{aligned}\right\} \qquad (9.4)$$

With $m=0.0633\ aU_0$ the ratio is $l/b=6$. The water-line coefficient for the same oval is $\alpha_{WL}=0.882$.

To a first approximation the effect of a rigid wall along the x axis, dividing the homogeneous flow far ahead of the body, is that produced by the image line source and sink at (a, id) and $(-a, id)$, respectively; the original oval is slightly distorted, however, and its complete restoration would require an infinite number of successive images in the rigid wall and in the oval boundaries. In the first approximation the complex potential is given by

$$w=U_0\xi-m[\ln(\xi-a+id)+\ln(\xi-a-id)]$$
$$+m[\ln(\xi+a+id)+\ln(\xi+a-id)] \tag{9.5}$$

and the equation of the stream function by

$$\frac{\Psi}{aU_0}=\frac{y}{a}+\frac{m}{aU_0}\left[\tan^{-1}\frac{2\left(\frac{y}{a}+\frac{d}{a}\right)}{1-\left(\frac{x}{a}\right)^2-\left(\frac{y}{a}+\frac{d}{a}\right)^2}\right.$$
$$\left.+\tan^{-1}\frac{2\left(\frac{y}{a}-\frac{d}{a}\right)}{1-\left(\frac{x}{a}\right)^2-\left(\frac{y}{a}-\frac{d}{a}\right)^2}\right] \tag{9.6}$$

Some calculations for the oval with $l/b=6$ have been performed by use of an analogue computer. In Fig. 24 are shown the (degenerated) contours and a few streamlines for ovals at distances $d=0.5a$ and $d=0.33a$ from the rigid wall. The velocity distribution along the wall is given by

$$\frac{U_x}{U_0}=-1-2\,\frac{m}{aU_0}\left[\frac{\frac{x}{a}+1}{\left(\frac{x}{a}+1\right)^2+\left(\frac{d}{a}\right)^2}-\frac{\frac{x}{a}-1}{\left(\frac{x}{a}-1\right)^2+\left(\frac{d}{a}\right)^2}\right] \tag{9.7}$$

and the dimensionless change of pressure, $\frac{\Delta p}{q_0}(x)=1-\left(\frac{U_x}{U_0}\right)^2$, is also shown in Fig. 24.

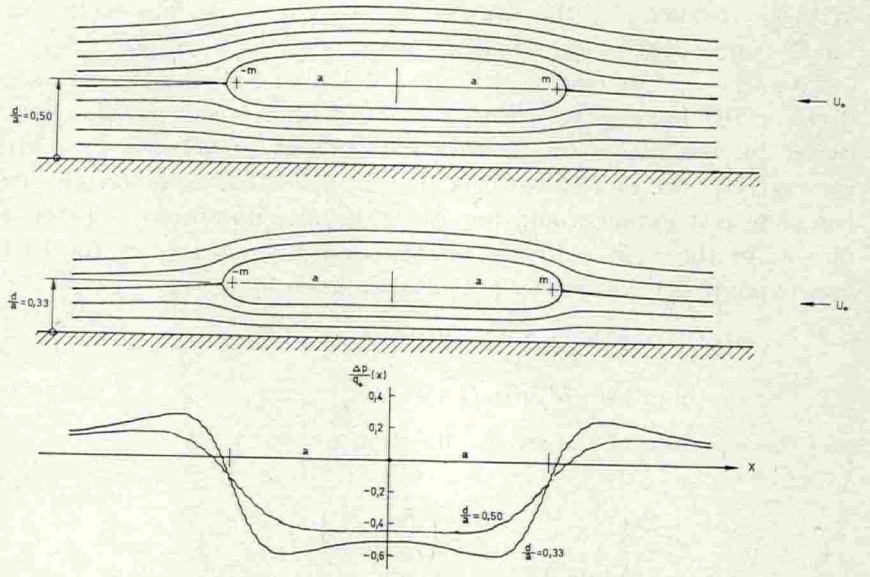

Fig. 24. Streamlines around degenerated ovals moving parallel to a vertical wall, and variation of pressure along the wall.

Close to the rigid wall the streamlines are forced to run almost parallel to it, but at some distance they are curved, which influences the velocity distribution in planes normal to the wall. For $d=a$ the supervelocity past the body midship section is 20 per cent higher than at the wall, but as the body is brought closer to the wall the variation of the velocity over the gap is progressively smaller. Finally the degenerating oval develops a camber, and the reversed curvature of the streamlines is now responsible for a velocity drop throughout the gap and especially close to the contour. From the curves of wall pressures in Fig. 24 it appears that the first order image theory for the oval here may perhaps be valid for a distance as small as $d=0.50a$, but certainly not for $d=0.33a$. (For $d=0.33a$ the gap between original body contour and wall equals $0.15a$, or $0.42B$.)

Far ahead of the body (where $\left(\frac{x}{a}-1\right)^2 \gg \left(\frac{d}{a}\right)^2$) the pressure on the wall is essentially independent of the distance d. End effects from short banks will be felt at a longitudinal distance of $1.5L$ forward of bow or aft of stern, and transient phenomena will dominate during

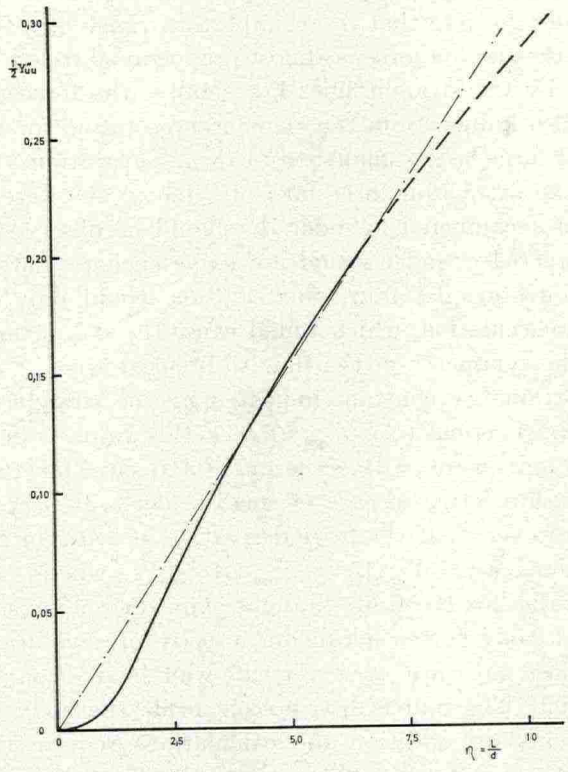

Fig. 25. Force derivative $\frac{1}{2}\, Y''_{uu}$ versus wall-distance parameter η for oval ($L/B=6$) moving parallel to vertical wall.

the passage of a bank which is, say, of a length less than six times the length of the body.

The area of negative pressures abreast the body is gradually shortened as wall distance is reduced, but within the validity of the theory the minimum pressure still becomes lower. Remembering that Y'' is the lateral force related to body weight the attraction-force-forward-speed derivative of interest is

$$\frac{1}{2}\, Y''_{uu} = -\frac{\frac{l}{b}}{2\alpha_{WL}\,\frac{l}{a}} \int_0^\infty \frac{\Delta p}{q_0}\; d\left(\frac{x}{a}\right) \tag{9.8}$$

where α_{WL} is the water-line coefficient. The result for $\frac{1}{2}\, Y''_{uu}$ is displayed versus the wall-distance parameter $\eta = \dfrac{L}{d}$ in Fig. 25.

It is of interest to note that in an important range of η for practical applications the suction force is almost proportional to this parameter, as indicated by the straight line. For small η the force grows more rapidly, as also known from the elementary solution for the circular cylinder. For large η, or small body-to-wall separations, the rate of increase of the attraction force falls off, due to the degeneration of the oval into a cambered cylinder. It should be observed, however, that the cambered cylinder would not experience any lateral force if alone in an irrotational flow; such a force could only develop in presence of a circulation, which would cause the stagnation points to move, and the symmetry of the flow to break down.

The proportionality constant indicated by the straight line shown in the diagram is equal to $\frac{1}{2} Y''_{uu\eta} \approx 0.030$; this value is in reasonable quantitative agreement with experimental results for three-dimensional model ship forms in case of small under-keel clearances. It is suggested, however, that the force derivative in water of finite depth will be obtained as $(\frac{1}{2} Y''_{uu\eta})_\zeta = \frac{1}{2} Y''_{uu\eta} + \frac{1}{2} Y''_{uu\eta\zeta}\zeta$, where $\frac{1}{2} Y''_{uu\eta}$ is the deep-water value for the finite-draught ship. (See next Section.)

The lateral body forces acting on a body of revolution in axial motion in close presence of a vertical wall have been studied by NEWMAN, [102]. The source distribution inside the body is mirrored in the wall, and in addition the calculations require the original distribution to be off-set towards the wall. This three-dimensional source distribution defines the velocity potential and so the forces may be found by use of the LAGALLY theorem. The result again is an attraction towards the wall, now increasing monotonically up to a finite value at body-and-wall contact. With present notation—and with ∇ equal to the displacement of the submerged half of a body of revolution at low FROUDE number—

$$\frac{1}{2} Y''_{uu} = -\frac{\pi}{4} \cdot \frac{b_0^3}{2\nabla} \int_{-1/2}^{1/2} \frac{\left\{ \dfrac{\partial}{\partial\left(\dfrac{x}{L}\right)} \left[\dfrac{A}{A_0}\left(\dfrac{x}{L}\right) \right] \right\}^2}{\left\{ \left(\dfrac{d}{b_0}\right)^2 - \dfrac{A}{A_0}\left(\dfrac{x}{L}\right) \right\}^{1/2}} \cdot d\left(\frac{x}{L}\right) \qquad (9.9)$$

In the analogue expression for the moment derivative $\frac{1}{2} N''_{uu}$ the integrand includes the factor x/L.

It is concluded that for geometrically related bodies with same sectional-area distribution the suction force will be inversely pro-

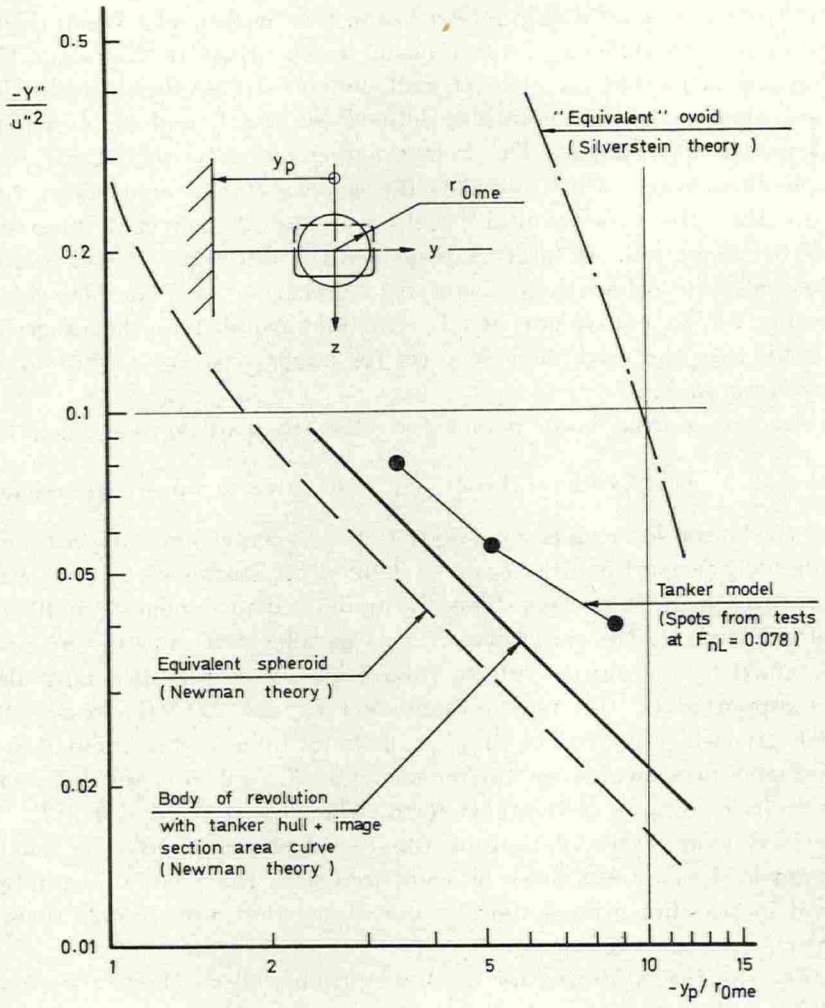

Fig. 26. Lateral force on a body moving parallel to a vertical wall. Measurements on propelled tanker model and theoretical results for bodies of revolution.

portional to the length, whereas the yawing moment will be independent of length variation. The results also indicate that there will be a bow-away-from-wall moment for bodies with a stern, which is blunt compared to the bow, and vice versa.

In Fig. 26 calculations by NEWMAN's method are compared with the results of force measurements on a tanker model towed along

the vertical wall of a ship model basin. (Cf. Section 11.) Basin depth was equal to $0.29 \cdot L_{pp}$, total basin width equal to $2.7 \cdot L_{pp}$. The diagram is plotted on ratio of wall distance to maximum radius of equivalent body of revolution, defined by length and displacement of model hull+image. The better agreement is obtained for that equivalent body, which also has the same sectional area curve, but even then the experimental results are some 25 per cent in excess of the prediction. At larger separations the difference is still larger. Comparative calculations using SILVERSTEIN's "not-too-near-wall" results for an equivalent ovoid, [82], are included in the diagram; in this case the prediction is better for larger separations, but in all much too high.

As long as the body is not too close to wall contact—i.e., for $\left(\frac{d}{b_0}\right)^2 \gg 1$—the NEWMAN theory, eq. (9.9), gives a linear dependence for the lateral force on ratio of body radius to centre-line wall distance; thus it is proportional to η_s or η_p defined for starboard or port wall distances in next Section. This linear dependence suggests that the lateral force on the ship between two parallel vertical walls may be obtained by adding the effects from each one, which idea may also be supported by the new presentation of old DTMB data [103, 104] given in Fig. 27. The diagram includes force and moment measurements on a twin-screw tanker model at $F_{nL}=0.05$ in several canal sections of simple rectangular form. The dotted curve for $h/T=1$, derived from extrapolation of the experimental results for small under-keel clearances, may be compared with the prediction for the oval in two-dimensional flow by use of the first-order image theory earlier given in Fig. 25.

The theoretical results for bow-away-from-wall moments are somewhat modified in practice, where bow wave and screw action contribute to make the tendency felt in ships of all types. Thus, in general a ship that moves off the centre-line of a canal must use helm towards the near wall and it takes up a small bow-from-wall equilibrium angle. Typical values derived from [103] for the 721′ tanker off-set 50′ from centre-line of the $500' \times 45'$ section are 15° helm and 1° drift.

On Changes in Lateral Cross Flow Drag

The motion in shallow port approaches may involve much larger drift angles, and the behaviour of the ship is markedly affected by

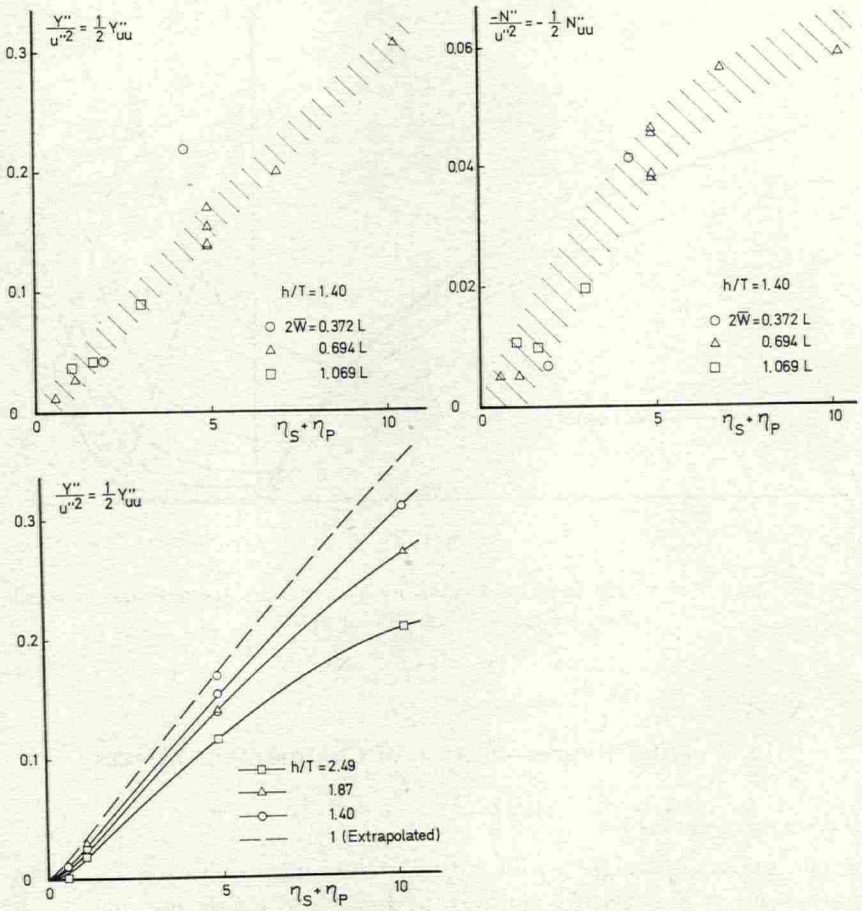

Fig. 27. Asymmetric forces and moments on a twin-screw tanker model moving parallel to the vertical walls of canals of differing widths and depths — $F_{nL} = 0.0505$.
(From DTMB test data.)
Upper curves: Constant depth. Lower curves: Varying depths.

the increase of lateral cross flow resistance due to under-keel blockage. The diagram in Fig. 28 is compiled from shallow water test data in ref. [50], and from Japanese data in ref. [105], which also includes measurements in presence of a wall. Again the parameters ζ and η are used for the presentation. For moderate ζ cross-flow drag increases in proportion to ζ, just as the linear force derivatives, but the dependence on η is of higher order. The cross-coupling between ζ and η may probably be ignored in practical applications.

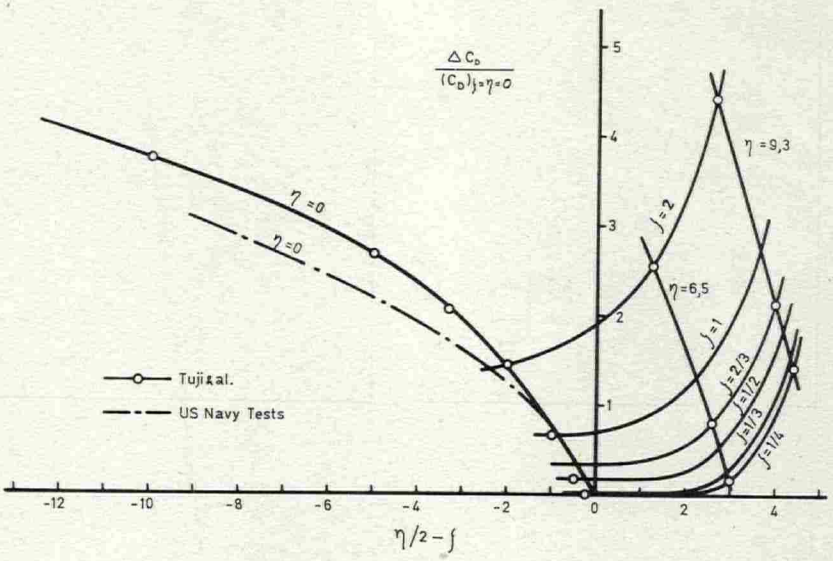

Fig. 28. Corrections to ship model cross-flow drag coefficients due to change of depth and presence of vertical wall.

10. Formal Representation of Confinement Effects

Waterway Description

The uniform straight canal with a rectangular section is the most simple case of a waterway confined in depth and width, but even there several parameters are required to characterize the flow phenomena taking place. It was seen in the last Section that the wall distance parameter η and the under-keel clearance parameter ζ both were useful tools for the description of certain effects. Their first merit, of course, is due to the zero values defined in unrestricted deep water.

Figs. 29 and 30 show a more general section of a canal. Such a canal is usually described by its mean depth between the bed lines, its widths at bed and beach lines, and its cross-section area, related to the midship section of a transiting ship by the blockage ratio. The position of the ship in the canal is mostly given by the off-centre distance, and by the angle to the canal centre-line. Here approximate expressions involving the new parameters only will be given for the main geometric characteristics.

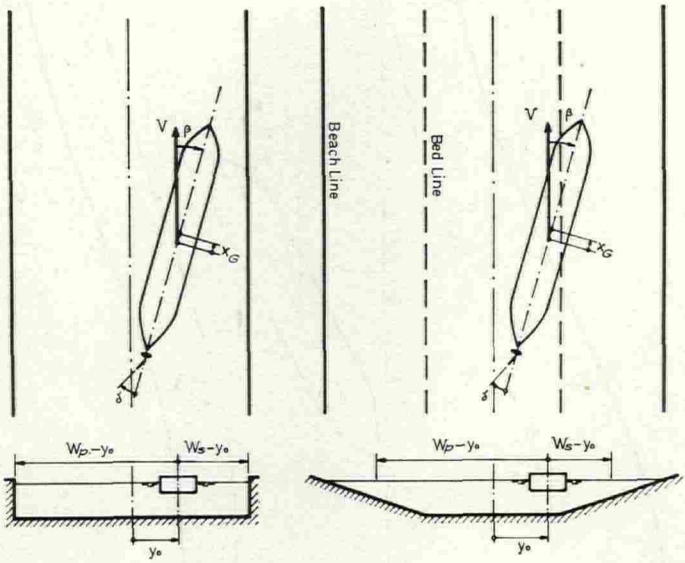

Fig. 29. Ship moving parallel to walls in a straight canal.

The depth h is considered constant between the bed lines. The mean width $2\overline{W}$ is defined as the quotient between cross-section area A_c and depth h. The ratio $2\overline{W}/B$ is a better parameter for width-to-beam relations the more shallow is the canal. For use with theoretical results for thin ships the width parameter will here not be related to beam but to ship length L.

As seen from Fig. 30 the bank and ship positions may be given by co-ordinates normal to a datum line essentially parallel to the main direction of the canal. The orientation of the ship is given by the heading angle ψ, measured from the same datum line. The basic geometric parameters are defined as

Under-keel clearance parameter	$\zeta=T/(h-T)$	
Port bank distance parameter	$\eta_p=L/(W_p-y_0)$	(10.1)
Stbd bank distance parameter	$\eta_s=L/(W_s-y_0)$	

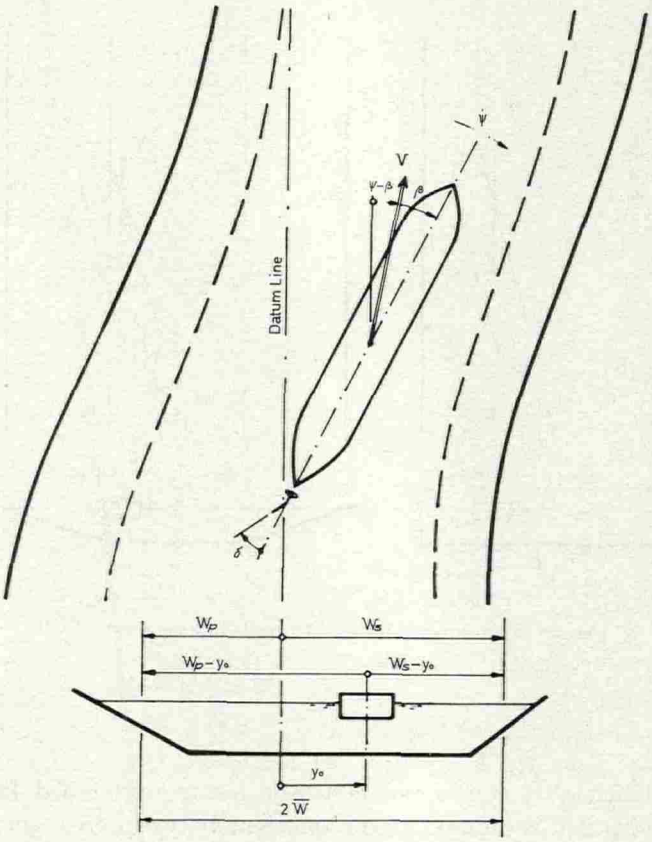

Fig. 30. Ship moving in a canal of slowly changing form.

Note that $W_s > y_0 > W_p$, so that $\eta_s > 0$ and $\eta_p < 0$. It is also convenient to introduce

$$\begin{aligned} \eta &= \eta_s + \eta_p \\ \bar{\eta} &= \eta_s - \eta_p \end{aligned} \tag{10.2}$$

The mean width of the canal at the station considered is

$$2\overline{W} = W_s - W_p = -\frac{\bar{\eta}}{\eta_s \eta_p} \cdot L \tag{10.3}$$

where the parameter ratio in the right member is constant for all lateral positions of the ship in the cross section. Especially, when ship on centre-line so that $\eta_s = -\eta_p = \bar{\eta}_0/2$, there is $\dfrac{L}{2\overline{W}} = \bar{\eta}_0/4$.

In fact $\bar{\eta}/4$ alone is an acceptable approximation to the "ship length-to-canal width" parameter ratio also at ship positions slightly off-set from the centre-line: with $y_0=\overline{W}/4$ $\bar{\eta}/4$ over-estimates the ratio $\frac{L}{2\overline{W}}=\bar{\eta}_0/4$ with less than 7 per cent. As a consequence $\bar{\eta}$ and ζ may be used to define an approximate blockage ratio

$$\frac{BT}{2\overline{W}h}=\frac{1}{4}\cdot\frac{B}{L}\cdot\frac{\bar{\eta}\zeta}{1+\zeta} \tag{10.4}$$

For small ζ the blockage ratio is proportional to $\bar{\eta}\zeta$, for large ζ to $\bar{\eta}$ alone.

Force Representation

The assymmetric forces appearing in presence of a single wall or in a canal are highly increased by an increase of the under-keel clearance parameter, and the general model will include complex couplings. If a single canal depth is studied on basis of special model tests it is of course possible to express the wall effect forces in terms of η_p and η_s only. Although the geometry of the inflow to the propeller may be modified in confined water it is assumed that the control derivatives remain unchanged and that changes of rudder forces are due to changes of screw loading only.

When suitable theoretical and experimental information becomes available it shall be possible to include the effects of ship motions towards the wall and of the angular orientation along it. At present solution to the problem of motions oblique to a wall seem to be known only for elementary singularities such as circular cylinders and spheres, [106]. In particular, these results give a repulsion by the wall on the body moving toward or away from it, but, again of course, an attraction on the body moving parallel to it.

For the present investigation it shall be assumed that the effects of the walls on a ship moving not to close to them will be approximated by the quasi-steady asymmetry, and that the added masses may be taken as those derived for low-frequency oscillations in the centre of the confinement.

In the previous Section was shown that the attraction force on the ship in motion parallel to a wall is essentially inversely proportional to the separating distance, i.e. $Y(u,\eta_s)=\frac{1}{2}Y_{uu\eta s}\cdot u^2\eta_s$, and

that the effects of two walls may be approximated by superposition. Thus for $Y(u, \eta_s, \eta_p)$

$$\tfrac{1}{2}\, Y_{uu\eta s} u^2 \eta_s + \tfrac{1}{2}\, Y_{uu\eta p} u^2 \eta_p = \tfrac{1}{2}\, Y_{uu\eta} u^2 \eta \qquad (10.5)$$

where $Y_{uu\eta} = Y_{uu\eta s} = Y_{uu\eta p}$.

As the ship moves closer to one of the walls, or as the walls are closer, this expression shall be completed by terms in η_s^2 and $|\eta_p|\eta_p$, or alternatively, in $\eta\bar{\eta}$.

The effect of a limited bottom depth is included by additional terms in $\eta\zeta$ and $\eta\bar{\eta}\zeta$. The forces due to steady sway and yaw are assumed to be increased in proportion to $uv\bar{\eta}$ and $ur\bar{\eta}$, and to $uv\bar{\eta}\zeta$ and $ur\bar{\eta}\zeta$ respectively. The dependence of added inertias on the confinements are represented by terms in $\dot{v}\zeta$ and $\dot{v}\bar{\eta}^2\zeta$, $\dot{r}\zeta$ and $\dot{r}\bar{\eta}^2$, all so far evaluated from the results published by FUJINO, [5].

11. Model Tests

Test Program and Model

Six years ago an experiment program was designed for a tanker model with a view to put to test and improve the analytical model set up as well as to obtain basic simulator data for a first canal transit study. Full scale measurements should subsequently be made with the 98,000 t.dw. prototype in the Suez Canal, but as things went about these plans could not be fullfilled.

In November 1965 a first series of three-component force measurements were ordered to be run with a 1:70 scale model at the VBD Laboratories in Duisburg. The test program included straight-line oblique towing of the propelled model in "deep" and shallow water in the large Shallow Water Tank and rotating arm tests at same depths in the Manoeuvring Tank. It also included straight-line oblique towing of the same propelled model in two Suez-Canal-type sections with a water depth equal to that of the shallow water tests. Most of these tests were run at self-propulsion point of model, determined from straight course speed runs in the waterways studied. All tests were performed at maximum "Suez draught". Resistance and propulsion tests had earlier been completed at SSPA with a 1:35 scale model on several draughts, and ship speed trials were analyzed to support the prediction of full scale screw loadings and control derivatives on model test draught. (Cf. Section 7.)

Additional tests in the VBD Shallow Water Tank were ordered in April 1966 to establish near-to-wall stiffness derivatives from straight-line motion close to one of the vertical basin walls in "deep" water. After a series of repeated tests with a modified recording system the full captive model test program was completed in April 1967. The preliminary test data are included in reports [107] and tables from VBD.

The test program is condensed in Table III and in Figs. 31 and 32, these illustrating the proportions involved. In all the tests the model was free to heave and trim in its xz-plane by fore and aft linkages attached to a heavy beam, this beam again hanging in a long parallel pendulum arrangement from the top of the carriage or rotating arm, and orientated according to the drift angle desired. Different damping devices were tried in order to control the long period surge and the mechanical oscillations induced by the carriage. There was no evidence of any effect on the lateral forces of a periodic shedding of vortices in the wake. The lateral forces at bow and stern as well as

Table III. Test program for the MALMÖHUS model ($L_{pp}=3.614$ m, $T=0.165$ m).

Series		FW	RAF	NW	SW	RAS	CS I	CS II
Waterway designation		Free water	Free water	Near to wall	Shallow water	Shallow water	Canal I	Canal II
Model dimensions:								
Water depth, h	mm	1050	1050	1050	214	214	214	214
Basin diameter, $2R_b$	mm	—	24500	—	—	24500	—	—
Tank width, W_{bed}	mm	9800	—	9800	9800	—	1020	1200
Tank width, W_{beach}	mm	9800	—	9800	9800	—	2300	2484
Tank width, $2\overline{W}$	mm	9800	—	9800	9800	—	1660	1842
$\zeta=T/(h-T)$		0.19	0.19	0.19	3.37	3.37	3.37	3.37
L/R_b		—	0.29	—	—	0.29	—	—
$\frac{\overline{\eta}_0}{4}=L/2\overline{W}$		0.37	—	0.37	0.37	—	2.18	1.96
Parameter variation:								
Range of $r'=L/R$		—	$-0.36-+0.54$	—	—	$-0.36-+0.54$	—	—
Max η_s or $\lvert\eta_p\rvert$		0	—	4.33	0	—	7.95	6.63
Range of β or ψ		± 6	0°	± 6°	± 6°	0°	± 6°	± 6°
Range of δ		± 25°	0°	0°	± 25°	0°	± 25°	0°

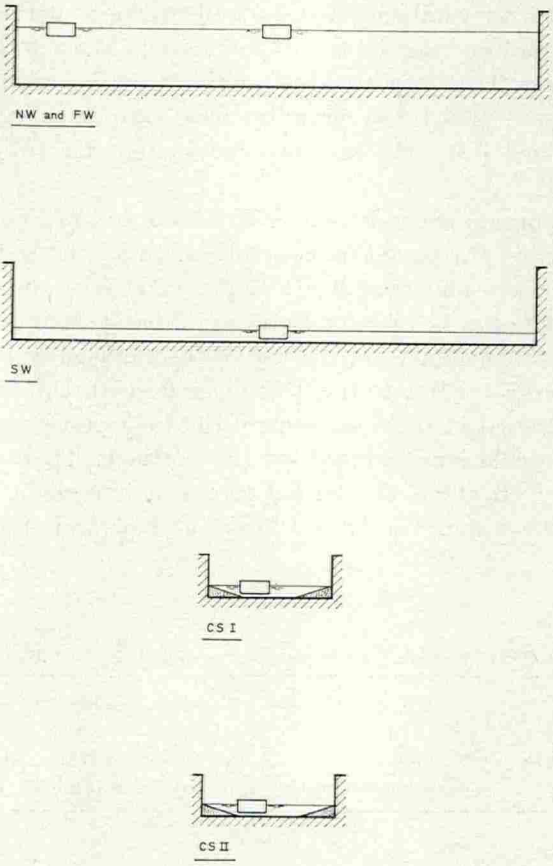

Fig. 31. Waterway sections in oblique towing tests. (Labels refer to test series in Table III.)

the unbalanced towing force supplied amidship were measured by means of electrical resistance wire strain gauges.

It shall be observed that no acceleration derivatives could be obtained from these tests. Most of the force measurements, were made at a model speed of 0.465 m/s, corresponding to a ship speed of 7.6 knots or 14 km/h.

The ship prototype was the 98,000 t.dw. single-screw/single-rudder turbin tanker MALMÖHUS delivered from K o c k u m s to M a l m-

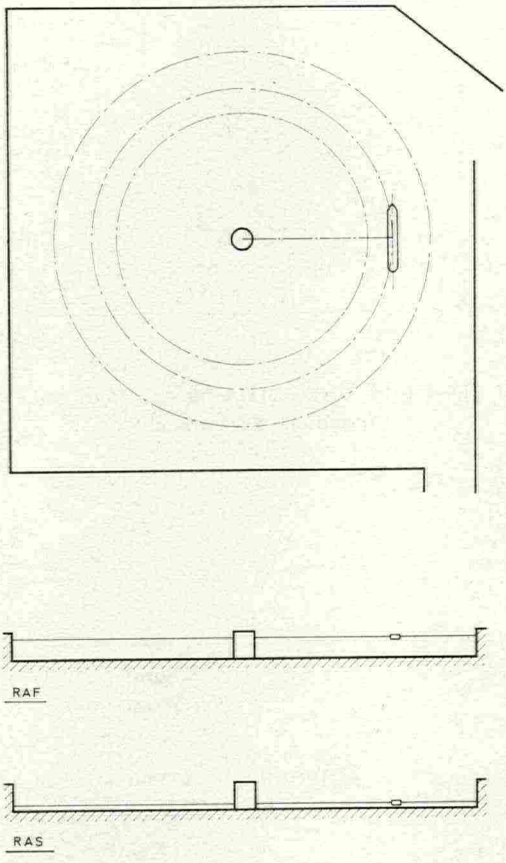

Fig. 32. Waterway sections in rotating arm tests.

ros Rederi AB in October 1965 for use in the crude oil trade through the Suez Canal on a reduced draught. The main dimensions of ship and 1:70 scale model are given in Table IV, and the body plan is shown in Fig. 33. The permission to publish these details is gratefully acknowledged.

The prototype has a Mariner-type rudder, normal bow and no bilge keels; a few tests were run to investigate the effects of a bulbous bow and of bilge keels of common design.

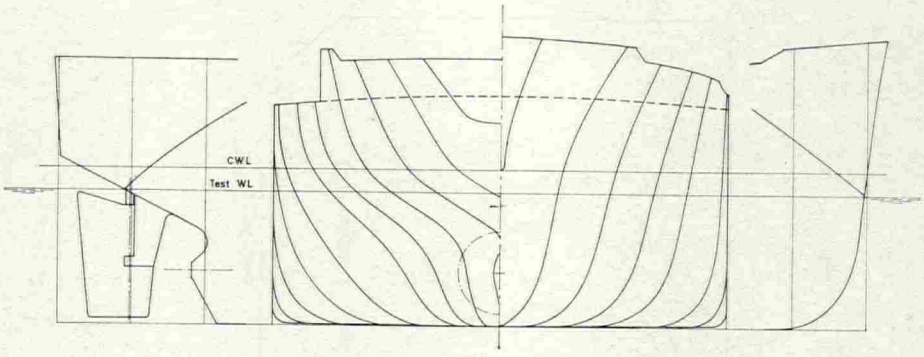

Fig. 33. Model of 98,000 t.dw. tanker MALMÖHUS — Body plan and profiles. Model tested on "Suez draught".

Table IV.

		Ship (T/T MALMÖHUS)		1:70 Model (VBD Model)
Length, $L_{pp}=L$	m	253.00		3.614
Beam, B	m	38.94		0.556
Design draught, T_{CWL}	m	13.45		0.192
Suez draught (38′), T	m	11.58		0.165
Displacement, Suez draught, ∇	m^3	91.933		0.2680
Slenderness ratio, Suez, $L_{pp}/\nabla^{1/3}$	—		5.606	
Midship coefficient, Suez, β	—		0.991	
CB forward of $L_{pp}/2$, x_G/L_{pp}	—		+ 0.0185	
Long. radius of gyration/L_{pp}	—		0.23	
Propeller diameter, D	m	7.15		0.1021
Pitch ratio, P/D	—		0.74	
Area ratio, A_d/A_0	—		0.65	
Number of blades, z	—		5	
Rudder area, total, A_r	m^2	64.8		0.0132
Horn area/A_r	—		0.182	
Relative rudder area, $A_r/L_{pp}T$	—		0.0221	
Height at stock, b	m	9.80		0.140

Results for Force and Moment Coefficients

Figs. 34–37 show plot of force and moment coefficients from tests in deep (free) and shallow water, and the analytical approximation obtained by stepwise regression analysis. Results from the near-to-wall experiments have been given in Fig. 26.

In the evaluation it was consistently assumed that the changes of first and second order derivatives due to finite depth could be approximated by terms proportional to ζ. As the tests did include two values of ζ only, one of which very small, this does not effect the derivatives derived for the setwo depth conditions, nor the "true-deep-water" values.

Further, because of the scatter of experimental data it proved suitable to perform the analysis with an assumed value for the deep-water cross-flow resistance corresponding to $C_D=0.7$; cf. Section 6.

In agreement with earlier findings the test results indicate a very marked influence of shallow water on the non-linear force contributions, and on the lateral force due to yaw in particular. It shall be observed that the analysis involves a change of sign in the first-order rotary force derivative as water depth is reduced.

The force and moment derivatives derived from shallow water and canal tests will be presented in the next Section.

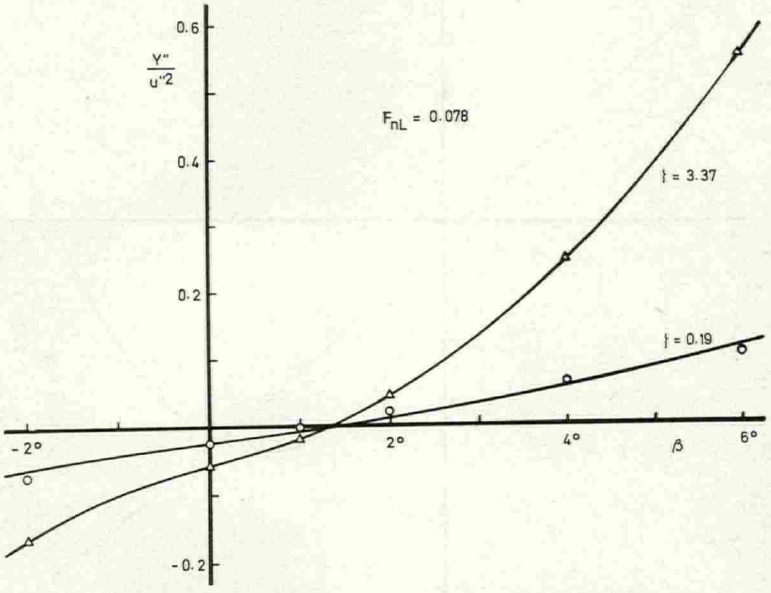

Fig. 34. The MALMÖHUS model — Force coefficient $Y''(\beta)/u''^2$ in deep and shallow water.

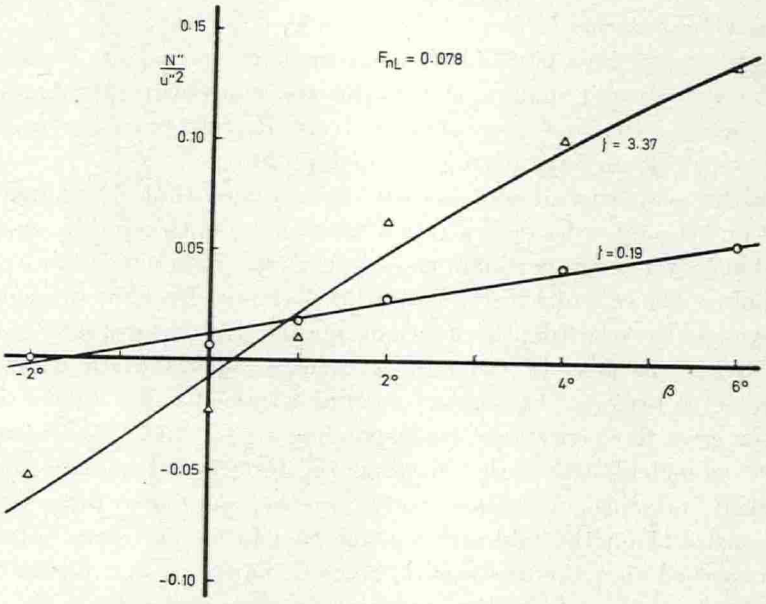

Fig. 35. The MALMÖHUS model — Moment coefficient $N''(\beta)/u''^2$ in deep and shallow water.

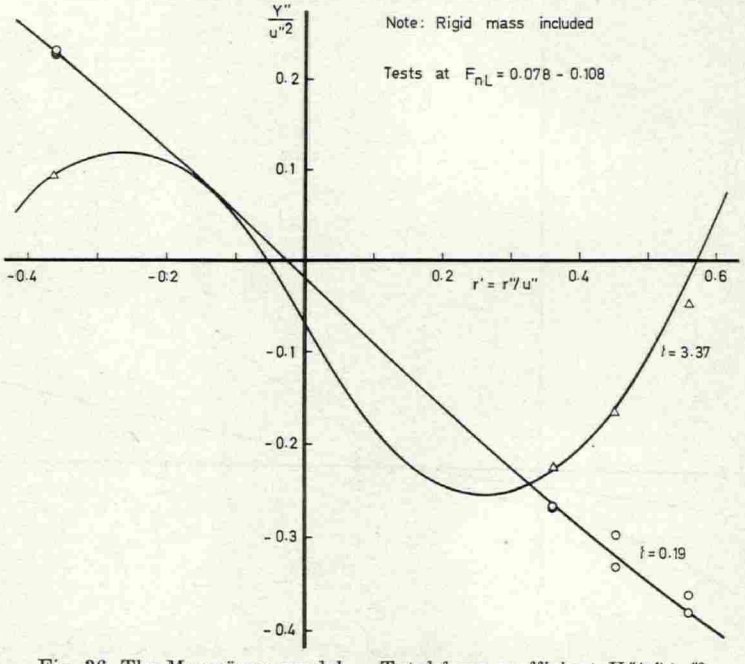

Fig. 36. The MALMÖHUS model — Total force coefficient $Y''(r')/u''^2$ in deep and shallow water.

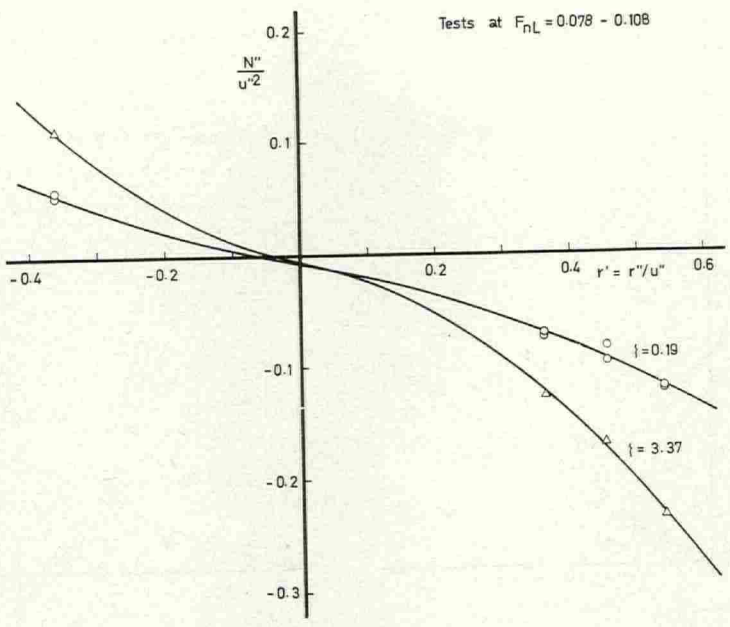

Fig. 37. The MALMÖHUS model — Moment coefficient $N''(r')/u''^2$ in deep and shallow water.

12. Results for Confinement Derivatives

Figs. 38–45 present some of the empirical or semi-empirical results available for the main lateral hydrodynamic derivatives, which appear in the confinement terms of the completed mathematical model. The derivatives $Y_{uv\eta}$ and $N_{uv\eta}$ as well as $\frac{1}{2}\, Y_{uu\eta}$ and $\frac{1}{2}\, N_{uu\eta}$ for the MALMÖHUS model have been derived from the near-to-wall tests in deep water, which results are not shown here. ($\frac{1}{2}\, Y''_{uu\eta}$ may be found from the diagram in Fig. 26, however.)

In Fig. 38 the shallow water results obtained for the MALMÖHUS model (SSPA tanker) are compared with similar experimental results published by FUJINO, [5], and with calculations by use of the theories of NEWMAN [97] and INOUE [98]. The SSPA test analysis is based on a linear dependence of the derivatives on ζ and the results are consequently given by plots on straight lines in the diagrams. FUJINO's derivatives are evaluated separately for each depth.

As already known from Fig. 23 the theory is in support of the

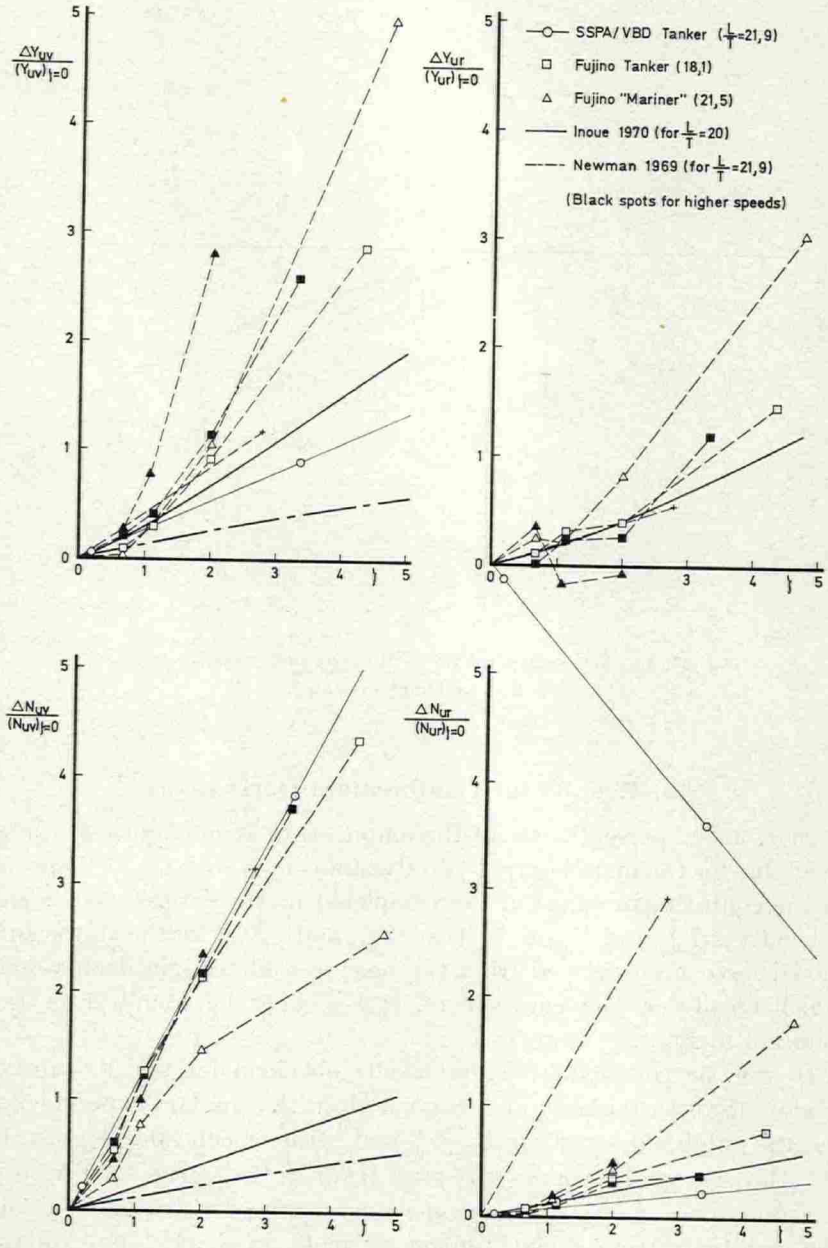

Fig. 38. Stability derivatives as influenced by finite depth — Results for SSPA model of tanker MALMÖHUS compared with FUJINO tests and with INOUE and NEWMAN theories.

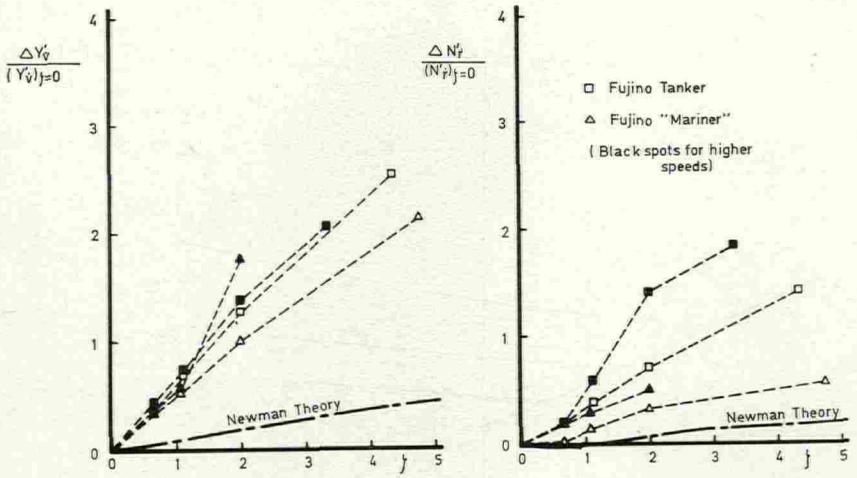

Fig. 39. Increase of linear and rotary acceleration derivatives with increase of parameter ζ according to FUJINO tests and NEWMAN theory.

mainly linear dependence on ζ, and this is essentially confirmed by the experimental results. In general the theory seems to underestimate the effects of the finite depth, however, especially in the stiffness moment. It is not impossible that some of the non-linearity with ζ inherent in the experimental curves for ΔY_{uv} and ΔN_{ur} may originate from an ignorance of the large cross-flow drags seen to exist in shallow water. (Cf. Fig. 28.) The strange results for ΔY_{ur} that are obtained for the SSPA tanker motivate a plea for tests always to be run at three or more depths.

Increases of added mass and added moment of inertia as obtained from FUJINO's experiments and NEWMAN's theory are shown in Fig. 39, again in poor agreement.

Figs. 40 and 41 include a comparison of lateral forces and yawing moments, respectively, in oblique towing in shallow waters and in the centre-line of canals as measured by FUJINO [5] and as derived from INOUE's theory, [99]. At least the effects due to the presence of the canal banks seem to be sufficiently well predicted.

The diagrams in Figs. 42–45 are all compiled from FUJINO's PMM measurements in shallow waters and canals, showing rotary force and moment derivatives, and the two main acceleration derivatives. The dotted curves again suggest a linear increase of these derivatives with ζ in unrestricted water, and a more complex dependence on ζ and η in a canal. (Cf. end of Section 10.)

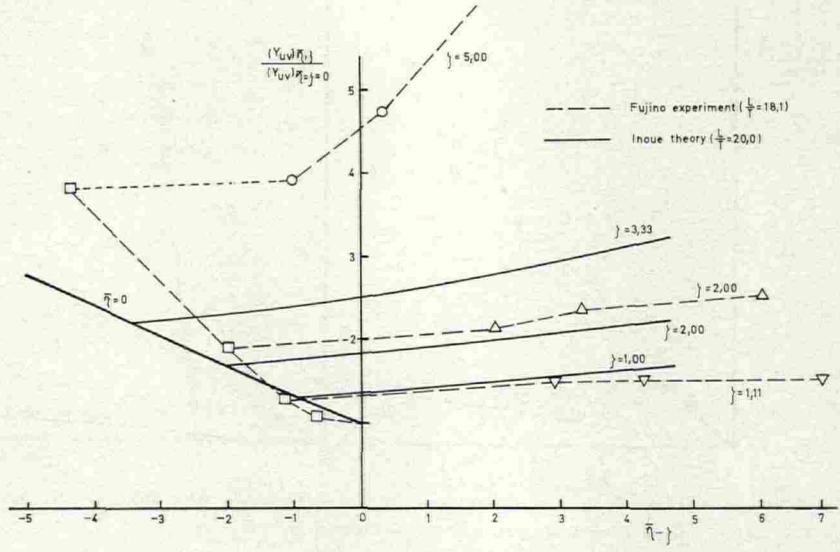

Fig. 40. Static force derivative for tanker as a function of waterway depth and width, replotted from FUJINO PMM data and compared with results from INOUE theory.

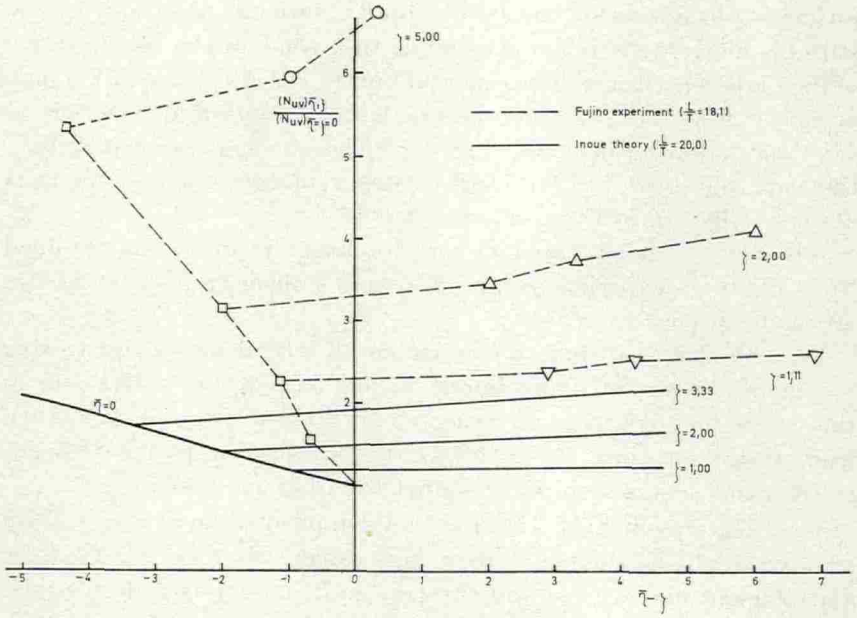

Fig. 41. Static moment derivative for tanker as a function of waterway depth and width, replotted from FUJINO PMM data and compared with results from INOUE theory.

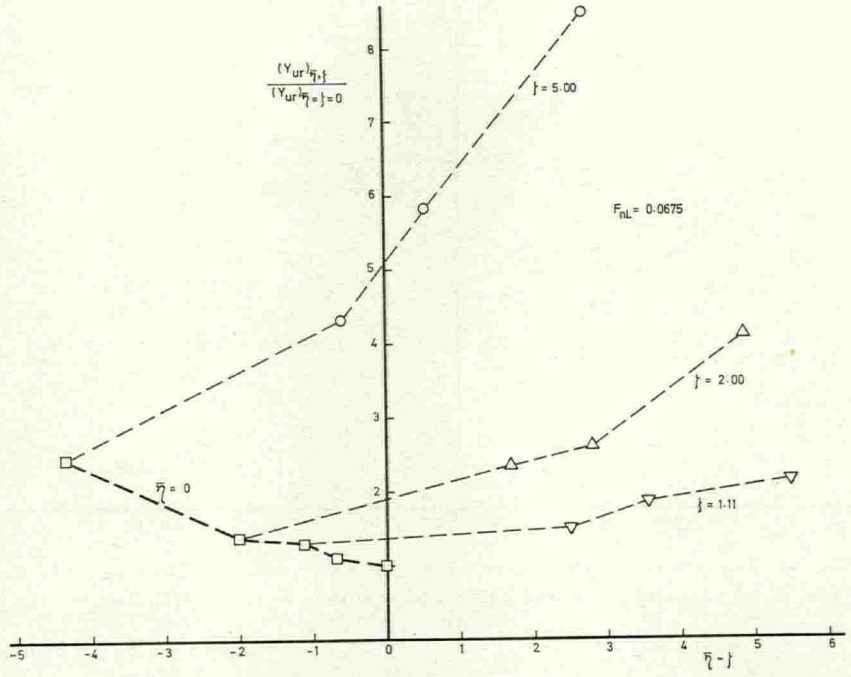

Fig. 42. Rotary force derivative for tanker as a function of waterway depth and width, replotted from FUJINO PMM data.

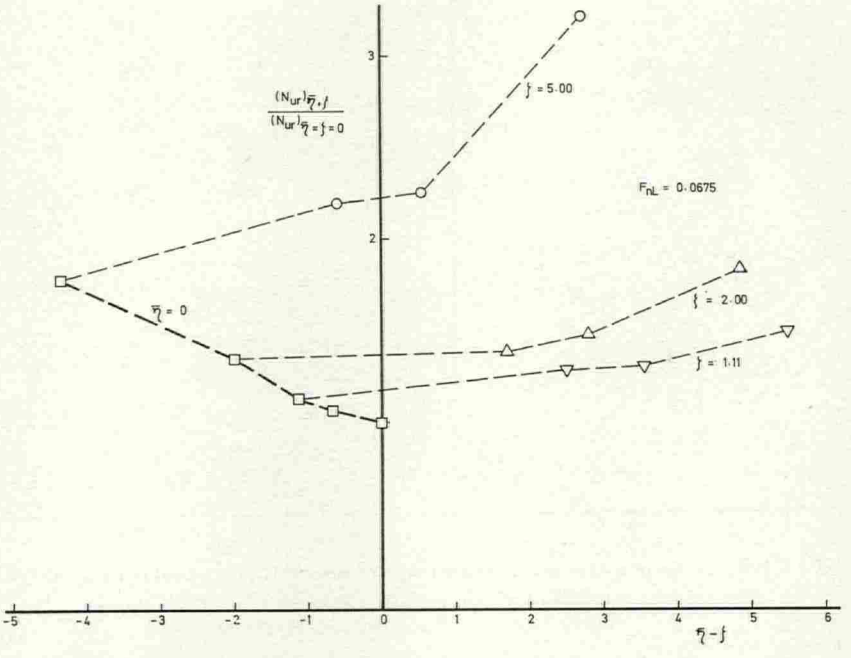

Fig. 43. Rotary moment derivative for tanker as a function of waterway depth and width, replotted from FUJINO PMM data.

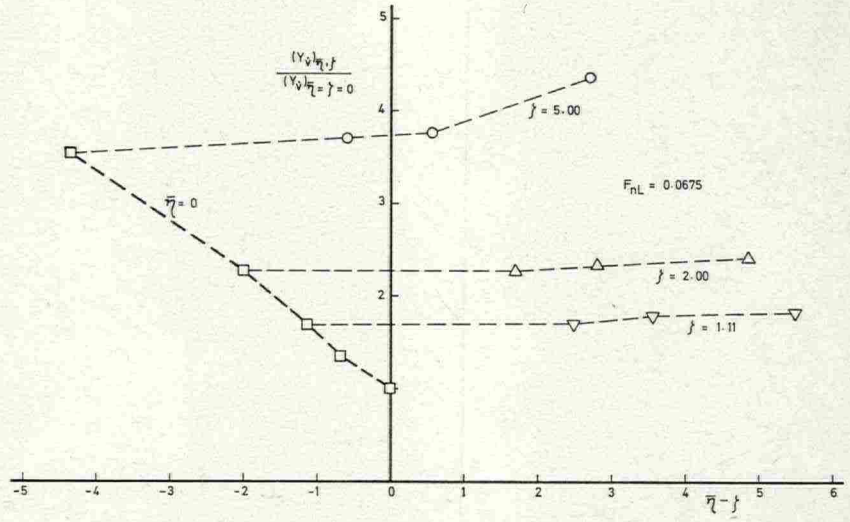

Fig. 44. Rel. change of lateral acceleration force derivative for tanker as a function of waterway depth and width, replotted from FUJINO PMM data.

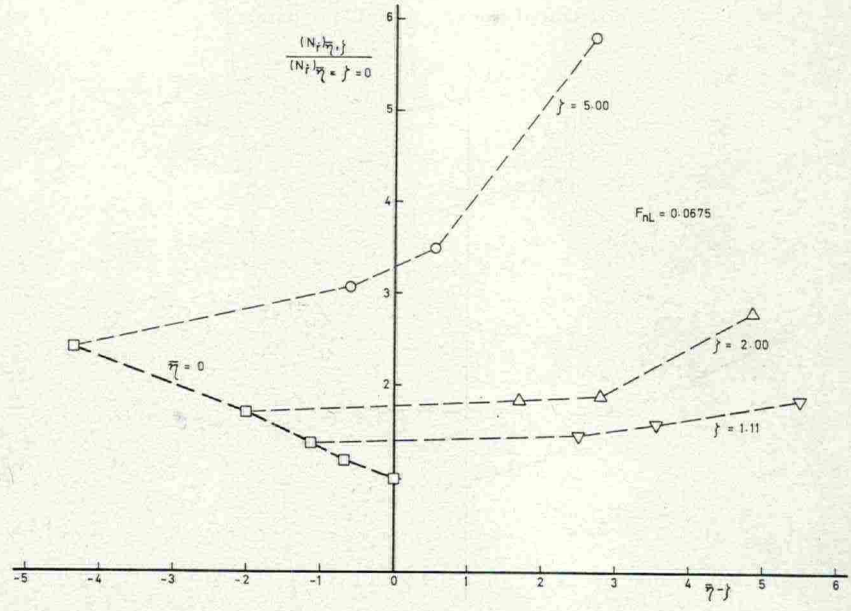

Fig. 45. Rel. change of rotary acceleration moment derivative for a tanker as a function of waterway depth and width, replotted from FUJINO PMM data.

13. Some Aspects of Ship Behaviour in Confined Waters

Here a few comments will be given on some of the results obtained in a computer and simulator study performed for the 98,000 t.dw. tanker. The diagrams in Figs. 46–53 all include results directly drawn on the analogue computer recorder.

The only full scale manoeuvring trials with the prototype ship so far available are a 20°/20° zig-zag test and a DIEUDONNÉ spiral, both run at full speed on full draught. These results are compared with the computer predictions—or hindcasts—for the ship on Suez draught in Figs. 46 and 47. As the difference in draught is not likely to have a significant influence the agreement is quite good. It shall be observed that the derivatives with respect to $|v|r$ and $v|r|$ are not derived from measurements with this model but taken from an analysis of rotating arm tests with another tanker form, and the almost exact prediction of overswing angles might be somewhat accidental.

The good correlation of speed loss in the zig-zag manoeuvre is satisfying. The phase difference is likely to be due in part to the stern position of the ship's pressure-type speed log.

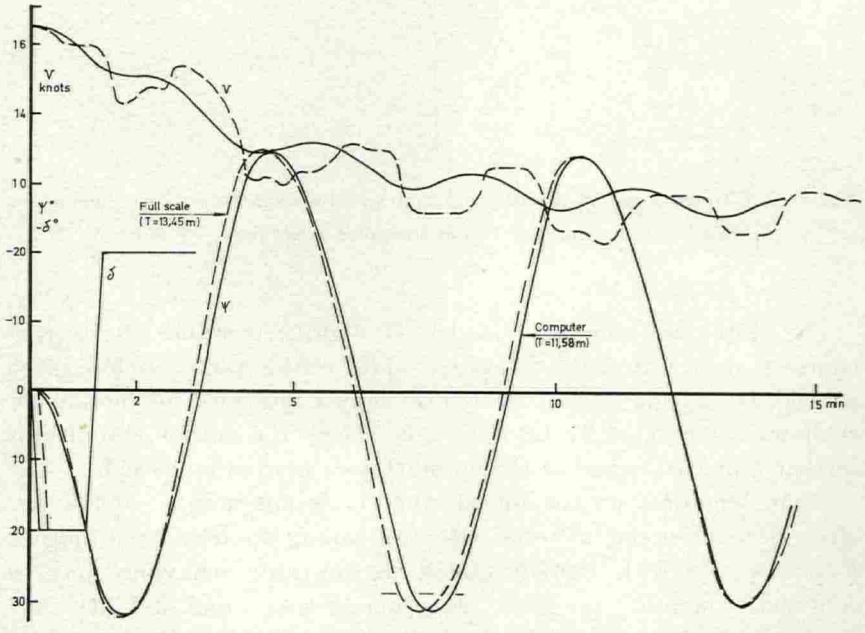

Fig. 46. T/T MALMÖHUS — 20°/20° zig zag test in deep water. Comparison of full scale trial and computer prediction.

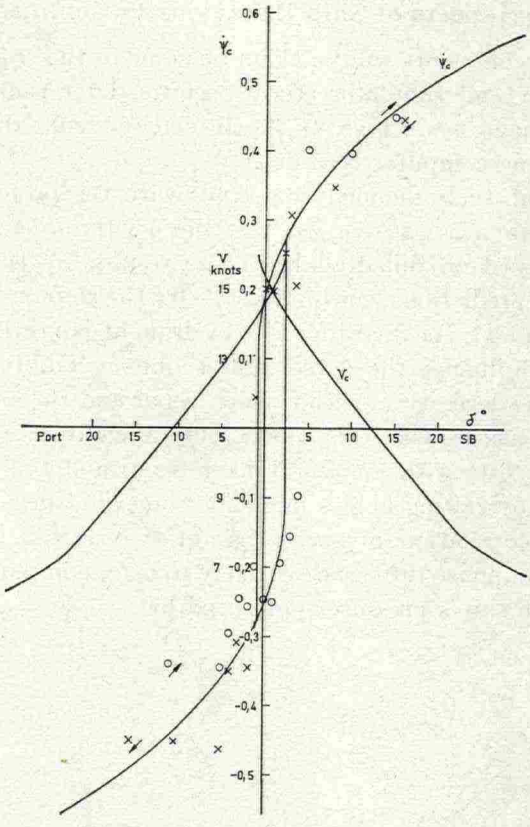

Fig. 47. T/T MALMÖHUS $-\dot{\psi}_c(\delta_c)$-diagram from spiral tests in deep water. Comparison of full scale trials ($\times$, o) and computer prediction (———).

The ship (and simulator model) is slightly unstable on straight course in deep water; the total loop width is about 3.5° at slow speed as well as at high. In Fig. 48 is also shown the spiral prediction for shallow water ($\zeta=3.37$ or $h/T=1.3$). Here the initial stability is further impaired, whereas the stability in a turn is increased.

A similar effect on the initial stability is not unique, and it has often been observed in tests with free-sailing models. According to FUJINO's tests with captive models the unstable behaviour may be confined to a finite range of "*dangerous depths*", and stability may be regained at very small under-keel clearances; this effect is traced back to a convex character of the lever l_v drawn to a base of varying ζ,

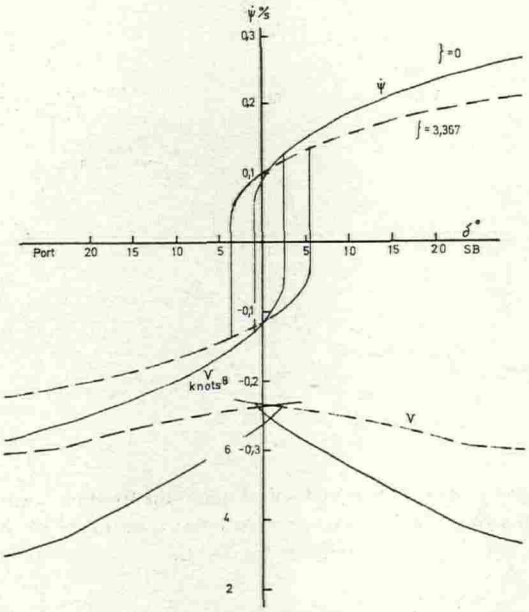

Fig. 48. T/T MALMÖHUS — Low speed spiral diagrams from computer predictions for deep and shallow water.

which is not supported by theory, but which may perhaps be explained by second order effects.

Another major factor governing the dependence of initial stability on water depth is the change of Y_{ur}, however. From Fig. 38 was seen that $Y''_{ur\zeta}$ came out negative for the MALMÖHUS model, so that the value of $l''_r = \dfrac{x''_G - N''_{ur} - N''_{ur\zeta}\zeta}{1 - Y''_{ur} - Y''_{ur\xi}\zeta}$ may diminish much faster with increasing ζ than does $l''_v = \dfrac{N''_{uv} + N''_{uv\zeta}\zeta}{Y''_{uv} + Y''_{uv\zeta}\zeta}$. It shall be borne in mind that Y''_{ur} essentially is a measure of the small difference between large damping forces on the after- and forebodies of the model and that effects which are not included in the simple theory may well be displayed in the negative $Y''_{ur\zeta}$. It is obvious, however, that rotating arm tests should include measurements at more than two depths of water. An alternative spiral prediction using zero $Y''_{ur\zeta}$ is presented in Fig. 49, but this alternative is not further considered below.

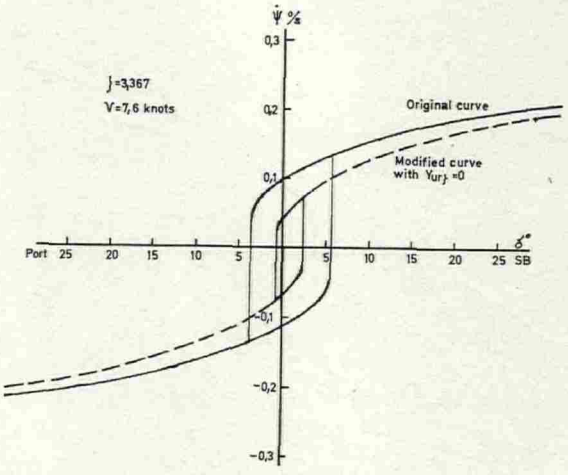

Fig. 49. T/T MALMÖHUS — Low speed spiral diagrams from computer predictions for shallow water, showing the importance of a correct estimate of the change of Y_{ur} with water depth.

Fig. 50 shows predictions for 20° rudder step responses in change of heading, yaw rate, and drift angle. The small drift angle obtained in the shallow water case is associated with the large increase of cross-flow drag. Similar results have earlier been reported by SCHMIDT-STIEBITZ, [108].

From simulator and full scale experience is known that the helmsman may have some difficulties of controlling the ship in manoeuvres that involve a change of course in shallow waters. Manoeuvres by use of auto pilots are repeatable and well suited for comparative studies. The diagrams in Figs. 51 and 52 refer to 10° course change manoeuvres predicted for the tanker at two speeds in deep water and at the lower speed in shallow water, all executed using the same normal setting of auto pilot controls. There are several overswings in shallow water, and checking helm is large.

The final diagrams in Fig. 53 furnish a condensed illustration to the changing problems of course control in shallow waters and in canals. These problems are also dealt with by EDA and SAVITSKY, [109], and in considerable detail by FUJINO, [110].

It is assumed that the ship is moving at low speed on a straight course parallel to the required track (in a buoyed channel, say) but off-set 20 m to the starboard side. A signal proportional to this

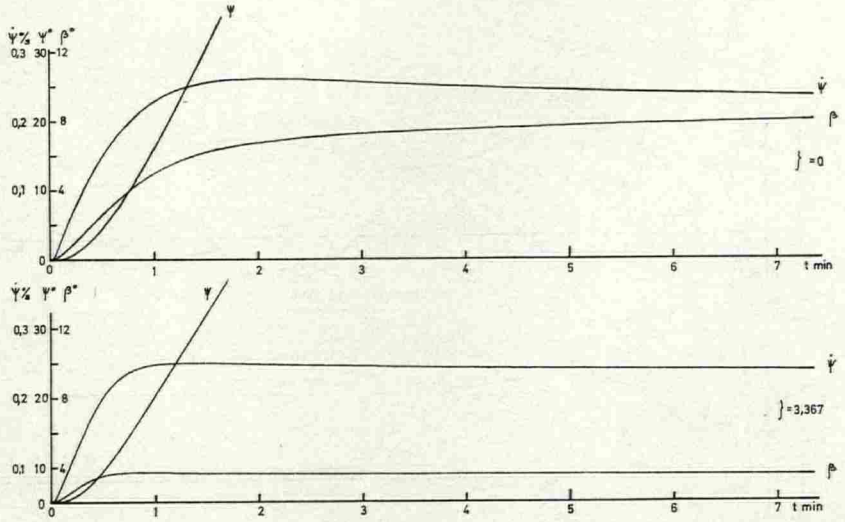

Fig. 50. T/T Malmöhus — Computer predictions of 20° rudder step response in deep and shallow water. Approach speed 7.6 knots.

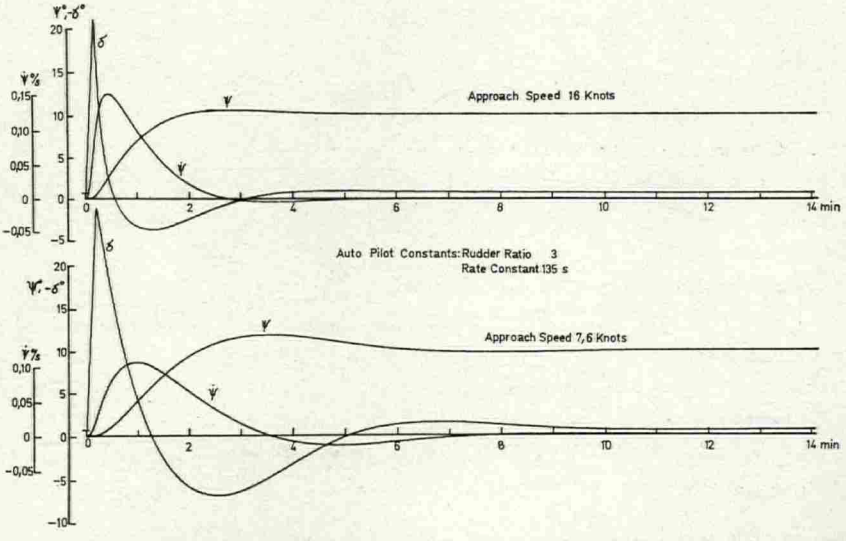

Fig. 51. T/T Malmöhus — Computer predictions of 10° course change manoeuvres by use of autopilot knob setting. Two speeds in deep water.

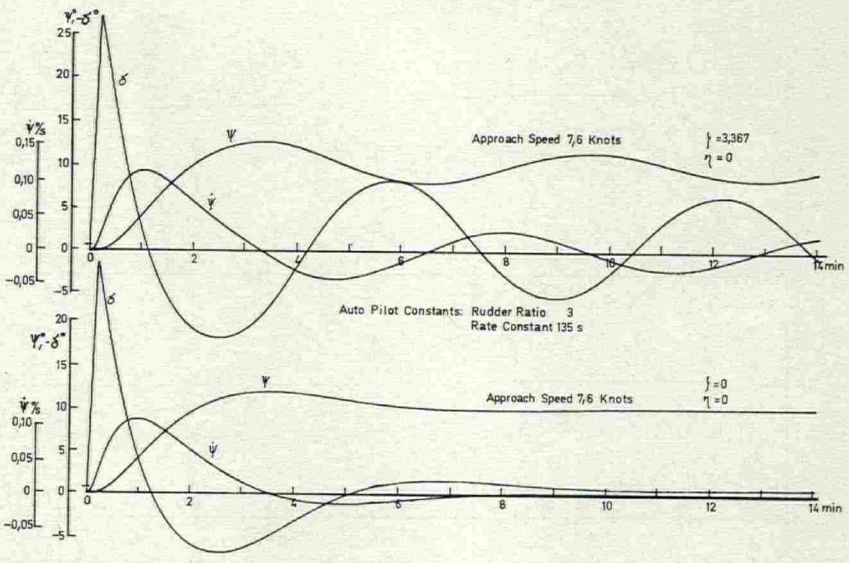

Fig. 52. T/T Malmöhus — Computer predictions of 10° course change manoeuvres by use of auto pilot knob setting. Shallow (top) and deep water.

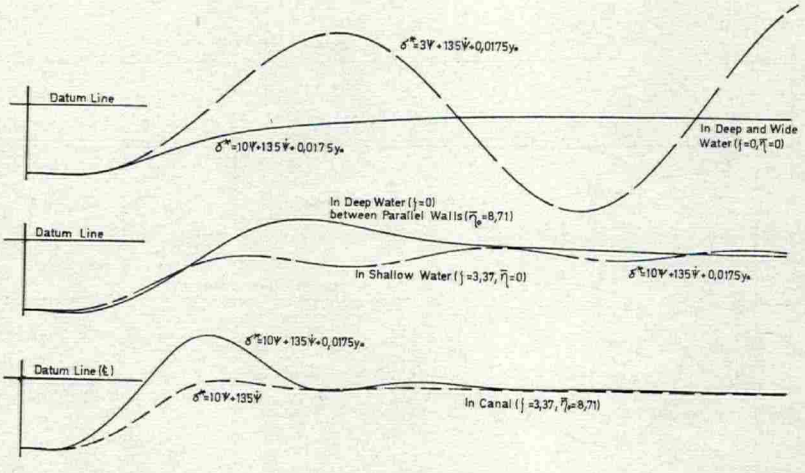

Fig. 53. T/T Malmöhus — Computer predictions of C. G. path in *on-track* control by auto pilots in deep and confined waters. Approach speed 7.6 knots. Initial off-set 20 m to starboard.

lateral error, calling for 1 degree rudder per m off track, is fed into the auto pilot. The upper curves for the free water conditions demonstrate that the rudder ratio setting must be increased (from normal 3 to say 10) in order to stabilize the ship on the required track. (In these diagrams off-track distance is increased compared to the distance parallell to original course in the proportion 20:1.) This control works reasonably satisfactory also in shallow water, but it tends to make the ship overshoot the centre-line in the alternative case between parallel walls in deep water. Obviously the presence of the near wall accelerates the first swing toward and beyond the centre-line.

The two lower curves of Fig. 53 relate to the ship in a typical part of the Suez canal. In the shallow water the effect of the near wall is even more pronounced, and the stern of the ship is in danger of hitting the bank. However, by turning down the lateral error knob to zero the auto pilot is made to behave like the experienced helmsman, already referred to in the introduction. Thus, the ship first sheers bow-off the wall before the auto pilot applies a counter-rudder in order to slowly press the ship laterally away from the wall. The ship is seen to be almost steady on to the centre-line within two ship lengths.

14. Some Conclusions, and Suggestions for Future Research

The main concern of this report has been the rational synthesizing of a mathematical model for use in analysis and simulator studies, and a critical examination of the elements of this model. The mathematical model here is a collective name for that set of equations of motion and state conditions, which controls the engines and rudders, and which describes the motions imposed by these controls and by outer disturbances. There is no evidence to say that memory effects in the presence of progressive ship surface waves or viscous phenomena will violate the use of ordinary differential equations with constant coefficients in a model designed for accurate predictions in practical applications.

Non-dimensional coefficients and parameters have been formed in a new system—here designated the "*bis*" system as different from the SNAME "*prime*" system generally in use—in which the units

for mass, length and time, respectively, are given by the mass of the ship, m, the length, L, and the time required for travelling one ship length at a speed corresponding to $V''=F_{nL}=1$, i.e. $\sqrt{L/g}$. One particular advantage of the new system is that the physical identity and magnitude is easily grasped. So, for instance, the derivative symbol Y''_{uv} indicates that it is a coefficient for the Y-force as a function of u and v and that its magnitude is directly related to the mass gravity of the ship. The non-linear force derivative $\frac{1}{2}\, Y''_{|v|v}$ is a coefficient for the cross-force, which is independent of the forward speed u (and of any other motion not displayed in the symbol). Other details of the model are pointed out below.

The complete model is designed to handle rather complex problems of ship operation by use of one or more rudders and propelling screws in shallow water and in canals. Whereas this same complete model will of course be applicable also to more simple studies, it may well be that its complexity will then obscure the basic disclosures.

It is shown that the linearized model in general is adequate for the simulation of course-keeping by automatic or manual control, and that the ship dynamics may be represented just by the virtual inertia forces as far as manual control of very large tankers is concerned. This latter implies that drift and yaw velocities both remain 90° out of phase with helm deflection, and, moreover, that the dynamic stability characteristics of the large tankers have no major effect upon their *on-straight-course* behaviour, which is dominated by the control blocks of the closed loop. Of course such a simplified model of the hydrodynamics is no longer valid as soon as a *change of course* has to be analyzed or simulated.

It is important that ship officers and pilots have an opportunity to learn how to handle the new large ships in transient manoeuvres. The mere access to a steady-state $\dot{\psi}(\delta)$-diagram from the trial spiral test will be of little use to them; this diagram is of more value to the analyst when checking the programmed simulator.

The manually controlled simulator is a versatile research tool as well as an effective training device. Experiences with the SSPA steering and manoeuvring simulator, which has been in continuous routine operation since the autumn 1967, do indicate that the bridge mock-up and environmental display may be rather simple, as long as the forward view in true perspective is wide enough. Emphasis has therefore been placed on a correct modelling of the dynamics of the operated systems.

Zero-frequency values of added masses shall be used in ship manoeuvring calculations. Suitable diagrams have been designed, which prove an acceptable correlation of experimental and theoretical results, and which may also be used for application to individual cases.

In a previous report by the author results from force measurements in oblique towing of a ship model and its divided double-body geosim were compared with calculations by use of the zero-aspect-ratio wing analogy. It was shown that the linear force contribution $Y_{uv}uv$ was dominated by the fore-body lift as predicted by the wing analogy, again using zero-frequency section added masses and zero-FROUDE number experiments. It was further shown that linear normal force and yawing moment increased by an increase of FROUDE number, much in the way given by HU's theory. The non-linear contributions were to be calculated from cross-flow resistances.

A certain number of stability derivative figures available to the author are here displayed in four diagrams, which, in principle, turn out to support the use of the wing analogy. These derivatives are all derived from cubic fits to experimental data. It is suggested—and so far confirmed by a limited re-analysis—that the bracketed square type fits would furnish linear derivatives for zero FROUDE number, which are in even better agreement with the simple wing analogy prediction. The present analysis adopted therefore involves a calculation of non-linear cross-flow second-order derivatives, then an evaluation of the first-order derivatives by use of an analogue computer and visual display, and finally a semi-empirical correction to zero FROUDE number. The finite speed correction is included in the full simulator model.

Screw and rudder contribute a (generally small) fin effect to a total stability derivative, for which effect at present only rough estimates can be made. (See above.)

The unsymmetric lateral force due to a single propeller as well as the lateral (suction) control made possible by a twin-screw arrangement are included in the mathematical model by means of contributions proportional to the axial thrusts.

The forward speed equation is dominated by the influence of the force $(m+X_{vr})vr$, recognized as the longitudinal component of the "centrifugal force" on lateral virtual mass. In ideal-flow theory X_{vr} equals the added mass in lateral acceleration, $-Y_{\dot{v}}$, and it is then expected to be almost as large as the ship mass proper. Viscous effects are likely

It has long been realized that the use of manually controlled scale models does not adequately simulate full-scale behaviour. By analogue computer simulation it is here shown that the limitations placed on model size scale factors are functions of prototype's size and steering characteristics. Human time constants may be adjusted to some small degree, but the dynamically scaled-down time constants for ship and steering engine must remain large compared to the helmsman's reaction time. In case of a 200,000 t.dw. tanker it appears that reliable free-sailing steering results will only be obtained from tests with models that are some 12 m long. (Programmed or automatically controlled tests may well be run with smaller models; REYNOLD's number effects on rudder lift curve slopes become critical only in case of models of lengths less than 5 or 4 meters. Viscous scale effects may also be present in separation phenomena on the after-body of full-form models of larger sizes, however.)

The simulator in each case makes use of the proper mathematical model, for which the hydrodynamic constants are derived from theory, from semi-empirical relations, or from new captive model tests, which are designed to furnish the particular coefficients required. Again, these model tests usually do not require model sizes of more than 4 or 5 m. However, tests in shallow water with small under-keel clearances are likely to suffer from viscous scale effects, which apparently tend to exaggerate the rate of increase of force with a further reduction of clearance. (See below.) Geosim tests in shallow water are therefore to be strongly advocated.

Whereas free sailing tests often fail to disclose the ultimate cause of the different behaviour of two alternative designs this difference is clearly explained by the captive test and computer technique. This technique has certain other advantages: in particular it is possible to apply the proper corrections for full scale wake and screw loading to the rudder forces measured in the captive model tests.

A simple procedure is here put forth for the calculation of control derivatives for a conventional stern rudder. This calculation is a prerequisite for the model-to-full-scale correction just mentioned. Further experimental information is required on the interference between hull after-body and rudder, i.e. on the control and total force derivatives from simultaneous measurements. It is suggested that the inherent coupling between forces and moments due to the rudder must be included as an additional constraint in a regression analysis of force and moment data.

to change this picture, and a recent analysis of speed loss in full-scale turning trials indicates a much smaller value of X_{vr}.

The forward speed equation here also includes a term $\frac{1}{6} X_{u|v|vv} u|v|v^2$, the form of which has been derived from an analysis of old data; in contrast to the drift-depending term of other models this one tends to zero with forward speed.

A correct prediction of forward speed is of special interest when comparing small losses experienced when under automatic control on a straight course, and it is absolutely essential to the successful simulation of turning rates and trajectories of hard-over manoeuvres. There is a need for new rotating arm tests with careful three-component force measurements on unpropelled models.

A large portion of this report is devoted to the extension of the mathematical model to cover the most important cases of confined water operations, i.e. manoeuvring in shallow water and steering in a canal. Previously existing models have been applied to these cases by the substitution of entirely new figures in place of the free-water derivates. The basic idea of the present approach is to simulate the influence of growing confinement by additional terms, which are proportional to growing confinement parameters and to their combinations. By a proper selection of these parameters it has been possible to extend the formally linear domain, and so to make way for a super-position technique; especially the suction effects due to a port and a starboard canal wall are added in this way.

The motion of a deep-draughted full-bodied ship parallel to a quay wall in very shallow water presents an almost two-dimensional flow picture, which essentially is that of a RANKINE oval moving parallel to a vertical wall. Some new results are here given from calculations by use of the simple image theory and an analogue computer; the theory should be valid for body-to-wall separations equal to the body beam or more. A bank wall is to be regarded as short if its length is less than fifteen times the length of the body, and transient phenomena are likely to dominate during the passage of a bank with a length less than six times the length of the body. The attraction force between body and a long wall is roughly inversely proportional to the distance between wall and body axis, within the range of practical interest, and the simple theory predicts forces, which are in a reasonable quantitative agreement with experimental results for ship forms in case of small under-keel clearances.

The three-dimensional case of a finite-draught ship moving parallel

to a bank in deep water may be handled by use of NEWMAN's theory for a body of revolution close to a wall. The theory predicts a suction force, which slightly underestimates the forces measured on a propelled tanker model towed along the side wall in a ship model basin; finite depth corrections tend to make the agreement better. The comparison of yawing moments is obscured by bow wave and screw action effects in the experiments. New tests with unpropelled bodies of revolution would be of great value.

Just as does the first-order two-dimensional image theory, NEWMAN's theory suggests that the suction force is essentially linearly proportional to the parameter $\eta=L/d$, where d is the distance from ship centre-line to wall, measured positive to starboard. For the problem of a ship between two parallel vertical walls it is possible to define one port and one starboard value of this parameter, η_p and η_s, and in the first approximation the force is proportional to $\eta=\eta_s+\eta_p$; in the middle of the canal $\eta=0$, and the bank effects are cancelled. The validity of this superposition principle is confirmed by an analysis of old DTMB model test data. Another parameter, $\bar{\eta}=\eta_s-\eta_p$, is used as a measure of the bank spacing, and it appears in coupling terms in the regression analysis of the forces on a ship well off the centre-line of a narrow canal. The immediate effect of a finite $\bar{\eta}$ is to counteract the effect of η, this to compensate for the first-order omission of the far wall image of the first image in the near wall. In most practical applications the canal is shallow, and if deep-water bank effects then are used it is necessary to include a complex coupling with the under-keel clearance parameter ζ.

The forces on a ship in turning motion have been seen to depend on the magnitude and distribution of section added masses as well as on the cross-flow viscous drag. Due to the under-keel blockage added masses and cross-flow drag figures are all higher in shallow water. Model experiment results indicate that the increase of the linear and to some extent also that of the non-linear force derivatives is roughly proportional to the parameter $\zeta=T/(h-T)$; the rate of increase is especially high for the cross-flow drag dependence.

Due to the striking non-linearities that appear in the lateral forces in shallow water any stringent analysis of captive model tests requires a relatively large number of data points. This is especially true when evaluating the total lateral force derivative from rotating arm tests, which have to be extrapolated to zero rate of yaw; that derivative is an essential factor characterizing the dynamic stability condition.

Viscous scale effects in effective under-keel clearance tend to exaggerate the forces at large ζ, and the need for illustrating geosim tests has already been pointed out. When making comparisons with theory the influence of sinkage on effective under-keel clearance must not be overlooked.

The results from INOUE's recent theory may be used for a prediction of the increase of the four stability derivatives proper in shallow water, as is proved by the comparatively good agreement with experiments. The general trend will be an increase of the inherent dynamical stability in shallow water, i.e. in the initial stability lever $l_r - l_v$ the first member will increase and the second will decrease monotonically. The theory fails to predict the existence of a range of "*dangerous depths*", in which, according to FUJINO's experiments, a ship that is dynamically stable in deep as well as in very shallow waters may loose that property; the convex character of the experimental curve of l_v versus under-keel clearance will probably have to be explained by second-order effects, such as a forward trim, which could move the sway damping force forward.

Up till now results from full scale trials with large tankers in deep and shallow waters are less conclusive with regard to changes of the stability characteristics reflected in the spiral test diagram. The large increase of virtual inertias will make it necessary to allow ample time for transient phases of the spiral manoeuvre, which also at a low speed is even more sensitive to disturbances from winds and currents. Again, the changes of the handling properties are of more practical concern, as shallow water manoeuvring usually involves frequent changes of course and speed.

There will be a smaller drift and a back-ward shift of the pivoting point position in turning, mainly due to the large increase of cross-flow drag with under-keel blockage. Due to the increased resistance to the turning of a deep-draught ship it may be difficult to bring her through shallow channel bends, which have been planned for ships with larger bottom clearances.

In closed canals the requirements on bottom clearances are usually higher than in open port approaches, as bed erosion due to canal water back-flow must be avoided. This back-flow is responsible for most of the increase of forward resistance in the canal—in the present model represented by additional terms in $u^2\bar{\eta}\zeta$ and $u^2\bar{\eta}\zeta^2$ — and the higher screw loading is favourable to the helm efficiency of the single-screw ship.

In a narrow one-way canal it is essential that the helmsman keeps the ship on the centre-line, but once off this line he should make only careful use of the rudder and take advantage of the bank suction effects, which, in the end, help to control the ship. This situation has here been studied within simulator investigations of the on-track control of a tanker with a flexible auto-pilot, moving in unrestricted deep and shallow water, between parallel walls and in a shallow canal. It is shown that the *lateral error* control of the auto-pilot is superfluous in the canal, and that the pilot with *heading error*+*rate*-control will handle the ship in the proper way: The ship sheers bow-off the wall, the auto-pilot then calls for rudder to bring the ship back parallel to the centre-line, and so the ship is slowly pressed laterally away from the near bank.

15. Acknowledgement

The results of this report are drawn from the author's work within the current research and development program on ship manoeuvring planned and sponsored by the Swedish State Shipbuilding Experimental Tank (SSPA). The author is indebted to Dr. HANS EDSTRAND, Director General, for his persistent support of this program, and for the interest he has shown.

The confined water model experiments reported on were performed to SSPA order in 1966 and 1967 by the VBD laboratories at Duisburg, to the Director and staff of which the author extends his thanks for the good co-operation offered. Part of the analysis was made possible by grants from the Hugo Hammar Foundations for Maritime Research and for International Research on Shipping.

To Mr. HANS LINDGREN, head of the research department of SSPA, to Mr. SIGURD GÖRANSSON in charge of the analogue computer facility, and to Mr. WILLEM VAN BERLEKOM and other colleagues of the staff the author is in debt for many a stimulating argueing. He also acknowledges the inspiration and criticism often obtained from discussions with Prof. J. N. NEWMAN of MIT. Further he owes a special thank to Mr. ANDERS IVARSSON and Mr. LARS MARCUSSON, who assisted in the evaluation and numerical analysis, and who prepared the graphs for this report.

16. List of References

1. NORRBIN, N. H., and GÖRANSSON, S.: "The SSPA Steering and Manoeuvring Simulator" (in Swedish), *SSPA Allm. Rapport No. 28*, April 1969.
2. MANDEL, PH.: "Ship Maneuvering and Control", in "*Principles of Naval Architecture*" (revised), New York 1967.
3. VAN BERLEKOM, W.: "Predictor Systems for Safer Manoeuvring of Nuclear Ships into Ports", *SSPA Paper prepared for the Symposium on Nuclear Ships*, Hamburg, May 1971.
4. BOHLIN, A.: "Problems Arising from the Use of Very Large Ships in Connection with the Alignment and Depth of Approach Channels and of Manoeuvring Areas", *Paper S. II-3, Proc. XXII^e Congrés International de Navigation*, Paris 1969.
5. FUJINO, M.: "Experimental Studies on Ship Manoeuvrability in Restricted Waters — Part I", *Intern. Shipb. Progr., Vol. 15, No. 168*, Aug. 1968.
6. NORRBIN, N. H., and SIMONSSON, E. Y.: "Observations onboard a 60,000 t.dw. Tanker Manoeuvring through the Suez Canal", *unpublished papers, SSPA* and *Uddevalla Shipyard*, Nov. 1964.
7. ITTC: "Recommended Symbols Classified by Subject", *Appendix II of Presentation Committee Report to the 10th ITTC*, London 1963.
8. SNAME: "Nomenclature for Treating the Motion of a Submerged Body Through a Fluid", *SNAME Technical and Research Bulletin No. 1–5*, New York 1950.
9. NORRBIN, N. H.: "A Study of Course Keeping and Manoeuvring Performance", *SSPA Publ. No. 45*, Göteborg 1960. (Also Publ. in *DTMB Report 1461*, Washington D.C. 1960.)
10. GLAUERT, H.: "A Non-Dimensional Form of Stability Equations of an Aeroplane", *ARC R & M No. 1093*, London 1927.
11. KIRCHHOFF, G.: "Über die Bewegung eines Rotationskörpers in einer Flüssigkeit", *Crelle, Vol. LXXI, Heft 237*, 1869.
12. LAMB, H.: "Hydrodynamics", *Cambridge University Press*, Cambridge 1932 (6th ed.).
13. MILNE-THOMSON, L. M.: "Theoretical Hydrodynamics", *MacMillan*, London 1955 (3rd ed.).
14. IMLAY, F. H.: "The Complete Expressions for Added Mass of a Rigid Body Moving in an Ideal Fluid", *DTMB Report 1528*, July 1961.
15. LAMB, H.: "The Inertia Coefficients of an Ellipsoid Moving in Fluid", *ARC R & M No. 623*, 1918.
16. KOTSCHIN, N. J., KIBEL, I. A., and ROSE, N. W.: "Theoretische Hydromechanik", Bd I (from Russian), *Akademie-Verlag*, Berlin 1954.

17. Munk, M.: "The Aerodynamic Forces on Airship Hulls", *NACA Report No. 184*, 1923.
18. Norrbin, N. H.: "Forces in Oblique Towing of a Model of a Cargo Liner and a Divided Double-Body Geosim", *SSPA Publ. No. 57*, 1965.
19. Weinblum, G.: "On Hydrodynamic Masses", *DTMB Report 809*, April 1952.
20. Grim, O.: "Die Hydrodynamischen Kräfte beim Rollversuch", *Schiffstechnik, 3. Bd, Heft 14/15*, Febr. 1956.
21. Landweber, L., and de Macagno, M. C.: "Added Mass of Two-Dimensional Forms Oscillating in a Free Surface", *J. Ship Research, Vol. 1, No. 3*, Nov. 1957.
22. Lewis, F. M.: "The Inertia of the Water Surrounding a Vibrating Ship", *Trans. SNAME, Vol. 37*, 1929.
23. Prohaska, C. W.: "The Vertical Vibration of Ships", *Shipb. and Mar. Eng. Builder*, Oct.–Nov. 1947.
24. Lockwood-Taylor, J.: "Some Hydrodynamical Inertia Coefficients", *Phil. Mag. (Series 7) Vol. 9, No. 55*, 1930.
25. Ursell, F.: "On the Heaving Motion of a Circular Cylinder on the Surface of a Fluid", *Quart. J. Mech. and Applied Math., Vol. II, Pt 2*, 1949.
26. Tasai, F.: "Hydrodynamic Force and Moment Produced by Swaying Oscillation of Cylinders on the Surface of a Fluid", *Journ. Soc. Nav. Arch. Japan, Vol. 110*, Dec. 1961.
27. Porter, W. R.: "Pressure Distribution, Added Mass, and Damping Coefficients for Cylinders Oscillating in a Free Surface", *University of California, Inst. of Engng Res., Series 82, Issue No. 16*, July 1960.
28. Frank, W.: "Oscillation of Cylinders in or below the Free Surface of Deep Fluids", *NSRDC Report 2357*, 1967.
29. Vugts, J. H.: "The Hydrodynamic Coefficients for Swaying, Heaving and Rolling Cylinders in a Free Surface", *Laboratorium voor Scheepsbouwkunde, Delft, Report No. 194*, Jan. 1968.
30. de Jong, B.: "Berekening van de hydrodynamische coëfficiënten van oscillerende cylinders", *Laboratorium voor Scheepsbouwkunde, Delft, Report No. 174*, March 1967.
31. Tuck, E. O.: "A New Approach to the Strip Theory of Forced Ship Motion", *NSRDC Tech. Note*, Sept. 1966.
32. van Leeuwen, G.: "The Lateral Damping and Added Mass of an Oscillating Shipmodel", *Shipbuilding Laboratory, Delft, Publ. No. 23*, July 1964.
33. Brard, R.: "Introduction à l'étude théorique du tangage en marche", *Bull. ATMA, No. 47*, 1948.
34. Newman, J. N.: "The Damping and Wave Resistance of a Pitching and Heaving Ship", *Journ. Ship Research, Vol. 3, No. 1*, June 1959.
35. Havelock, T.: "The Resistance of a Submerged Cylinder in Accelerated Motion", *Quart. Journ. Mech. Appl. Math., Vol. 2, Part 4*, Dec. 1949.
36. Motora, S.: "On the Measurement of Added Mass and Added Moment of Inertia of Ships in Steering Motion", *Proc. First Symposium on Ship Maneuverability*, Washington 1960, *DTMB Report 1461*, 1960.
37. Motora, S., Fujino, M., Sugiura, M., and Sugita, M.: "Equivalent Added Mass of Ships in the Collision", *Journ. Soc. Nav. Arch. Japan, Vol. 126*, Dec. 1969.

38. JONES, R. T.: "Properties of Low-Aspect-Ratio Pointed Wings at Speeds Below and Above the Speed of Sound", *NACA Report No. 835*, 1946.

39. SMITT, L. W.: "Skibes Styre- og Manøvreevne. Fuldskala- og Modelforsøg" (in Danish), *HyA Paper presented to NSTM 70 in Göteborg*, Sept. 1970.

40. EDA, H., and CRANE, C. L. JR.: "Steering Characteristics of Ships in Calm Water and Waves", *Trans. SNAME, Vol. 73*, 1965.

41. JACOBS, W. R.: "Estimation of Stability Derivatives and Indices of Various Ship Forms, and Comparison with Experimental Results", *Dav. Lab. Report 1035*, Sept. 1964.

42. HU, P. N.: "Forward Speed Effect on Lateral Stability Derivatives of a Ship", *Dav. Lab. Report R-829*, Aug. 1961.

43. NEWMAN, J. N.: "Some Hydrodynamic Aspects of Ship Maneuverability", *Proc. Sixth Symposium on Naval Hydrodynamics*, Washington, D.C. 1966.

44. BRARD, R.: "A Vortex Theory for the Manoeuvring Ship with Respect to the History of Her Motion", *Proc. Fifth Symposium on Naval Hydrodynamics*, Bergen 1964.

45. NOMOTO, K., and KARAANO, K.: "A New Procedure of Manoeuvring Model Experiment", *Journ. Soc. Nav. Arch. Japan, Vol. 126*, Dec. 1969.

46. NOMOTO, K.: "Unusual Scale Effect on Manoeuvrabilities of Ships with Blunt Bodies", *Proc. 11th ITTC*, Tokyo 1966.

47. BOTTOMLEY, G. H.: "Manoeuvring of Ships, Parts II–IV", *Trans. IESS, Vols. 67, 70, and 74*, 1923–1931.

48. KENT, J. L.: "Ships in Rough Water", *Thomas Nelson and Sons Ltd.*, London 1958.

49. THIEME, H.: "Schleppversuche bei Queranströmung", *Schiff und Hafen, 6. Jahrg., Heft 6*, 1954.

50. SNAME: "Notes on Ship Controllability", *SNAME Technical and Research Bulletin No. 1–27*, New York 1966.

51. CRANE, C. L., JR.: "Studies of Ship Manoeuvring—Response to Propeller and Rudder Actions", *Proc, Ship Control Systems Symposium, Encl. to Vol. 1, US Marine engng. Lab.*, Annapolis 1966.

52. ABKOWITZ, M. A.: "Lectures on Ship Hydrodynamics—Steering and Manoeuvrability", *HyA Report No. Hy-5*, May 1964.

53. GERTLER, M., and HAGEN, G. R.: "Standard Equations of Motion for Submarine Simulation", *NSRDC Report 2510*, June 1967.

54. LINDGREN, H.: "Ship Trial Analysis and Model Correlation Factors", *SSPA Publ. No. 54*, 1963.

55. SAUNDERS, H.: "Hydrodynamics in Ship Design", *Vol. II, Chapter 56, publ. by SNAME*, New York 1957.

56. MOTORA, S., and KOYAMA, T.: "Some Aspects of Automatic Steering of Ships", *Japan Shipb. & Marine Engng*, July 1968.

57. NOMOTO, K., *et al.*: "On the Steering Qualities of Ships", *Intern. Shipb. Progress, Vol. 4, No. 35*, July 1957.

58. NOMOTO, K.: "Analysis of Kempf's Standard Manoeuvre Test and Proposed Steering Quality Indices", *First Symposium on Ship Maneuverability*, Washington D.C., *DTMB Report 1461*, Oct. 1960.

59. NORRBIN, N. H.: "The Technique and Analysis of the Zig Zag Test" (in Swedish), *SSPA Allmän Rapport Nr. 12*, 1965. (English translation in *BSRA Transl. No. 2188.*)

60. NORDÉN, I.: "Fartyg med två roder" (in Swedish), *Götaverken Journal Skeppsbyggaren, No. 4*, 1960.

61. NORRBIN, N. H.: "Steuern bei geringer Fahrt", *Hansa, 101. Jahrg., Heft 10*, May 1964.

62. RIBNER, H. S.: "Propellers in Yaw", *NACA Report No. 820*, 1945.

63. DITLEV JÖRGENSEN, H., and PROHASKA, C. W.: "Wind Resistance", *Appendix IV of Performance Comm. Report to the 11th ITTC*, Tokyo 1966.

64. WERELDSMA, R.: "Experimental Determination of Thrust Excentricity and Transverse Forces Generated by a Screw Propeller", *Intern. Shipb. Progr., Vol. 9, No. 95*, July 1962.

65. NORRBIN, N. H.: "Circle Tests with a Radio-Controlled Model of a Cargo Liner", *SSPA Publ. No. 53*, Göteborg 1963.

66. LÖTVEIT, M.: "A Study of Rudder Action with Special Reference to Single-Screw Ships", *Trans. NECI, Vol. 75*, 1959/60.

67. BAKER, G. S., and BOTTOMLEY, G. H.: "Manoeuvring of Ships, Part I — Unbalanced Rudders of Single-Screw Ships", *Trans. IESS, Vol. 65*, 1921/22.

68. WEISSINGER, J.: "Über die Auftriebsverteilung von Pfeilflügeln", *Forschungsbericht deutscher Luftfahrtforschung Nr 1553*, 1942. (Transl. *NACA TM 1120.*)

69. SPREITER, J. R.: "The Aerodynamic Forces on Slender Plane- and Cruciform-Wing and Body Combinations", *NACA Report No. 962*, 1950.

70. MIRELS, H.: "Lift Effectiveness of Slender Wings on Cylindrical Bodies", *J. Aero. Sci., Vol. 20, No. 7*, July 1953. (Readers Forum.)

71. YAZAKI, A., and YOKOO, K.: "On the Roughness Allowance and the Scale Effect on the Wake Fraction of Super-Tankers", *Proc. 11th ITTC*, Tokyo 1966.

72. STRØM-TEJSEN, J., and CHISLETT, M. S.: "A Model Testing Technique and Method of Analysis for the Prediction of Steering and Manoeuvring Qualities of Surface Ships", *Proc. Sixth Symposium on Naval Hydrodynamics*, Washington D.C., 1966. (Also *HyA Report Hy-7*, Copenhagen 1966.)

73. HOOFT, J. P.: "The Manoeuvrability of Ships on a Straight Course", *Intern. Shipb. Progress, Vol. 15, No. 162*, Feb. 1968.

73. NORDSTRÖM, H. F.: "Screw Propeller Characteristics", *SSPA Publ. No. 9*, Göteborg 1948.

75. BAKER, D. W., and PATTERSON, C. L. JR.: "Some Recent Developments in Representing Propeller Characteristics", *Proc. Second Ship Control Systems Symposium*, Annapolis, Maryland 1969.

76. HARVALD, S. A.: "Wake and Thrust Deduction at Extreme Propeller Loadings", *SSPA Publ. No. 61*, Göteborg 1967.

77. RITTERHOFF, J.: "Beitrag zur Erhöhung der Sicherheit von Schiffsantriebsanlagen durch Untersuchung ihres Manöververhaltens", *Schiff und Hafen, 22. Jahrg., Heft 3*, March 1970.

78. SAUNDERS, H.: "Hydrodynamics in Ship Design", *Vol. III, Chapter 6, publ. by SNAME*, New York 1965.

79. BRARD, R.: "Maneuvering of Ships in Deep Water, in Shallow Water, and in Canals", *Trans. SNAME Vol. 59*, 1951.

80. Weinblum, G.: "Theoretische Untersuchungen der Strömungsbeeinflussung zweier Schiffe aufeinander beim Begegnen und Überholen auf tiefem und beschränktem Wasser", *Schiffbau, 34. Jahrg.*, 1933.
81. Havelock, T. H.: "Wave Resistance—The Mutual Action of Two Bodies", *Proc. Roy. Soc., Series A, Vol. 155*, London 1936.
82. Silverstein, B. L.: "Linearized Theory of the Interaction of Ships", *Inst. Engng Research, Report Series 82, Issue 3, Univ. of California*, Berkeley 1957.
83. Schuster, S.: "Untersuchungen über Strömungs- und Widerstandsverhältnisse bei der Fahrt von Schiffen in beschränktem Wasser", *Jahrb. STG, 46. Bd.*, 1952.
84. Weinblum, G.: "Wellenwiderstand auf beschränktem Wasser", *Jahrb. STG, 39. Bd.*, 1938.
85. Müller, O.: "Aus dem Grenzgebiet des wasser- und schiffbaulichen Modellversuchswesens", *Schiffbau, 36. Jahrg.*, 1935.
86. Constantine, T.: "On the Movement of Ships in Restricted Waterways", *J. Fluid Mechanics, Vol. 9, Part 2*, Oct. 1960.
87. Hooft, J. P.: "On the Critical Speed Range of Ships in Restricted Waterways", *Intern. Shipb. Progress, Vol. 16, No. 177*, May 1969.
88. Sturtzel, W., and Graff, W.: "Untersuchungen über die Zunahme des Zähigkeitswiderstandes auf flachem Wasser", *85. Mitteilung der VBD, Forschungsberichte des Landes Nordrhein-Westfalen Nr. 1777*, 1967.
89. Kirsch, M.: "Die Erzeugung von Rotationskörpern aus gegebenen Singularitäten-Verteilungen", *Schiff und Hafen, 11. Jahrg., Heft 11*, 1959.
90. Sturzel, W., und Heuser, H. H.: "Widerstands- und Propulsionsmessungen für den Normalselbstfahrer Typ Gustav Koenigs", *Forschungsberichte des Landes Nordrhein-Westfalen, Heft 868*, 1960.
91. Graff, W.: "Untersuchungen über Änderungen von Sog und Nachstrom auf beschränkter Wassertiefe in stehendem und strömendem Wasser", *Schiffstechnik, 8. Bd, Heft 44*, Nov. 1961.
92. Sjostrom, C. H.: "Effect of Shallow Water on Speed and Trim", *Naval Engineers Journal*, April 1967.
93. Tuck, E. O.: "Shallow Water Flows Past Slender Bodies", *Journ. Fluid Mechanics, Vol. 26, Part 1*, Sept. 1967.
94. Tuck, E. O.: "Sinkage and Trim in Shallow Water of Finite Width", *Schiffstechnik, 14. Bd, Heft 73*, Sept. 1967.
95. Hay, D.: "Harbour Entrances, Channels and Turning Basins", *The Dock and Harbour Authority*, Jan. 1968.
96. Kan, M., and Hanaoka, T.: "Analysis for the Effect of Shallow Water upon Turning" (in Japanese), *Journ. Soc. Nav. Arch. Japan, Vol. 115*, 1964.
97. Newman, N. J.: "Lateral Motion of a Slender Body Between Two Parallel Walls", *Journ. Fluid Mechanics, Vol. 39, Part 1*, Oct. 1969.
98. Inoue, S., and Murayama, K.: "Calculation of Turning Ship Derivatives in Shallow Water" (in Japanese), *J. Seibu Zōsen Kai, No. 37*, Febr. 1969.
99. Inoue, S., and Kijima, K.: "Force Calculation of a Rectangular Plate Moving Obliquely in Water Channels" (in Japanese), *J. Seibu Zōsen Kai, No. 39*, March 1970.
100. Bollay, W.: "A Non-Linear Wing Theory and its Application to Rectangular Wings of Small Aspect Ratio", *ZAMM, 19. Bd, Nr 1*, Febr. 1939.

101. Borden, A.: "Wall Corrections for Flow about Two- and Three-Dimensional Symmetrical Bodies in Rectangular Channels of Infinite and Finite Lengths", *DTMB Report 864*, Dec. 1954.

102. Newman, N. J.: "The Force and Moment on a Slender Body of Revolution Moving Near a Wall", *DTMB Report 2127*, Dec. 1965.

103. Garthune, R. S., Rosenberg, B., Cafiero, D., and Olson, C. R.: "The Performance of Model Ships in Restricted Channels in Relation to the Design of a Ship Canal", *DTMB Report 601*, Aug. 1948.

104. Schoenherr, K. E.: "Data for Estimating Bank Suction Effects in Restricted Water and on Merchant Ship Hulls", *Proc. First Symposium on Ship Maneuverability*, Washington D.C., *DTMB Report 1461*, Oct. 1960.

105. Tuji, T., Mori, N., and Yamanouchi, Y.: "On the Water Force Acting on a Ship in Oblique Flow (Restricted Water Effect)", *Contr. to the 12th ITTC*, Rome 1969.

106. Kennard, E. H.: "Irrotational Flow of Frictionless Fluids, Mostly of Invariable Density", *DTMB Report 2299*, Feb. 1967.

107. Nussbaum, W.: "Messung von Quer- und Längskräften am Modell eines Grosstankers", *VBD Berichten Nr. 396 I–II* and *406*, June–Sept. 1966. (Contract Reports.)

108. Schmidt-Stiebitz, H.: "Die Manövriereigenshaften der Schiffe in Abhängigkeit von Schiffsform und Fahrwasser", *Schiff und Hafen, 16. Jahrg., Heft 2*, Feb. 1964.

109. Eda, H., and Savitsky, D.: "Experimental and Analytical Studies of Ship Controllability in Canals", *Dav. Lab. Techn. Note 809*, Sept. 1969.

110. Fujino, M.: "Experimental Studies on Ship Manoeuvrability in Restricted Waters — Part II", *Intern. Shipb. Progr., Vol. 17, No. 186*, Feb. 1970.

Contents